NASA Tech Briefs

Official Publication of
National Aeronautics and
Space Administration
Volume 14 Number 4

Transferring Technology to
American Industry
and Government
April 1990

Special Report On NASA High-Speed Aircraft Research

In space: looking back to look forward.

What can the nature and origin of the universe tell us about the future of Earth? To help answer that question, we make craft and instruments for traveling billions of miles in space and seeing as far as 15 billion years back in time. Martin Marietta was the integrator and builder of two Viking landers, which sent back remarkable photos of the surface of Mars, examined soil samples, and studied Martian weather and seismic activity. For the Voyagers we provided instrumentation that reported on electromagnetic activity near Jupiter and Saturn–Voyager 2 went on to Uranus, some 2 billion miles from Earth. That was nine years after launch; next destination, Neptune, in 1989. These are but a few results of Martin Marietta's ability to create survivable, mystery-solving craft and their instruments–from concept through mission completion.

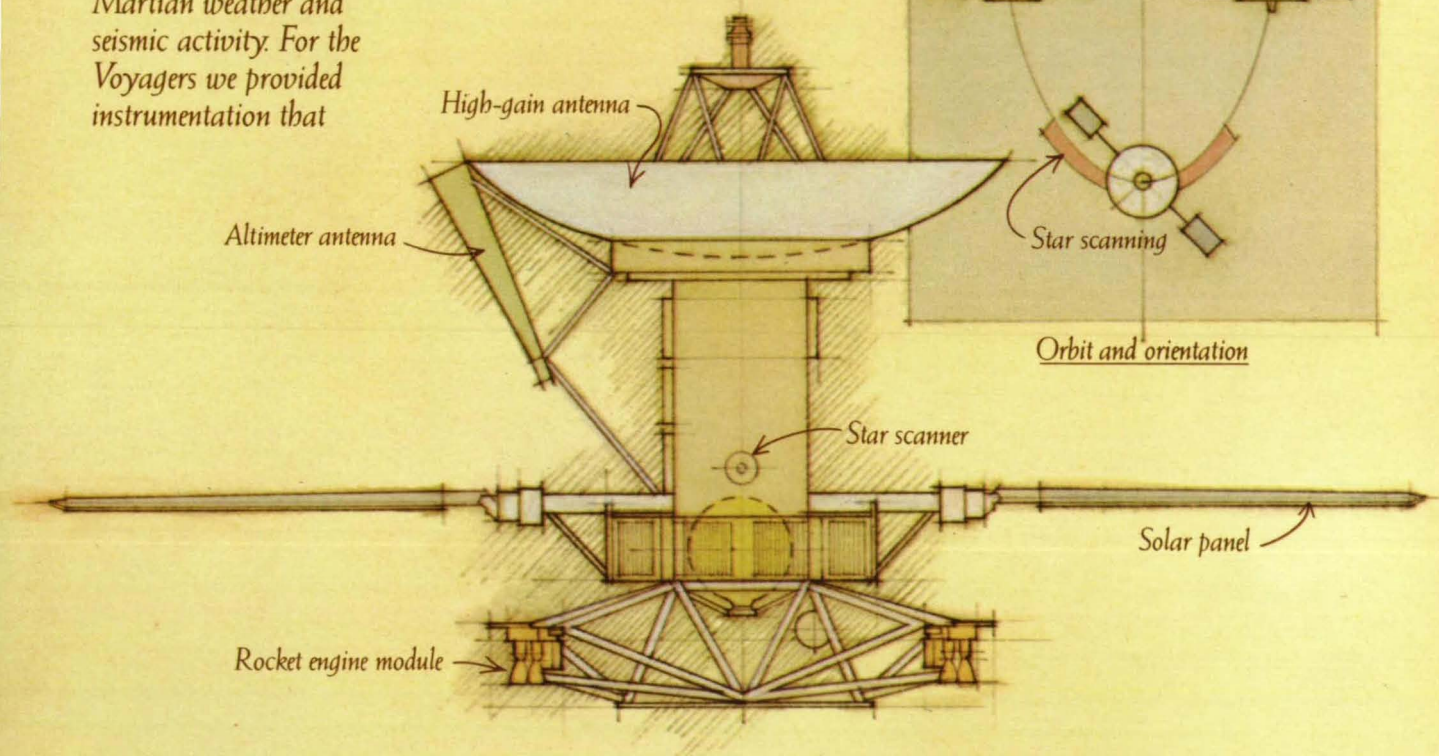

Magellan Spacecraft

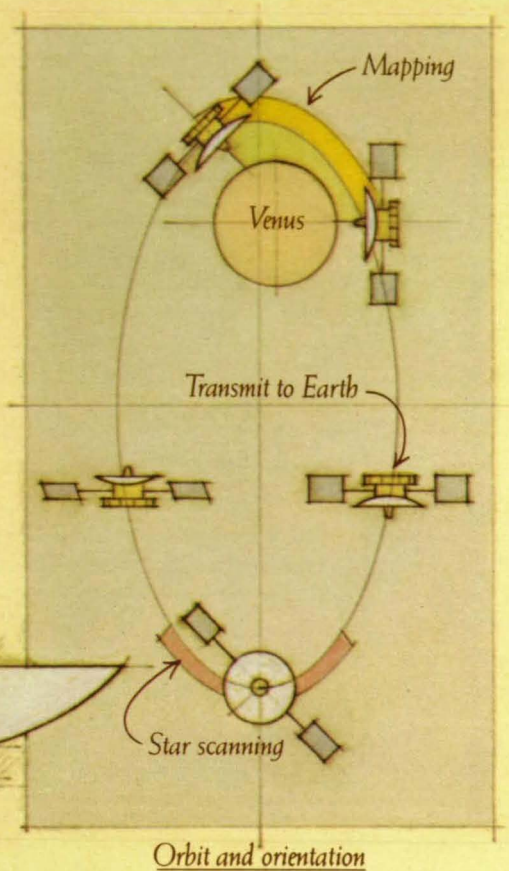

Orbit and orientation

Mission: map Venus.

From orbit, Magellan's radar will penetrate the planet's thick, gaseous cloud cover and send back photo-like images of nearly 90% of its surface. Our role: design, integrate, build and test the craft.

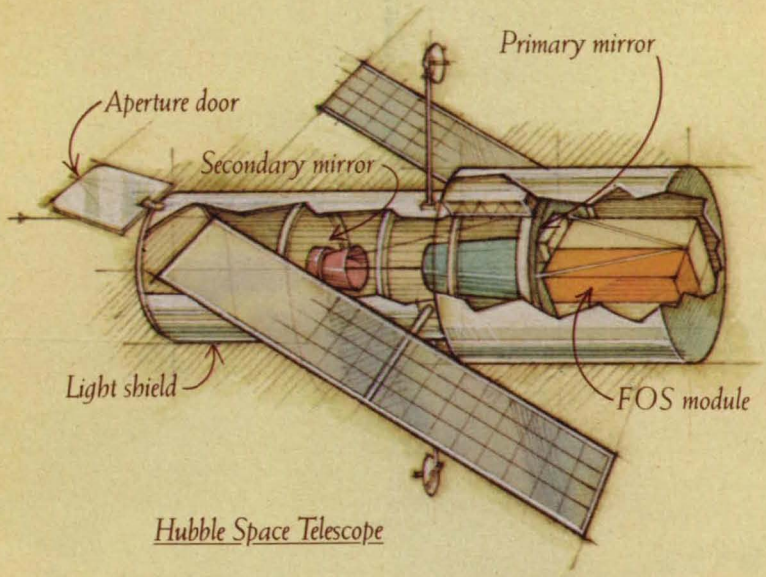

Hubble Space Telescope

Viewing the infant universe.

For the Hubble Space Telescope we are providing the Faint Object Spectrograph (FOS), which will see objects up to 15 billion light-years away. Since the universe is estimated to be 18-20 billion years old, astronomers will witness events close to its birth.

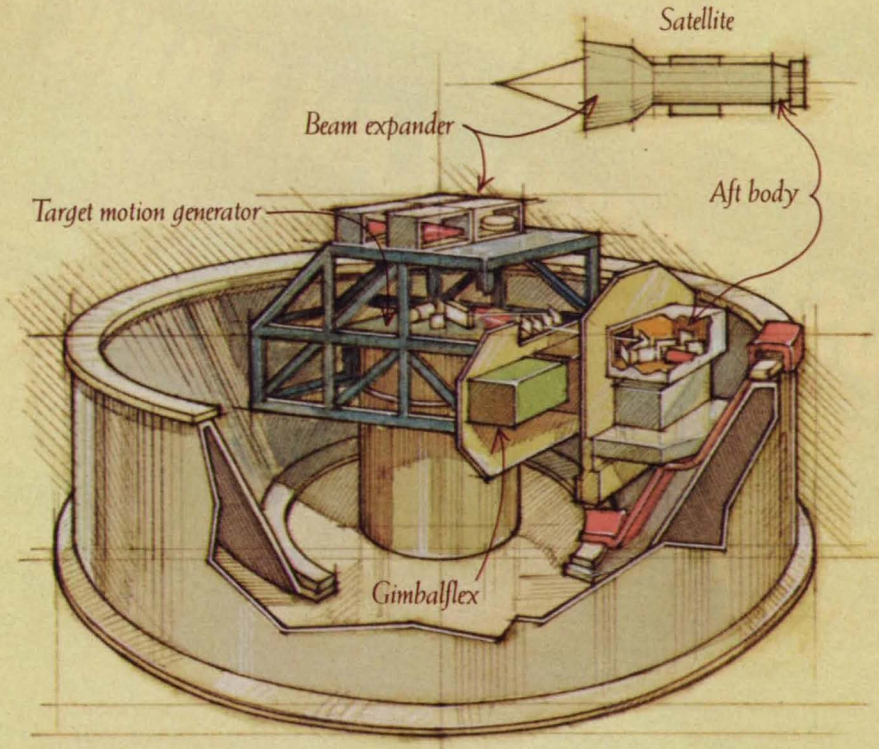

Fine Pointing Simulator

The fine points of fine pointing.

Precisely controlled, space-spanning energy delivery and collection systems create difficult pointing and retargeting challenges, which we can now simulate. This new lab is working toward the precision to zero in on a football-size object 3,000 miles away, in support of the Strategic Defense Initiative research program.

Masterminding tomorrow's technologies

MARTIN MARIETTA

6801 Rockledge Drive, Bethesda, Maryland 20817, USA

AEROSTRENGTH

COMPOSITES YOU CAN BANK ON.

Hercules® graphite composites finish ahead of the competition when high performance is on the line.

These strong, lightweight materials are delivering speed and crashworthiness to World Champion, Marlboro McLaren Honda race cars. Trimming weight and enhancing aerodynamics for supersonic fighters. And increasing payload for space launch vehicles. Just what you'd expect from America's largest producer and the world's foremost user of graphite fiber.

Hercules high performance composites. First choice worldwide when second best isn't good enough.

For more information, contact:
Hercules Advanced Materials & Systems Company
U.S.A. - (801) 251-5372, Fax: (801) 251-3268
Europe - (1) 47 51 29 19, Fax: (1) 47 08 50 75

Circle Reader Action No. 488

HERCULES

A Unit of Hercules Incorporated

MATLAB™

High-Performance Numeric Computation and Data Analysis

MATLAB has rapidly become an industry standard for engineering and scientific research. Its unique interactive interface, algorithmic foundation, easy extensibility, and speed make MATLAB the software system of choice for ***high productivity and high creativity*** research.

Problems and solutions are expressed just as they are written mathematically – ***without the need for traditional programming***. As a result, you can solve numerical problems in a fraction of the time required to write a program in Fortran, Basic, or C. Then plot the results as 2-D and 3-D graphics, with publication-quality output to plotters, dot-matrix printers, and laser printers.

"I can create algorithms so easily that it almost seems like cheating."

Amnon Aliphas, Personal Engineering & Instrumentation News

Add to MATLAB your choice of tools for digital signal processing, system identification, control system design, and more. MATLAB's open-system design lets you see the algorithms and the implementations, even change them to suit your specific requirements.

MATLAB is developed by The MathWorks, a leader in software for data analysis and mathematics. Our users – in thousands of companies and universities – know that MATLAB enables them to work more creatively and productively. Take a look at how MATLAB can do the same for you.

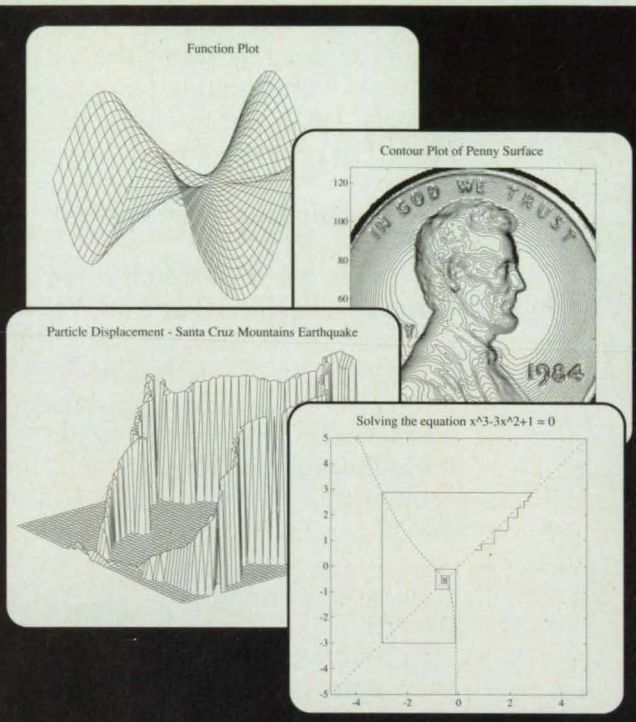

Over 300 Built-In Functions

- eigenvalues
- matrix arithmetic
- matrix decompositions
- convolution
- spectrum estimation
- complex arithmetic
- 1-D and 2-D FFTs
- filtering
- curve fitting
- cubic splines
- Bessel functions
- elliptic functions
- nonlinear optimization
- linear equation solving
- differential equations
- polynomial arithmetic
- descriptive statistics
- 2-D and 3-D graphics

Plus Toolboxes for:

- digital signal processing
- parametric modelling
- control system design
- chemometric analysis, and more

"MATLAB is the undisputed choice for computation-intensive engineering work."

Charles Seiter, Macworld

"MATLAB's power and ease of use go a long way toward taking the drudgery out of repetitive analysis projects."

Richard Santalesa, IEEE Spectrum

Computers supported

PCs and ATs
386-based PCs
Macintosh
Sun
Apollo
HP 9000/300
DECstation
VAX/VMS
VAX/Ultrix
Stardent
Convex
Encore
Alliant
Cray
and more

To find out more about MATLAB, call us at **(508) 653-1415**. Or simply return the completed coupon to the address below.

Name _____

Company _____

Department _____

Address _____

City, State _____

Zip _____ *Country* _____

Telephone _____

Computer(s) _____

The MATH WORKS Inc.

21 Eliot Street
South Natick, MA 01760
Phone: (508) 653-1415
Fax: (508) 653-2997

NASA 4/90

Circle Reader Action No. 503

Get a close look at the big picture.

With the new HI JetPro™ printer/plotter.

Select your drawing. Preview it on your monitor. Zoom in on the tightest detail. Clip it, scale it, mark a "window." Then press a key to get a high-quality hardcopy of the segment you want.

You can do all of this—*plus* high-speed draft and letter-quality printing—with one machine: the HI JetPro printer/plotter.

The flexible hardcopy control system

Whether it's an E-size drawing or a scanned data file, HI JetPro delivers the flexibility you need and the image you want. With HI's JetPro, you have a complete hardcopy control system that includes hardware and software for high-speed, high-resolution printing and plotting—in both vector and raster environments.

Convenient, quiet, and precise

HI JetPro produces your images on ordinary paper, in sizes up to 16.5 × 23.3 inches (DIN A2), with the incredibly sharp clarity of 360 dpi. And because it's a bubble-jet, it prints and plots quickly and quietly.

Simple to use and easy to maintain, the HI JetPro printer/plotter is fully backed by Houston Instrument's reputation for price-performance, quality, and support.

To get a closer look, call *1-800-444-3425* or 512-835-0900.

HOUSTON INSTRUMENT™
A DIVISION OF AMETEK

8500 Cameron Road, Austin, TX 78753

Houston Instrument and HI JetPro are trademarks of AMETEK, Inc.

Circle Reader Action No. 550

Inframetrics infrared imaging: to see, to quantify, to understand.

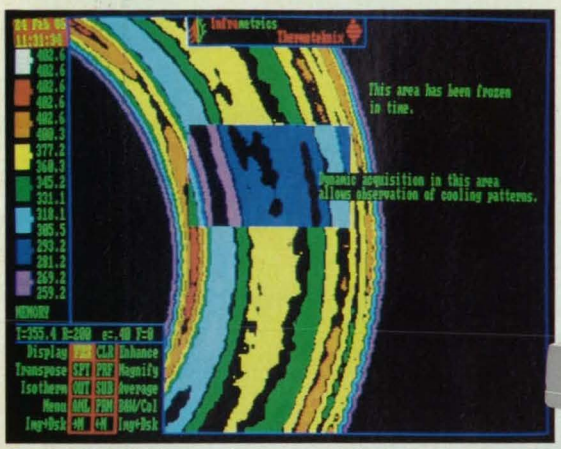

ThermaGRAM® image of an automotive brake rotor.

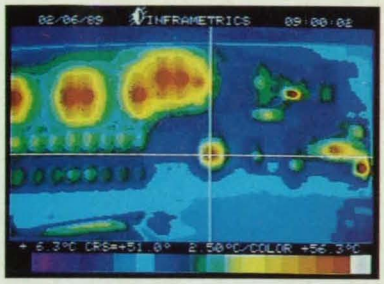

Model 600 provides spot temperatures of components on PC board. Line scan profiling, isotherm contouring and area measurement are all standard, without computer interface.

Model 600 on the lab bench...stalwart of sophisticated radiometers.

Whether you're looking for pressure leaks in an aircraft fuselage or fluid ingress in the flaps; electrical system hot spots or excessive bearing friction; delamination in composite structures or shorts in a multilayer printed circuit board...the infrared diagnostic technology of Inframetrics systems will quickly give you the answers you need.

Our concentration on *practical infrared imaging and temperature measurement* — the delivery of useful results, under real-world conditions, at reasonable prices — has made us a leader in infrared imaging radiometers, and producers of the widest variety of thermal imaging instruments in the world.

A complete system, cart-mounted, with optional VCR and Polaroid hard copy system, goes anywhere.

TV-compatible, compact and field-portable, Inframetrics Imaging Radiometers and Thermal Imagers provide real time imagery with excellent picture quality for the *highest total performance* commercially available today. Combine these capabilities with the most versatile image-processing system in the market; ThermaGRAM® performs histogram analysis, time vs. temperature studies, real time image analysis, and countless other functions.

Just consider the possibilities.

Inframetrics systems adapt to a wide variety of applications, including R&D, nondestructive testing, electronic diagnosis, quality control, facilities maintenance and medicine.

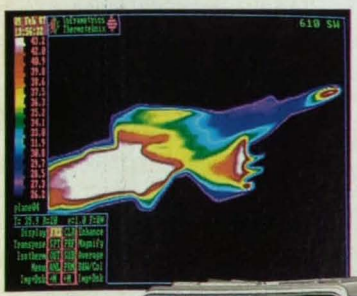

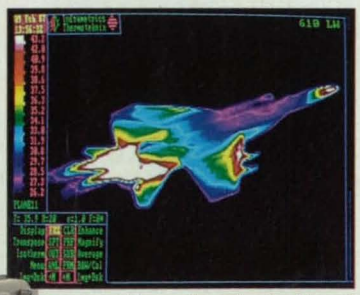

Model 610 acquires the dual-band IR signature of a fighter.

Model 445 high resolution thermal imager shows delamination in a composite panel. Ideal for qualitative analysis, nondestructive testing, security systems, more.

Inframetrics systems open the door to another engineering perspective on your problems. To learn more, tell us your application.

inframetrics The Infrared Specialists

16 Esquire Rd., No. Billerica MA 01862-2598 *Offices worldwide*
TEL 508-670-5555 • FAX 508-667-2702 • TWX 710-326-0659

Circle Reader Action No. 370

NASA Tech Briefs

Transferring Technology to
American Industry and Government

APRIL 1990
Volume 14 Number 4

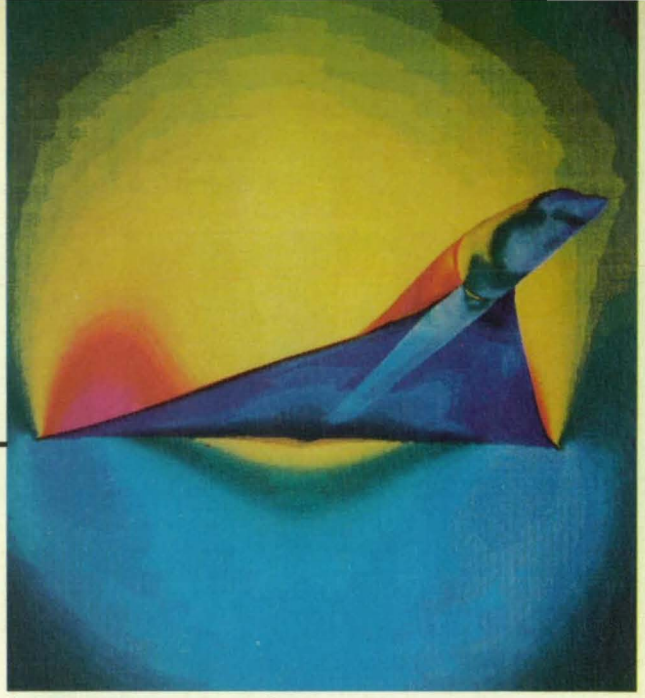

Photo courtesy McDonnell Douglas Corp.

This High-Speed Civil Transport (HSCT) concept shows a computational fluid dynamics solution of the flowfield static pressure distribution up to the engine inlet plate. The blue shading on the lower surface indicates higher than freestream local pressure and a compression of the flow; the red above the configuration represents lower pressures. For more on HSCT research, turn to page 10.

SPECIAL FEATURES

TECHNICAL SECTION

ABP BPA

DEPARTMENTS

On The Cover: A Cray XMP-18 supercomputer generated this prediction of the pressure fields around a supersonic aircraft. High-pressure regions on the wing leading edge and the fuselage appear red, while low-pressure regions on the wing upper surface are in blue. Graphics were produced by ARTIS software. (Photo courtesy McDonnell Douglas Corporation)

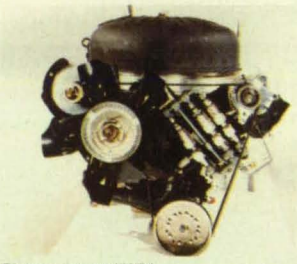

Photo courtesy NASA

NASA is developing high-temperature materials for piston rings and cylinder coatings in automotive Stirling engines. The materials help increase engine power and reduce fuel consumption by as much as seven percent. See page 56.

NASA Tech Briefs, ISSN 0145-319X, USPS 750-070, copyright © 1990 in U.S., is published monthly by Associated Business Publications Co., Ltd., 41 E. 42nd St., New York, NY 10017-5391. The copyrighted information does not include the individual tech briefs which are supplied by NASA. Editorial, sales, production and circulation offices at 41 East 42nd Street, New York, NY 10017-5391. Subscription for non-qualified subscribers in the U.S. , Panama Canal Zone, and Puerto Rico, $75.00 for 1 year; $125.00 for 2 years; $200.00 for 3 years. Single copies $10.00. Remit by check, draft, postal or express orders. Other remittances at sender's risk. Address all communications for subscriptions or circulation to NASA Tech Briefs, 41 East 42nd Street, New York, NY 10017-5391. Second-class postage paid at New York, NY and additional mailing offices.

POSTMASTER: please send address changes to NASA Tech Briefs, 41 E. 42nd Street, Suite 921, New York, NY 10017-5391.

To show you what our new DataGraf recorder can do,

GOULD
Electronics

No matter how advanced your recorder is, it still has to meet your most basic recording needs. That's why our new DataGraf offers everything you'd expect from a computer-based recorder—plus unique hard copy output flexibility.

How advanced is DataGraf? It offers 16-channel recording capability, all in a rugged, portable package weighing less than forty pounds. With DataGraf, you can store events on disk and replay them as often as you like. You can also expand or compress traces, overlay signals, and even label key points.

What's more, using advanced waveform analysis software, DataGraf automatically analyzes your data, virtually eliminating the need for manual interpolation and long-hand math. Whether you're interested in the entire signal or just a specific section, the touch of a button will calculate Max/Min, Standard Deviation, dY/dX, RMS, and much more.

And when it comes to seeing your results on paper, DataGraf can output your traces to hundreds of printers, plotters and traditional oscillographic recorders.

It's exactly the kind of solution you'd expect from Gould, a company with over fifty years of recorder development experience. By applying new technology to the real needs of today's engineers, we've developed a unit that offers real advantages. Advantages that go beyond advanced features. Advantages you can put on paper.

Send for a free DataGraf demo disk. Use the coupon below, or fax your request to (216) 361-0559.

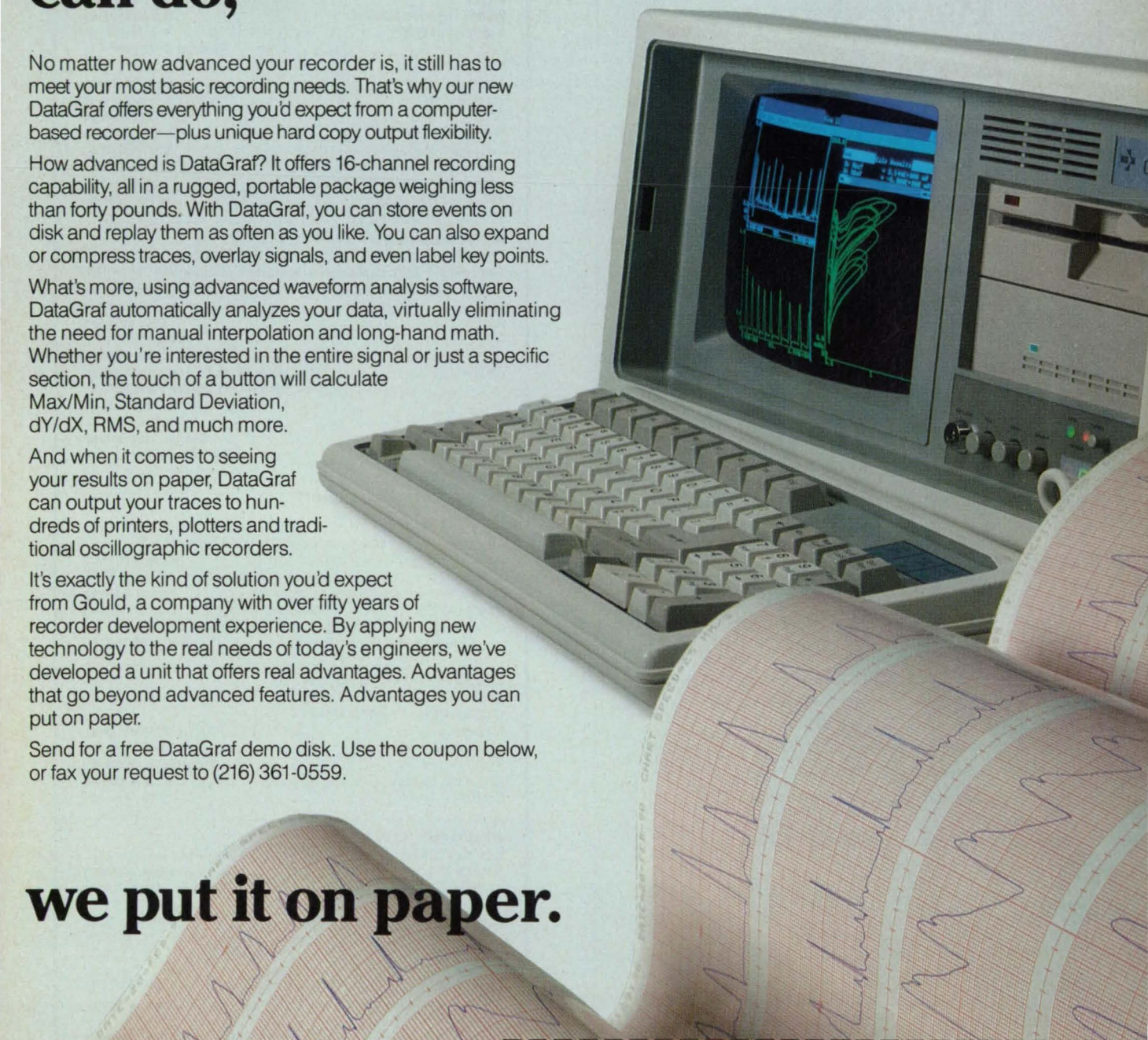

we put it on paper.

Free demo disk!

NTB4/90

Yes! I'd like to see what DataGraf can do. Send me a free demo disk and product information package.

NAME: _____ TITLE: _____

COMPANY: _____

STREET: _____

CITY: _____ STATE: _____ ZIP: _____

PHONE: _____

Send to: Gould, Inc., Test and Measurement, 3631 Perkins Avenue, Cleveland, Ohio 44114, or call (216) 361-3315. Fax: (216) 361-0559.

NASA Tech Briefs

Official Publication of
National Aeronautics and
Space Administration

ABP BPA

NASA Tech Briefs:

Published by ..... **Associated Business Publications**
Editor-in-Chief/Publisher ..... **Bill Schnirring**
Associate Publisher ..... **Frank Nothaft**
Editor ..... **Joseph T. Pramberger**
Managing Editor ..... **R. J. Laer**
Assistant Editor ..... **Theresa M. Detko**
Technical Advisor ..... **Dr. Robert E. Waterman**
Production Manager ..... **Rita Nothaft**
Traffic Manager ..... **James E. Cobb**
Circulation Manager ..... **Cheryl Golden**
Advertising Coordination Manager ..... **Maya V. Falek**
Telecommunications Specialist ..... **Evelyn Mars**
Reader Service Manager ..... **Sylvia Valentin**

Briefs & Supporting Literature:
Provided to National Aeronautics and Space Administration by **International Computers & Telecommunications, Inc.**, NY, NY with assistance from **Logical Technical Services**, NY, NY
Technical/Managing Editor ..... **Ted Selinsky**
Art Director ..... **Luis Martinez**
Administrator ..... **Elizabeth Texeira**
Chief Copy Editor ..... **Lorne Bullen**
Staff Writers/Editors ..... **Dr. James Boyd, Dr. Larry Grunberger, Dr. Theron Cole, Jordan Randjelovich, George Watson, Oden Browne**
Graphics ..... **Vernald Gillman, Charles Sammartano**
Editorial & Production ..... **Bill Little, Ivonne Valdes, Frank Ponce, Susan Finelli**

NASA:
NASA Tech Briefs are provided by the National Aeronautics and Space Administration, Technology Utilization Division, Washington, DC:
Administrator ..... **Richard H. Truly**
Assistant Administrator for Commercial Programs ..... **James T. Rose**
Deputy Assistant Administrator (Programs) ..... **Henry J. Clarks**
Acting Director TU Division (Publications Manager) ..... **Leonard A. Ault**
Manager, Technology Utilization Office, NASA Scientific and Technology Information Facility ..... **Walter M. Heiland**

Associated Business Publications
41 East 42nd Street, Suite 921, New York, NY 10017-5391
(212) 490-3999 FAX (212) 986-7864
President ..... **Bill Schnirring**
Executive Vice President ..... **Frank Nothaft**
Vice President ..... **Domenic A. Mucchetti**
Operations Manager ..... **Rita Nothaft**
Controller ..... **Felecia Lahey**

Advertising:
New York Office: (212) 490-3999 FAX (212) 986-7864
Director of Advertising Sales ..... **James G. McGarry**
Account Executive (NY, NJ) ..... **Brian Clerkin** at (201) 285-0880
Account Executive (VA, DC, MD, DE, WV) ..... **John D. Floyd** at (215) 399-3265
Account Executive ..... **Debby Crane** at (201) 967-9838
Account Executive (Midwest, Northwest) ..... **Paul Lesher, CBC** at (708) 501-4140
Regional Sales Manager (South-Central) ..... **Douglas Shaller** at (212) 490-3999
Account Executives (Eastern MA, NH, ME, RI) ..... **Paul Gillespie** at (508) 429-8907; **Bill Doucette** at (508) 429-9861
Account Executives (Western MA, CT, VT) ..... **George Watts** or **David Haggett** at (413) 253-9881
Account Executives (Southeast) ..... **Newton Collinson** or **Jonathan Kiger** or **Lawrence Mischik** at (404) 939-8391
Account Executives (Calif., AZ, NV, NM) ..... for Area Codes 818/213/805 —**Thomas Stillman** for Area Codes 408/415/916/209 —**Elizabeth Cooper** and for Area Codes 619/714 —**Karen Mock** at (213) 372-2744

NTBM-Research Center
Account Supervisor ..... **Lourdes Del Valle**

digital™

How to improve your station in life.

It's easy.

From now until June 30, 1990, just trade in your VAXstation™ 2000 workstation and Digital will give you $2,000 off the purchase price of our VAXstation 3100 workstation.

When you do, you're getting a lot more than just money off.

The VAXstation 3100 workstation delivers 3 to 4X the performance of the 2000.

The VAXstation 3100 workstation lets you run DECwindows™ software. It gives you a consistent user interface for accessing applications on your network whether they're running VMS,™ UNIX®/ ULTRIX™ or MS-DOS.® You choose what you want and it shows up on screen the way you want.

	VAXstation 2000	VAXstation 3100
VUPs	1	4
Memory	6–14 MB	8–32 MB
Disk Capacity	70–1.3 GB	104–1.3 GB
Resolution	1,024 × 864	1,024 × 864
Planes	1, 4, 8	1, 8

And, even though the VAXstation 3100 workstation is an upgrade, you can use all the same software you've been using on the 2000. With no rewriting.

Take the all-important first step toward improving your station in life. Call 1-800-343-4040, ext. 874 to take advantage of this special $2,000 offer.

Digital has it now.

NASA Leads Research On High-Speed Civil Transport

Supersonic Aircraft Would Meet Need For Fast Transoceanic Travel

Editor's note: The following report is the first of two parts on NASA's High Speed Research Program.

The growing need to travel quickly to the economic centers of the Pacific Basin is expected to create a market for as many as 1200 supersonic airliners by the year 2015. To help the United States gain a competitive edge in this potentially lucrative market, NASA has teamed with U.S. aircraft makers to explore the feasibility of developing a fleet of long-range supersonic transports for commercial introduction in the 2000-2010 time frame. Cruising at two to three times the speed of sound (1350-2000 mph), the advanced aircraft would cut flight times dramatically; a trip from Los Angeles to Tokyo, for example, would be reduced from ten hours to approximately four hours.

As now envisioned by aircraft designers, this high-speed civil transport (HSCT) would carry 250-300 passengers and be able to fly 6500 miles without refueling. By comparison, the Anglo-French Concorde holds only 103 passengers and has a range of 3500 miles. And while the Concorde caters mainly to the jet set, the HSCT would offer standard tri-class seating, with fares only slightly higher than those for subsonic planes.

"The challenge is to build a plane that's both environmentally acceptable and economically sound," said Donald Graf, HSCT Business Unit Manager for the McDonnell Douglas Corporation. Studies by McDonnell Douglas and the Boeing Company determined that substantial demand for an HSCT will materialize only if the aircraft meets community noise standards, has no harmful effects on the atmosphere, and is cost-competitive with future long-haul subsonic airliners. The reports emphasized that the technology to build a high-speed transport satisfying these requirements does not yet exist.

In late 1989, NASA initiated the industry-government High Speed Research Program to tackle the technical and economic challenges of making a supersonic transport an "environmental good neighbor." The six-year, $284 million program, involving the agency's Ames, Langley, and Lewis research centers, is initially focused on three major environmental issues: atmospheric effects, airport community noise, and sonic boom. "We have to make some headway in solving these environmental problems before we can move on to a more focused technology development program," said Howard Wesoky, NASA's program manager for HSCT research and technology.

Probing The Atmosphere

The most serious concern, and the top priority of NASA's new program, is the potential for damaging the Earth's fragile ozone layer. Because the plane would fly at 55,000 to 60,000 feet, scientists fear that nitrogen oxides (NOx) emitted from its kerosene-burning engines could destroy the stratospheric ozone that blocks the sun's ultraviolet rays. NASA and its industry partners are investigating advanced combustor designs that offer reduced emissions without compromising engine efficiency, and are experimenting with NOx destructive additives such as methane and propane. One approach is to introduce the additive into the exhaust gas stream so that elemental nitrogen is formed rather than NOx, but experts caution that a variety of technical issues must still be addressed. And there are potential drawbacks: additives increase aircraft weight and the cost of ground handling.

Space Agency researchers also plan to use sophisticated atmospheric chemistry and dynamics models to analyze the dispersion and long-term effects of emissions. Their goal is to develop a technical basis for the establishment of emissions standards. "We're not going to be able to progress very far in the combustor technology until we understand how the upper atmosphere handles emissions and determine what level of emissions is acceptable," Wesoky stated.

Noise Control

The HSCT's engines will need to quieter than those of the Concorde if the plane is to gain approval from local communities to take off as frequently as subsonic transports. Researchers are evaluating low-noise exhaust nozzle and inlet configurations for the craft's propulsion system, and are applying high-lift aerodynamics technology to proposed wing designs. A wing with good takeoff lift performance would help reduce perceived noise by quickly carrying the offending engines to high altitudes.

In contrast to the needle-like shape of the Concorde, the HSCT is likely to have broad, triangular wings with the desired high-lift characteristics. This wing planform is called a double delta because the forward portion of the wing slopes backward in a sharp triangle while the back half spreads out at a wide angle. To determine the optimal shape for the aircraft's wings and fuselage, engineers are employing computational fluid dynamics (CFD) techniques to model the high-speed air flow over a hypothetical HSCT.

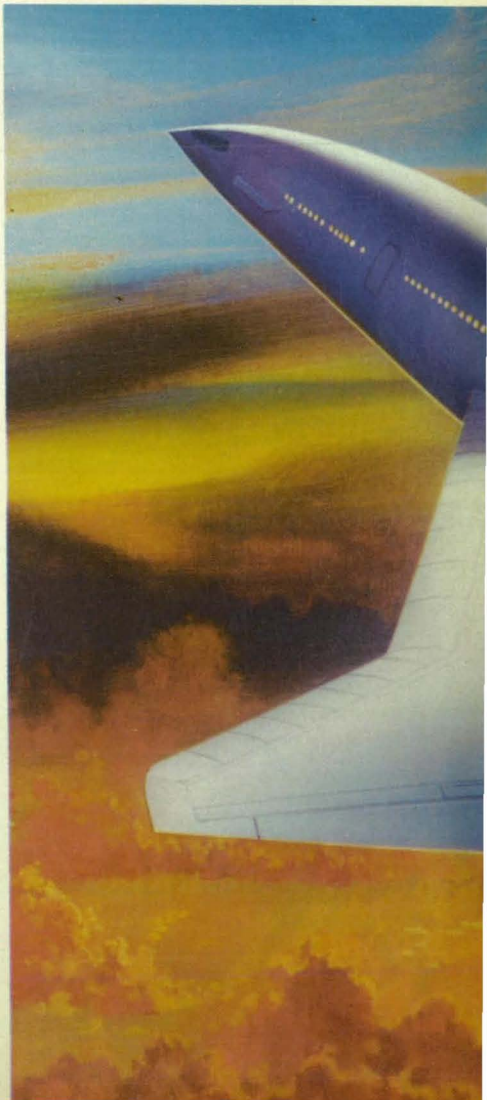

Lowering The Boom

Engine emissions and noise aren't the only barriers to public acceptance: HSCT researchers must also deal with sonic boom, the explosive sound produced when a shock wave formed at the nose of a supersonic aircraft reaches the ground. Aircraft designers want to limit the boom impact enough for the HSCT to win permission for supersonic flight over land, which would save passengers time and increase the aircraft's productivity and economic viability. The effort to minimize sonic boom involves a synergistic approach, combining advances in the understanding of human and structural responses to booms with modifications to the aircraft's geometry to reduce the annoyance level. Scientists are using technical, statistical, and psychological means to measure response characteristics and establish what levels of sonic boom noise are acceptable for overland flight. The acceptability criteria will be used to guide the design of low-boom configurations and to evaluate the designs through computer analysis, wind tunnel experiments, and flight tests.

A less direct but extremely important way to alleviate sonic boom and other environmental problems is to reduce the aircraft's weight, which in turn results in a lower boom level and in smaller engines that produce less emissions and noise. This necessitates developing lightweight structural materials capable of handling the high temperatures and pressures that an HSCT would encounter. The Boeing study identified toughened thermosetting, high-temperature thermoplastic or polyimide polymeric composites as the most promising structural materials for a next-generation supersonic transport. Boeing projected that by the year 2015 the maturation of metal matrix composites and rapid solidification technology will enable their application on the HSCT. Current material forms, processes, and production equipment are not adequate to produce the large structures required for the HSCT program, the study concluded.

The HSCT's weight could also be lowered by applying supersonic laminar flow control, which would increase the vehicle's lift-to-drag ratio and therefore its fuel efficiency, since less fuel would be needed to overcome drag forces. Researchers are studying a system that combines air suction near the wing leading edge with contouring of the wing surface to reduce friction drag. Even with penalties for suction system weight and engine power extraction, a 6.5 percent or greater reduction in takeoff gross weight is anticipated for a typical high-speed transport, an amount comparable to the aircraft's payload.

The Next Step

If researchers can show significant progress in resolving the environmental problems and further studies confirm the supersonic aircraft's importance to the transportation system and the U.S. economy, a larger scale vehicle technology development effort "could be considered as a next step," according to Wesoky. Ultimately, he said, the decision to produce a supersonic commercial transport will rest with the nation's aerospace industry. ❐

Next month: A close-up look at HSCT research at NASA's Ames, Langley, and Lewis research centers.

Photo courtesy Boeing Commercial Airplanes

Artist's conception of a high-speed civil transport with a double-delta wing planform

New Product Ideas

New Product Ideas are just a few of the many innovations described in this issue of *NASA Tech Briefs* and having promising commercial applications. Each is discussed further on the referenced page in the appropriate section in this issue. If you are interested in developing a product from these or other NASA innovations, you can receive further technical information by requesting the TSP referenced at the end of the full-length article or by writing the Technology Utilization Office of the sponsoring NASA center (see page 14). NASA's patent-licensing program to encourage commercial development is described on page 14.

Crystal Oscillators Operate Beyond Rated Frequencies

A class of crystal oscillators is based on the use of negative-voltage-gain amplifiers at frequencies well into the "roll-off" frequency regions of their gain-versus-frequency curves. This characteristic eliminates the need for expensive amplifiers and extra passive components used in more conventional oscillator designs.
(See page 30)

Header for Laser Diode

A laser-diode header provides electrical and thermal connections to the diode and optomechanical adjustments to focus and aim the laser beam. This relatively inexpensive optical communications package features a simple mechanical configuration and commercially available lenses.
(See page 16)

Feeder System for Particle-Size Analyzer

A feeder system meters a precise stream of powder into a precise flow of gas feeding a light-scattering particle-size analyzer. The feeder makes dry analysis of a powder more practical than in the past. Such an analysis takes about one-third the time of conventional wet analysis and consumes less powder.
(See page 61)

Improved Liquid-Electrode/ Solid-Electrolyte Cell

A rechargeable solid-electrolyte electrochemical cell features a new mixture of organic and inorganic materials in a liquid cathode. The cell operates at a temperature about 120 to 170 °C lower than that of sodium/sulfur cells and has comparable energy density of about 150 Wh/kg.
(See page 51)

Durable Bipolar Plates for Lead/Acid Batteries

A new structure for the positive faces of bipolar plates increases the longevity of lead/acid batteries. The positive-electrode layer is divided into many isolated segments so that defects cannot spread across the layer. The materials that support the electrochemically active components are lightweight and resistant to acid.
(See page 22)

Acoustic Humidity Sensor

An industrial humidity sensor measures the volume fraction of water in the air via its effect on the speed of sound. The sensor is rugged enough for such harsh environments as in paper mills and can measure water-vapor content to within 0.5 percent.
(See page 47)

How to meet your recommended daily Ada requirements on all Intel-based systems.

Now, the leader in Ada Compilers in the 286/386 DOS world offers a compatible family for all Intel-based systems.

Whatever chip: 80386; 80286; 80186; 8086. Whatever operating system: DOS 16-bit with Alsys Extender; DOS 32-bit with Phar Lap; OS/2; 386/ix, AIX PS/2, SunOS, XENIX, and other UNIX variants; bare 80x86 applications; and, soon, BTOS/CTOS targets. Whatever host platform: PC AT; PS/2; Z-248; 386-based PS/2; Compaq 386; and Sun386i, to name a few.

Whatever you use, it can be fortified with the power and flexibility of an Alsys Ada compiler.

Just complete the coupon or call 617-270-0030 for more information on Alsys Ada Compilation Systems. Because to get everything you require from your Intel-based system, you need a compiler that's technology-enriched.

alsys

Check boxes that interest you.
Please send me information on Alsys Ada compilers for: ☐ 286 DOS ☐ 386 DOS ☐ 386 UNIX ☐ OS/2
Please send me more information on: ☐ Ada Education ☐ Other Alsys Ada compilers

NTB4/90

Name _____

Company _____

Address _____

City _____ State ____ Zip _____

Phone ( ) _____

Mail to: Alsys, Inc., 67 South Bedford St., Burlington, MA 01803-5152

AdaNow.

In the US: Alsys Inc., 67 South Bedford St., Burlington, MA 01803-5152, Tel: (617) 270-0030; In the UK: Alsys, Partridge House, Newtown Road, Henley-on-Thames, Oxon RG9 1EN, Tel: 44(491)579090; In France: Alsys, 20 Avenue de Versailles, 78170 La Celle St. Cloud, France, Tel: 33(1) 3918.12.44

Circle Reader Action No. 341

HOW YOU CAN BENEFIT FROM NASA'S TECHNOLOGY UTILIZATION SERVICES

If you're a regular reader of TECH BRIEFS, then you're already making use of one of the low- and no-cost services provided by NASA's Technology Utilization (TU) Network. But a TECH BRIEFS subscription represents only a fraction of the technical information and applications/engineering services offered by the TU Network as a whole. In fact, when all of the components of NASA's Technology Utilization Network are considered, TECH BRIEFS represents the proverbial tip of the iceberg.

We've outlined below NASA's TU Network—named the participants, described their services, and listed the individuals you can contact for more information relating to your specific needs. We encourage you to make use of the information, access, and applications services offered by NASA's Technology Utilization Network.

How You Can Utilize **NASA's Industrial Applications Centers**—A nationwide network offering a broad range of technical services, including computerized access to over 100 million documents worldwide.

You can contact NASA's network of Industrial Applications Centers (IACs) for assistance in solving a specific technical problem or meeting your information needs. The "user friendly" IACs are staffed by technology transfer experts who provide computerized information retrieval from one of the world's largest banks of technical data. Nearly 500 computerized data bases, ranging from NASA's own data base to Chemical Abstracts and INSPEC, are accessible through the ten IACs located throughout the nation. The IACs also offer technical consultation services and/or linkage with other experts in the field. You can obtain more information about these services by calling or writing the nearest IAC. User fees are charged for IAC information services.

Aerospace Research Applications Center (ARAC)
Indianapolis Center for Advanced Research
611 N. Capitol Avenue
Indianapolis, IN 46204
Dr. F. Timothy Janis, Director
(317) 262-5036

Central Industrial Applications Center/NASA (CIAC)
Rural Enterprises, Inc.
P.O. Box 1335
Durant, OK 74702
Dr. Dickie Deel, Director
(405) 924-5094

Science and Technology Research Center (STRC)
Post Office Box 12235
Research Triangle Park,
NC 27709-2235
H.L. (Lynn) Reese, Director
(919) 549-0671

NASA Industrial Applications Ctr.
823 William Pitt Union
University of Pittsburgh
Pittsburgh, PA 15260
Dr. Paul A. McWilliams, Exec. Director
(412) 648-7000

NASA/Southern Technology Applications Center
Box 24
Progress Ctr., One Progress Blvd.
Alachua, FL 32615
J. Ronald Thornton, Director
(904) 462-3913
(800) 354-4832 (FL only)
(800) 225-0308 (toll-free US)

NASA/UK Technology Applications Program
University of Kentucky
109 Kinkead Hall
Lexington, KY 40506-0057
William R. Strong, Director
(606) 257-6322

NERAC, Inc.
One Technology Drive
Tolland, CT 06084
Dr. Daniel U. Wilde, President
(203) 872-7000

Technology Application Center (TAC)
University of New Mexico
Albuquerque, NM 87131
Dr. Stanley A. Morain, Director
(505) 277-3622

NASA Industrial Applications Center
University of Southern California
Research Annex
3716 South Hope Street
Los Angeles, CA 90007-4344
Robert Stark, Director
(213) 743-6132
(800) 642-2872 (CA only)
(800) 872-7477 (toll-free US)

NASA/SU Industrial Applications Center
Southern University Department of Computer Science
P.O. Box 9737
Baton Rouge, LA 70813-9737
Dr. John Hubbell, Director
(504) 771-6272

If you represent a public sector organization with a particular need, you can contact NASA's Application Team for technology matching and problem solving assistance. Staffed by professional engineers from a variety of disciplines, the Application Team works with public sector organizations to identify and solve critical problems with existing NASA technology. **Technology Application Team, Research Triangle Institute, P.O. Box 12194, Research Triangle Park, NC 27709. *Doris Rouse, Director,* (919) 541-6980**

How You Can Access Technology Transfer Services At NASA Field Centers:

Technology Utilization Officers & Patent Counsels—Each NASA Field Center has a Technology Utilization Officer (TUO) and a Patent Counsel to facilitate technology transfer between NASA and the private sector.

If you need further information about new technologies presented in *NASA Tech Briefs,* request the Technical Support Package (TSP). If a TSP is not available, you can contact the Technology Utilization Officer at the NASA Field Center that sponsored the research. He can arrange for assistance in applying the technology by putting you in touch with the people who developed it. If you want information about the patent status of a technology or are interested in licensing a NASA invention, contact the Patent Counsel at the NASA Field Center that sponsored the research. Refer to the NASA reference number at the end of the Tech Brief.

Ames Research Ctr.
Technology Utilization Officer: Laurance Milov
Mail Code 223-3
Moffett Field, CA 94035
(415) 694-4044
Patent Counsel: Darrell G. Brekke
Mail Code 200-11
Moffett Field, CA 94035
(415) 694-5104

Lewis Research Center
Technology Utilization Officer: Anthony F. Ratajczak (acting)
Mail Stop 7-3
21000 Brookpark Road
Cleveland, OH 44135
(216) 433-5568
Patent Counsel: Gene E. Shook
Mail Code LE-LAW
21000 Brookpark Road
Cleveland, OH 44135
(216) 433-5753

John C. Stennis Space Center
Technology Utilization Officer: Robert M. Barlow
Code HA-32
Stennis Space Center, MS 39529
(601) 688-1929

John F. Kennedy Space Center
Technology Utilization Officer: Thomas M. Hammond
Mail Stop PT-PMO-A
Kennedy Space Center, FL 32899
(407) 867-3017
Patent Counsel: James O. Harrell
Mail Code PT-PAT
Kennedy Space Center, FL 32899
(407) 867-2544

Langley Research Ctr.
Technology Utilization Officer: John Samos
Mail Stop 139A
Hampton, VA 23665
(804) 864-2484
Patent Counsel: George F. Helfrich
Mail Code 279
Hampton, VA 23665
(804) 864-3523

Goddard Space Flight Center
Technology Utilization Officer: Donald S. Friedman
Mail Code 702.1
Greenbelt, MD 20771
(301) 286-6242
Patent Counsel: R. Dennis Marchant
Mail Code 204
Greenbelt, MD 20771
(301) 286-7351

Jet Propulsion Lab.
NASA Resident Office
Technology Utilization Officer: Gordon S. Chapman
Mail Stop 180-801
4800 Oak Grove Drive
Pasadena, CA 91109
(818) 354-4849
Patent Counsel: Thomas H. Jones
Mail Code 180-801
4800 Oak Grove Drive
Pasadena, CA 91109
(818) 354-2734
Technology Utilization Mgr. for JPL: Dr. Norman L. Chalfin
Mail Stop 156-211
4800 Oak Grove Drive
Pasadena, CA 91109
(818) 354-2240

George C. Marshall Space Flight Center
Technology Utilization Officer: Ismail Akbay
Code AT01
Marshall Space Flight Center,
AL 35812
(205) 544-2223
Fax (205) 544-3151
Patent Counsel: Bill Sheehan
Mail Code CC01
Marshall Space Flight Center,
AL 35812
(205) 544-0021

Lyndon B. Johnson Space Center
Technology Utilization Officer: Dean C. Glenn
Mail Code IC-4
Houston, TX 77058
(713) 483-3809
Patent Counsel: Edward K. Fein
Mail Code AL3
Houston, TX 77058
(713) 483-4871

NASA Headquarters
Technology Utilization Officer: Leonard A. Ault
Code CU
Washington, DC 20546
(202) 453-8377
Assistant General Counsel for Patent Matters: Robert F. Kempf, Code GP
Washington, DC 20546
(202) 453-2424

A Shortcut To Software: **COSMIC®**—For software developed with NASA funding, contact COSMIC, NASA's Computer Software Management and Information Center. New and updated programs are announced in the Computer Programs section. COSMIC publishes an annual software catalog. For more information call or write: **COSMIC®**, 382 East Broad Street, Athens, GA 30602 *John A. Gibson, Dir.,* (404) 542-3265

If You Have a Question . . . **NASA Scientific & Technical Information Facility** can answer questions about NASA's Technology Utilization Network and its services and documents. The STI staff supplies documents and provides referrals. Call, write or use the feedback card in this issue to contact: **NASA Scientific and Technical Information Facility,** Technology Utilization Office, P.O. Box 8757, Baltimore, MD 21240-0757. *Walter M. Heiland, Manager,* (301) 859-5300, Ext. 242, 243

Tufoil®

WE'VE SAVED MILLIONS FOR OEM'S IN RECENT YEARS WITH OUR PATENTED, LOW FRICTION TECHNOLOGY

- TUFOIL'S STEEL ON STEEL FRICTION IS .029 THATS SLIPPERIER THAN TEFLON® at [.04]

SUPER-LOW FRICTION LUBRICATION PRODUCTS

TUFOIL®, the world's most advanced lubricant does for lubrication what the transistor did for electronics. Spectacular low friction and wear confirmed by one of the U.S. Government's most prestigious labs, and others worldwide. TUFOIL is slipperier than Teflon® according to their data. A patented family of lubricants based on TUFOIL has been developed for the age of computers.

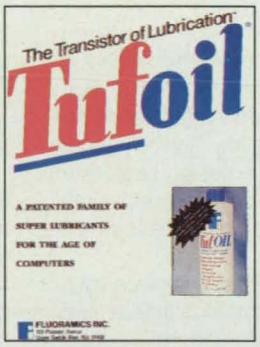

INDUSTRIAL TUFOIL®

Many manufacturers are putting Tufoil in compressor oils, engine crankcase oils, gear boxes, transmissions and lift truck hydraulic systems as an additive to their regular lubricants. Others use it straight from the bottle with our special drip tip to lubricate machine ways, guides, cross-slides and bearings.
Your machinery will run smoother, quieter, using less power than you ever thought possible. No other lubricant even comes close!™

TUFOIL LUBIT-8®

Superior lubricity. Specified by a major manufacturer of automatic machines for inserting components in printed circuit boards. Protective qualities remain almost indefinitely. Compatible with all oils and greases. Lubit is an excellent cleaning agent and can be applied over old lubricants. Great for locks, sewing machines, printers, power tools, automatic machinery and countless other uses!

TUFOIL LIGHTNING GREASE®

Easily sheared grease! Scanning Electron Microscope photos show friction and wear are drastically reduced resulting in longer machine life. Great on instruments, recorders, precision bearings, gears or sliding mechanisms that succumb to friction. Especially suitable for silky smooth robotics!
One-tenth the wear of conventional greases.

TUFOIL COMPU-LUBE®

Very low viscosity Tufoil. Tiny particles, 0.5 to .05 microns, easily get between finest working surfaces for long lasting protection. A microscopic amount does the job. Use on mechanical disk drives, daisy wheels, tractor feeds, robot arms, etc. High tech lubrication for high tech machinery! Works well at very low temperatures (-40°F) and at very high speeds.

TUFOIL GUN-COAT®

In development over 5 years with a major Federal law enforcement training center. Lubricates and rustproofs all firearms and virtually eliminates jamming and leading. Excellent lubricant and preservative for any application where rust is a problem. Law enforcement groups specify it for guns that must work all the time on short notice.
If your life depends on your weapons -- - be sure to use GUN-COAT.

LUBRICATION IS OUR BUSINESS!

Give us a call with your specific problem. We've been solving lubrication problems for major auto manufacturers, Fortune 500 computer companies and OEM's all over the world.

Send $50 for a lubrication sample pack so you can test and see for yourself! We'll send you one each of the above plus FORMULA-8 & LOX-8 PASTE oxygen resistant pipe joint sealers.

Tufoil® is reg trademark of Fluoramics Inc.. Teflon® is reg trademark of DuPont

FLUORAMICS INC.
18 Industrial Avenue
Mahwah, NJ 07430

Phone: 201-825-8110 FAX: 201-825-7035
Technical service: 1-800-922-0075

Electronic Components and Circuits

Hardware, Techniques, and Processes

Header for Laser Diode

A package provides for focusing and aiming.

Goddard Space Flight Center, Greenbelt, Maryland

A header has been designed to contain a laser diode, the output of which is to be combined incoherently with the outputs of other laser diodes in a grating laser-beam combiner in an optical communication system. The header is a package that provides the electrical connections to the laser diode, cooling to thermally stabilize the laser operation, and optomechanical adjustments that steer and focus the laser beam. The range of adjustments provides for correction of the worst-case decentering and defocusing of the laser beam typically encountered with laser diodes.

The mechanical configuration of the header is made relatively simple to promote stability and keep the cost low. The cost is also kept down by the use of commercially available lenses. The number of lenses is made as small as possible, consistent with the needed adjustments, to keep reflection losses low. The only major disadvantage of these design choices is that alignment has to be performed manually in a process that can be tedious and time-consuming.

The header includes a two-piece cylinder, 0.75 in. (19.05 mm) in diameter, consisting of the diode housing and the optical-assembly housing (see figure). The laser diode is held in the diode housing by a threaded retainer ring, which presses down on the flange of the diode package. Three 0-80 screws (not shown) protrude radially outward from the diode housing. These serve as a diode-centering adjustment, providing a worst-case diode decenter of 12.7 μm. They are removed once the diode is centered and the diode-retaining ring is tightened. The optical-assembly housing holds the entire optical system, which consists of the coarse collimator, the fine-focus system, and the vernier steering system.

The coarse collimator (4.7-mm focal length) is positioned so that when the diode and optical-assembly housings are screwed together, it collimates the output of the laser diode. The degree of collimation is determined by the accuracy of the diode-to-collimator separation, which is set by shim-stock spacers to obtain a despacing accuracy of 12.7 μm. The worst-case despacing of 12.7 μm results in an excess divergence of 0.6 mrad. The fine-focus system is used to eliminate this excess divergence.

The fine-focus system consists of two lenses, one planoconcave (focal length −10 cm) and one planoconvex (focal length +10 cm). When the lenses are butted together, the fine-focus system has no optical power, but as the lenses are moved apart, their optical power increases. A separation range of 6.0 mm corrects for the excess divergence. Separation, again, is effected with shim stock spacers, with a worst-case despacing of 12.7 μm. Because the focal lengths of the fine-focus elements are 21 times that of the coarse collimator, the fine-focus system is much less sensitive to spacing errors. The worst-case spacing error of 12.7 μm results in a defocus of 20 μrad, which is less than 10 percent of the diffraction limit and is considered acceptable.

The worst-case decentering of the laser diode, 12.7 μm, corresponds to a beam-steering error of ~2.5 mrad, and, therefore, a vernier pointing lens is included to correct for this. This lens, which has a diameter of 7 mm and a focal length of 1 m, is mounted in a pair of nested eccentrics, which provide ±2.5 mm of lateral movement in any direction. Once the desired alignment is achieved, all optical elements are locked in place with the threaded retaining rings.

This work was done by Jonathan A. R. Rall and Paul L. Spadin of **Goddard Space Flight Center**. *For further information, Circle 73 on the TSP Request Card.*
GSC-13234

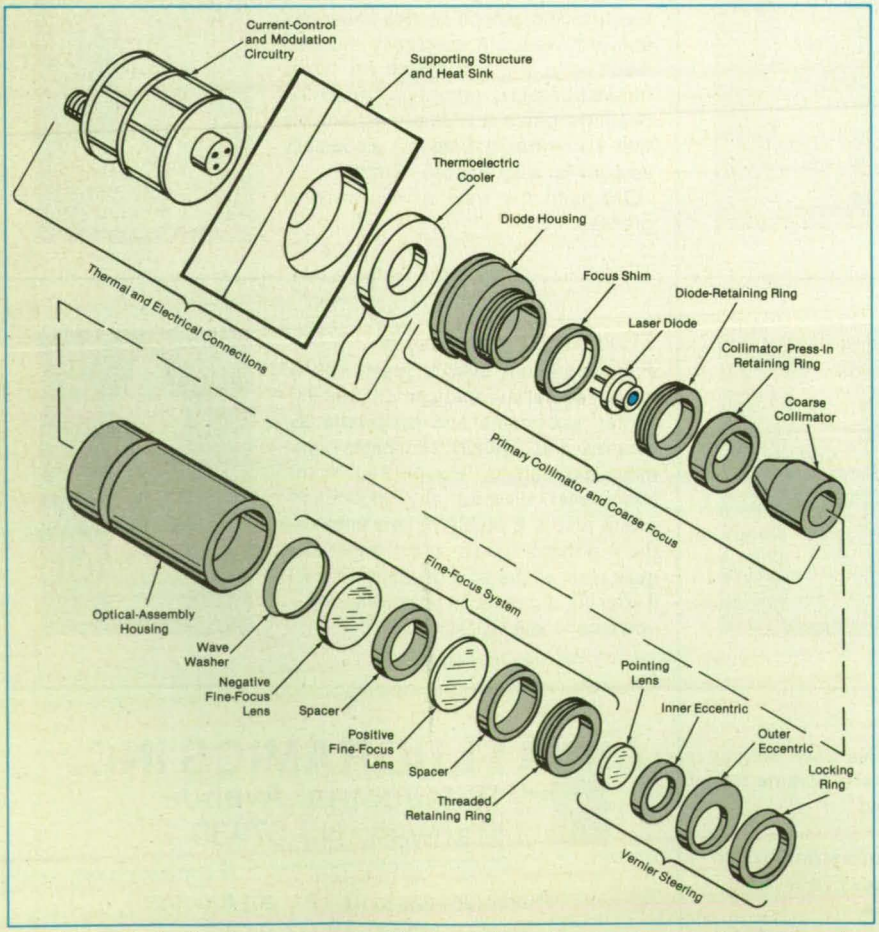

The **Laser-Diode Header** provides electrical and thermal connections to the diode and optomechanical adjustments to focus and aim the laser beam.

Quantized-"Gray-Scale" Electronic Synapses

Parallel resistors at each node would be switched to adjust conductive strength.

NASA's Jet Propulsion Laboratory, Pasadena, California

A proposed array of programmable synaptic connections for electronic neural network applications offers multiple quantized levels of connection strength using only simple, two-terminal, binary microswitch devices. Such simple device structures promise implementations of quantized-"gray-scale" synaptic arrays with very high density. Synaptic arrays for electronic neural networks have been fabricated in the past, using programmable binary (on/of) microswitches and passive thin-film resistor elements with equal connection strengths at all nodes, useful for content-addressable, high-density associative memories. However, multivalued, gray-scale synaptic connection strengths are required for neural network architectures with capabilities that involve higher-level learning and adaptability to solve ill-posed problems.

The basic structure of this quantized gray-scale synaptic array resembles a programmable binary synaptic grid with resistive connections at the intersections of row and column conductors. However, in this case, several adjoining rows and columns of the grid are connected in parallel externally, to form "subgrids" of chosen size. Thus, each subgrid constitutes several row/column intersections of a finer grid and forms one synaptic node with programmable multivalued connection strength (see figure).

Within each subgrid, the individual microswitches associated with their respective resistive connections at the nodes of the finer grid can be turned on in various combinations to obtain discrete synaptic strengths. The parallel external connections create sets of parallel resistors. Thus the conductance of each internal connection of the subgrid adds to the total conductance (connection strength) of the node represented by the subgrid. The scheme can, of course, be applied to an array of synapses with analog strengths to extend their range.

The design of a subgrid and the achievable conductance values depend predominantly on the conductance of individual elements and precision in their values. For example, in a subgrid of n elements with equal conductance values, it is possible to obtain either zero conductance or any integral multiple of the unit conductance from 1 to n. Further, if different conductance values (e.g., a binary string of values proportional to 1, 2, 4, 8...) are provided in a subgrid, then the maximum achievable number of subgrid conductances is 2^n.

The practical number and sizes of conductance increments are, however, restricted by the need to avoid overlap of conductance levels due to the limitations in the achievable resistor precision. For example, with ±3-percent precision, an array is limited to 16 distinct conductance levels (in addition to zero), even with subgrids larger than 16 nodes. Programmable,

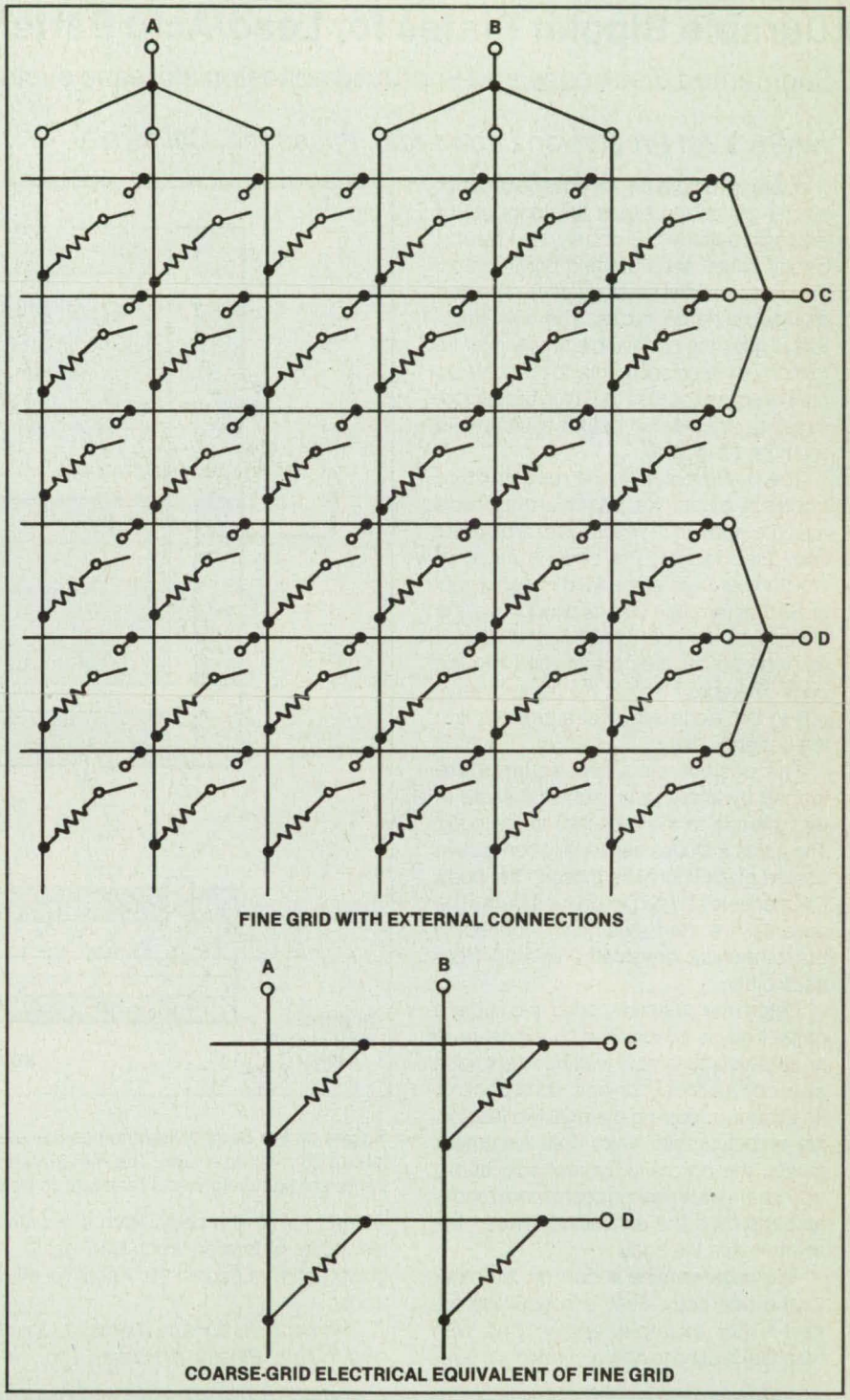

Subgrids in a Fine Grid of programmable resistive connections would be connected externally in parallel to form a coarser synaptic grid. By selection of the pattern of connections in each subgrid, the connection strength of the synaptic node represented by that subgrid would be set at a quantized "gray level."

40-by-40 binary synaptic arrays have been fabricated with an identical connection strength at each node of one megohm resistances having a precision of ±3-percent and can thus provide a 4-bit gray scale with this scheme. The extra "real estimate" occupied by the binary elements to provide for a gray scale in such an array is more than compensated by the overall structural simplicity and the potential high density.

This work was done by James L. Lamb, Taher Daud, and Anilkumar P. Thakoor of Caltech for **NASA's Jet Propulsion Laboratory**. *For further information, Circle 155 on the TSP Request Card.*
NPO-17579

Durable Bipolar Plates for Lead/Acid Batteries

Segmented electrodes and improved adhesion increase cycle life.

NASA's Jet Propulsion Laboratory, Pasadena, California

A new structure for the positive faces of bipolar plates increases the longevity of lead/acid batteries. Ordinarily, the layers in bipolar plates separate and positive-electrode material flakes away after repeated charge/discharge cycles. The new structure divides the positive-electrode layer into many isolated segments so that defects cannot spread across the layer. In addition, surfaces are treated before assembly to promote adhesion.

The positive plate in the new structure consists of tilelike positive-electrode squares arrayed in recesses in a platelike body (see figure). The body is made of woven fiberglass embedded in epoxy resin. So that the plate body is conductive, the glass fibers are coated with fluoride-doped tin oxide before they are molded into the body. The epoxy makes the plate impervious to the electrolyte that surrounds it in the battery.

The positive-electrode squares are formed by applying an aqueous paste of lead dioxide to the recesses in the body. The paste includes electrically-conductive coated glass fibers like those in the body. The paste is allowed to dry and cure. The squares are then electrically connected but otherwise physically isolated from each other.

Before the paste is applied, the surface of the body is conditioned by exposure to an oxidizing plasma, a wetting agent such as a conventional nonionic surfactant, or an aqueous coupling material like lead oxide in polyacrylic acid. This treatment makes the normally hydrophobic epoxy accept the water-based paste more readily and improves the adhesion between the squares and the body.

The negative side is built on the other face of the body. First, a conductive adhesive (for example, epoxy filled with graphite) is used to hold a conductive layer of lead foil on the body. Then a negative electrode is formed from lead paste. A glass scrim supports the negative electrode.

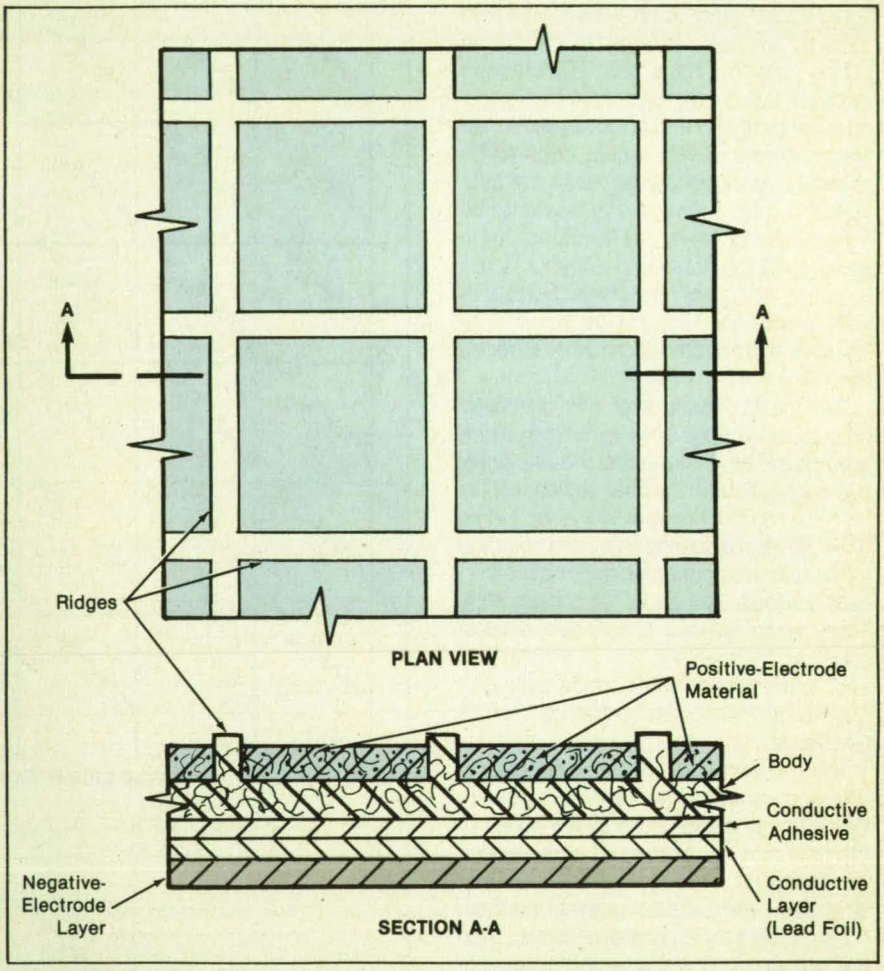

Ridges on the Body divide the positive electrode into isolated squares, each typically 1 in. (about 25 mm) on a side. The materials that support the electrochemically active components are lightweight and resistant to acid.

This work was done by Thomas J. Clough and Naum Pinsky of Ensci, Inc., for **NASA's Jet Propulsion Laboratory**. *For further information, Circle 43 on the TSP Request Card.*
NPO-17662

Interferometric Fiber-Optic Gyroscope

An integrated three-waveguide directional coupler functions as a polarizer and splitter.

NASA's Jet Propulsion Laboratory, Pasadena, California

A fiber-optic gyroscope (see Figure 1) incorporates a novel three-waveguide directional coupler that functions both as a polarizer and as a splitter. The coupler is intended for eventual fabrication as in a mass-producible integrated optical circuit that would

THE WAVE OF THE FUTURE

Rise above any waveform measurement challenge with the new Nicolet System 500.

It's the most powerful and flexible digital waveform acquisition system available. With more channels. More speed. More memory. Greater resolution. And in the optimum configuration, starting as low as $1,645 per channel.

Available in portable or rack mount, this premier *turnkey* system features:

Independent digitizer boards with maximum sampling rates of up to 10 MS/s.

Multichannel flexibility. Whether it's two or 200 channels, the 500 can handle it.

Local processing. Lightning-fast on board calculation capabilities save you time.

And . . . *Instant start-up.* The System 500 is ready to start working almost as soon as it's out of the box. Send now for free brochure.

Nicolet Test Instruments Division

5225 Verona Road, Madison, WI 53711-4495, 608/273-5008 or 800/356-3090

Circle Reader Action No. 696

Nicolet

INSTRUMENTS OF DISCOVERY

provide advantages including low drive voltage, large-bandwidth phase modulation, preservation of polarization in transmission between the devices on the same substrate, and low cost.

The design of the new coupler avoids a deficiency noted in the "Y-tap" configuration tried in an earlier multifunction circuit. In that configuration, when the front-end splitter was fabricated in a single integrated optical circuit, power radiating from one tap recoupled into the other tap.

The source of light for the gyroscope is a superluminescent laser diode that has a middle wavelength of 1,300 nm and a bandwidth of 20 nm. An output of 130 μW of output from the diode is coupled into a single-mode optical-fiber "pigtail" connected to one port of a 3-dB polished fiber coupler. An InGaAs positive/intrinsic/negative field-effect-transistor detector is connected to another port of the coupler. Yet another port of the coupler is connected to the integrated optical substrate, and the fourth port is connected to a power-monitoring detector (not shown). The polished fiber coupler is made from the polarization-maintaining fiber. The coupler has polarization cross coupling of less than -18 dB for all ports and has a 0.9 dB insertion loss.

The integrated circuit consists of the three-waveguide directional coupler with a phase modulator on one of the waveguides. The coupler is designed with transverse electric (TE) polarization in the bar state (two coupling lengths) and transverse magnetic (TM) polarization in the cross state (one coupling length). The TM light entering the middle waveguide splits into the outer guides, which are connected to the sensing coil of the gyroscope. The integrated circuit is fabricated in Z-cut, Y-propagating lithium niobate, by diffusing titantium and indium into the $LiNbO_3$ substrate to make a waveguide structure for single-mode operation. A 2,000-Å-thick SiO_2 buffer layer deposited from chemical vapor prevents TM loading of the aluminum electrodes. When used passively in the gyroscope, the integrated circuit has a polarization extinction ratio of 20 dB and a TM splitting ratio of 1.01.

The sensing coil of the gyroscope is 16 cm in diameter and quadrupole-wound with 884 m of polarization-maintaining fiber. The coil has a polarization extinction ratio of 8.6 dB (compared to 19 dB when loosely wound) and a loss of 1.0 dB. During open-loop testing without phase modulation and with no rotation, the power reaching the detector is 0.18 μW. The total loss in the system is 26.6 dB; 7.8 dB due to the round trip through the fiber coil, and 18.8 dB due to the two passes through the integrated optical circuit.

Nonoptimum coupling of the TM mode in the polarizer/splitter contributes 3.2 dB of the 9.4 dB total loss per pass through the integrated optical circuit. The remaining 6.2 dB of insertion loss is due to coupling between the fibers. To reduce the 4-percent Fresnel reflections at the interfaces between the fibers and the lithium niobate, the interfaces are angled. However, the angling increases the coupling loss from 1.1 dB to 3.1 dB per interface.

Figure 2 shows the data obtained when the gyroscope was used to detect the rotation of the Earth with the axis of the coil held horizontally at a latitude of 40°38′. The phase modulator was driven by a ± 4.5 V square wave to produce a $\pm 90°$ phase shift at the coil eigenfrequency of 115 kHz. The gyroscope exhibited a phase noise of 0.63(°/h)/Hz$^{1/2}$ with a lock-in amplifier time

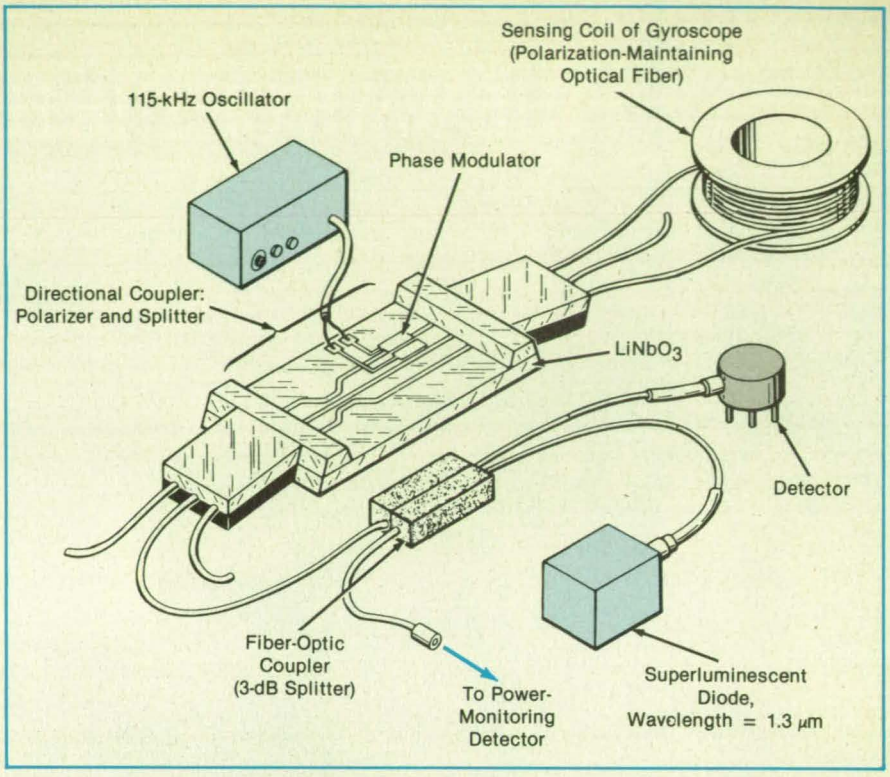

Figure 1. The **Interferometric Fiber-Optic Gyroscope** includes a combined polarizer and splitter that can be implemented as a single integrated optical circuit.

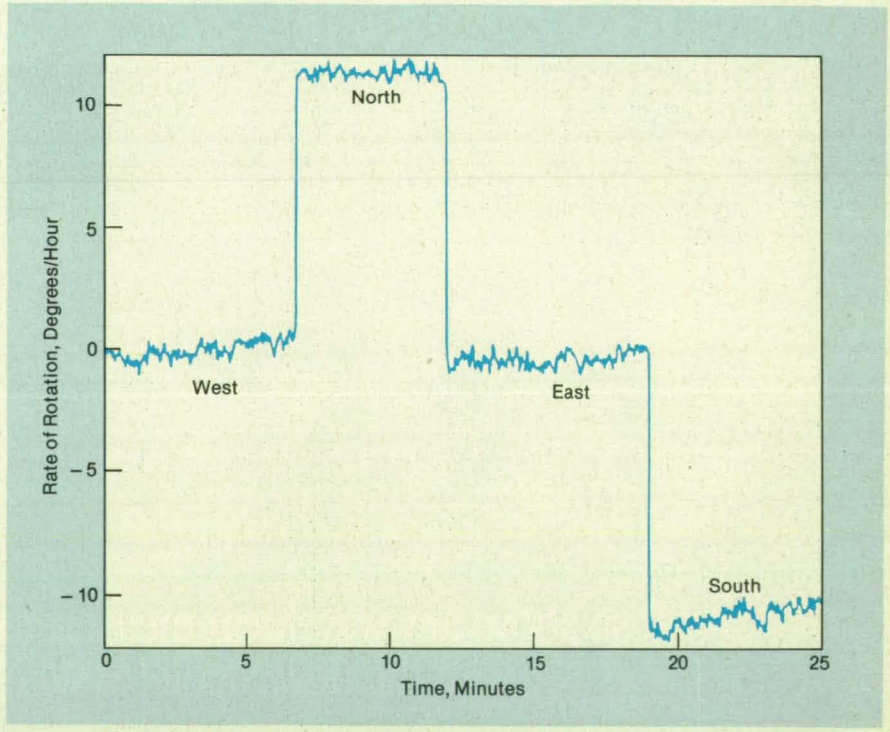

Figure 2. The **Fiber-Optic Gyroscope Detects** the 11.4°/h horizontal component of the Earth's rotational velocity at Allentown, PA. (latitude 40° 38′). The graph shows the output of the gyroscope with the axis of the sensing coil pointing in the indicated directions.

TEAM WORK

PUBLICIS ZB-A2

ARIANE PUTS SATELLITES INTO SPACE THAT SPEAK 27 LANGUAGES. As industrial architect Aerospatiale cooperates with 11 European countries providing space-age technology and management skills. With the number of satellites launched for american companies, we prove our capability of working together. And Aerospatiale has built more than 40 technically diversified satellites, many of them with american partners. Working and creating together keeps us up there. Meet the team.

aerospatiale

AEROSPATIALE INC. 1101. 15TH STREET N.W WASHINGTON DC 20005
PHONE: 202 293 0650

constant of 1.0 s and a 12-dB/octave rolloff. This corresponds to a random walk of 0.011 °/h$^{1/2}$, which is within a factor of 3 of the shot noise limit, 0.0042 °/h$^{1/2}$.

This work was done by Ramon P. DePaula of Caltech and Gail A. Bogert and William J. Minford of AT&T Bell Laboratories for **NASA's Jet Propulsion Laboratory**. *For further information, Circle 18 on the TSP Request Card.*
NPO-17515

Upper-Bound Estimates of SEU in CMOS

Limited experimental information can be used to make conservative design estimates.

NASA's Jet Propulsion Laboratory, Pasadena, California

The theory of single-event upsets (SEU) (changes in logic state caused by energetic charged subatomic particles) in complementary metal oxide/semiconductor (CMOS) logic devices has been extended to provide upper-bound estimates of rates of SEU when limited experimental information is available and the configuration and dimensions of SEU-sensitive regions of devices are unknown. The method of estimation is based partly on the chord-length-distribution method, which is a popular method for SEU calculations, and in which the configurations and dimensions of devices are normally required.

The method requires experimental data on the normal incident SEU cross section as a function of linear energy transfer (LET). The method involves the partition of the device into an arbitrary number of assumed parallelepiped-shaped sensitive regions, which may or may not represent the real (but unknown) sensitive regions of the device.

The cross sections and the threshold LET's of the assumed sensitive regions are adjusted to obtain a composite, stepped cross-section-vs.-LET curve that bounds the experimental curve (see figure). During this curve-bounding process, the depths and length-to-width ratios of the parallelepipeds are adjusted to obtain maximum rates of upset. Several theorems regarding this process have been proved to justify the principal statement of the method regarding estimation, which is simply that the rate of upset of the hypothetical device composed of the parallelepipeds is an upper bound on the rate of upset of the real device.

The fundamental conclusion of the theorems is that when length-to-width ratios and depths are varied to produce a maximum upset rate, the rate for any collection of parallelepipeds (all having the same threshold LET) is proportional to the total area. It is shown that this implies that the same upper bound estimate (constructed from an experimental cross-section-versus-LET curve) can be applied whether the device contains a few large sensitive regions or many small identical or nonidentical regions. This "invariance" of upset rate per area implies that it is possible to construct an effective flux (which is defined to be the upper bound upset rate per area) versus LET curve (one curve for each environment) such that the same curve can be used to produce upper bound upset rate estimates for any parallelepiped-shaped region or any collection of such regions in an isotropic environment.

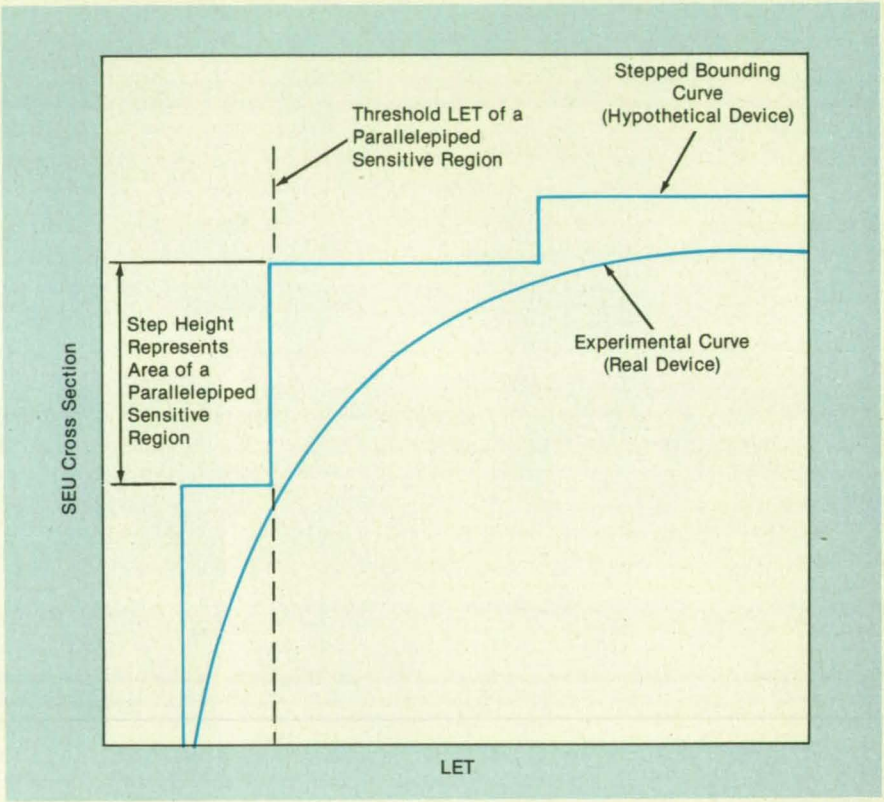

The **Stepped Curve** is a theoretical curve. Each step represents a sensitive region in a hypothetical device. Under appropriate conditions, upset rates for the hypothetical device are upper bounds on the rate for the real device.

The validity of this upper-bound estimate depends on the following conditions:

- The experimental data represent the device with adequate accuracy for the conditions that will apply (e.g., temperature, total dose degradation).
- The component of the ionizing radiation in question is sufficiently energetic so that the LET does not vary appreciably along the chord through the device and, therefore, the chord-length-distribution method can be applied.
- Delayed charges are unimportant compared to prompt charges.
- The sensitive regions can be treated as having well-defined shapes (i.e., the effects of funneling can be approximated by assuming some appropriate effective shape for each sensitive region), and for each region the shape can be adequately approximated as a parallelepiped.
- The sensitive regions are independent of each other, and each can be characterized by a well-defined critical charge for SEU.
- Every SEU in the device can be attributed to the liberation of charge in excess of the critical charge in one of the sensitive regions.

Most of these conditions are required whenever the chord-length-distribution method is used. The popularity of the chord-length-distribution method suggests that the conditions are approximately satisfied when CMOS devices are exposed to cosmic rays.

This work was done by Larry D. Edmonds of Caltech for **NASA's Jet Propulsion Laboratory**. *For further information, Circle 59 on the TSP Request Card.*
NPO-17566

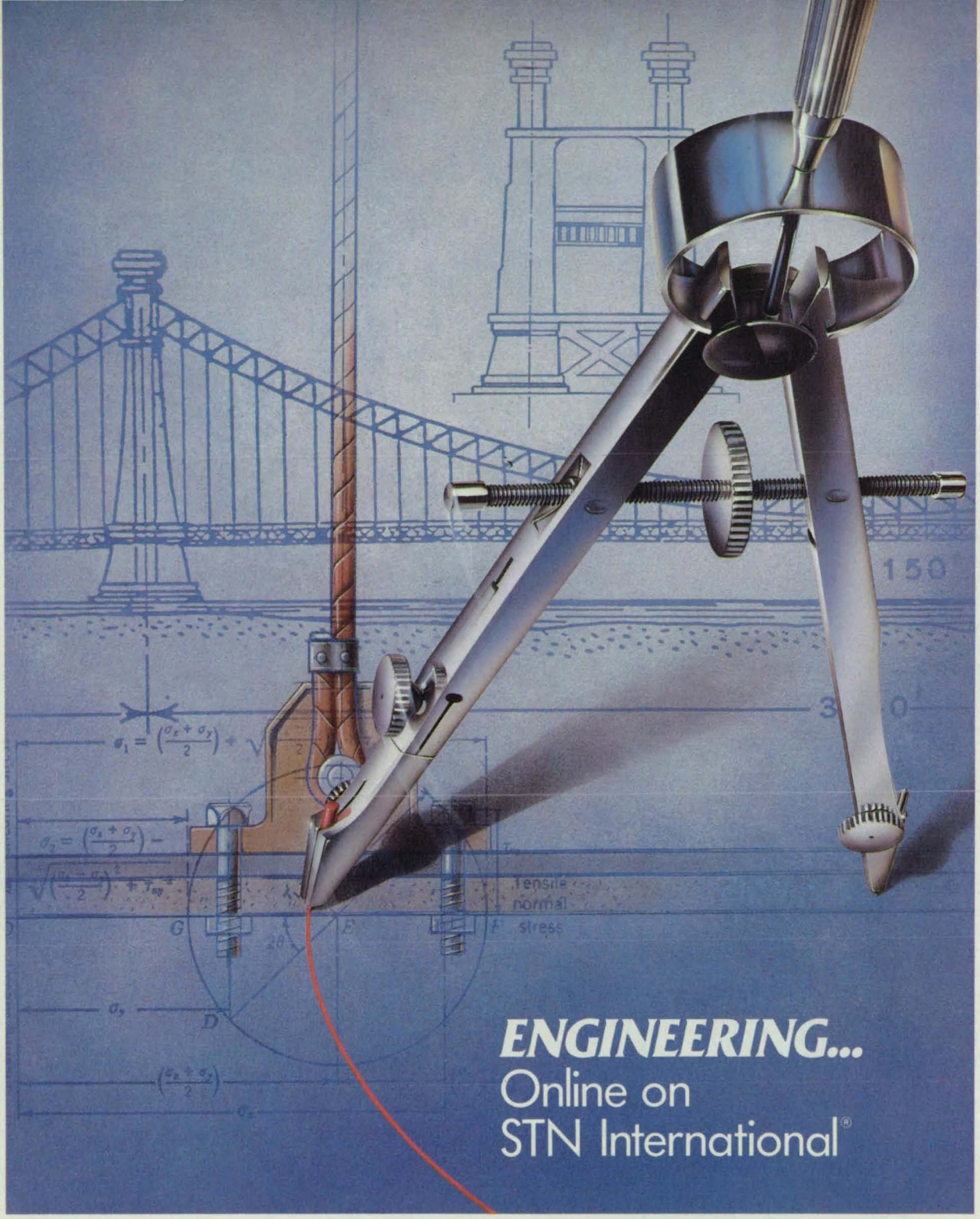

For more information about STN International, write or call: STN International, Marketing, Dept. 30689, P.O. Box 02228, Columbus, OH 43202. Phone 800-848-6538

STN International is operated in North America by Chemical Abstracts Service, a division of the American Chemical Society; in Europe, by FIZ Karlsruhe; and in Japan, by JICST, the Japan Information Center of Science and Technology.

Circle Reader Action No. 464

Forward Bias Inhibits Single-Event Upsets

Bipolar integrated circuits are made more resistant to ionizing radiation.

NASA's Jet Propulsion Laboratory, Pasadena, California

Tests show that the resistance of a bipolar integrated logic or memory circuit to single-event upsets can be increased by imparting forward bias to the diode constituted by the buried layer of the substrate and the collector. The susceptibility of the conventional design to single-event upsets is illustrated in Figure 1. The buried-layer/substrate diode is reverse-biased to prevent the leakage of current between adjacent transistors. Because of this reverse bias, an energetic ion that penetrates the buried layer can cause the collection of charge at the buried-layer/substrate junction. Schematically, this is represented as a pulse of current $I_S(t)$ in the buried-layer/substrate diode D_S.

An integrated-circuit chip containing four random-access memory cells (also shown schematically in Figure 1) was built to test its behavior under irradiation at various degrees of forward bias. Transistors T_1 and T_2 are for data storage. Diodes D_1 and D_2, which are formed by short circuiting the base and collector contacts of transistors, are used to read and write data in the memory cell. The lateral dimensions of three of the cells were 2, 4, and 10 times, respectively, those of the smallest cell. The cells were laid out at the corners of the chip, away from each other, so that they would not interfere with each other when the buried-layer/substrate diodes were forward-biased.

During the tests, each of the cells was powered with a cell current of 50 μA during irradiation by 150-MeV iron ions. As the bias on the buried-layer/substrate diode was varied from full reverse (−10 V) to slightly forward (+0.1 V), the single-event-upset cross section of the largest cell decreased by a factor of about 1,000 (see Figure 2). The cross section began to increase again as the forward bias rose to 0.2 V because the logic-voltage margin decreased with the increase in forward bias.

The single-event-upset cross sections of

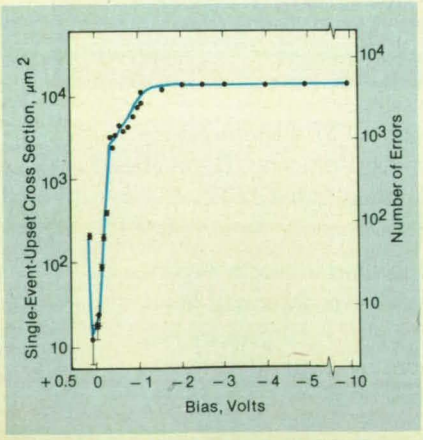

Figure 2. The **Single-Event-Upset Cross Section** of the largest test cell decreases dramatically as the bias changes from −10 V to +0.1 V.

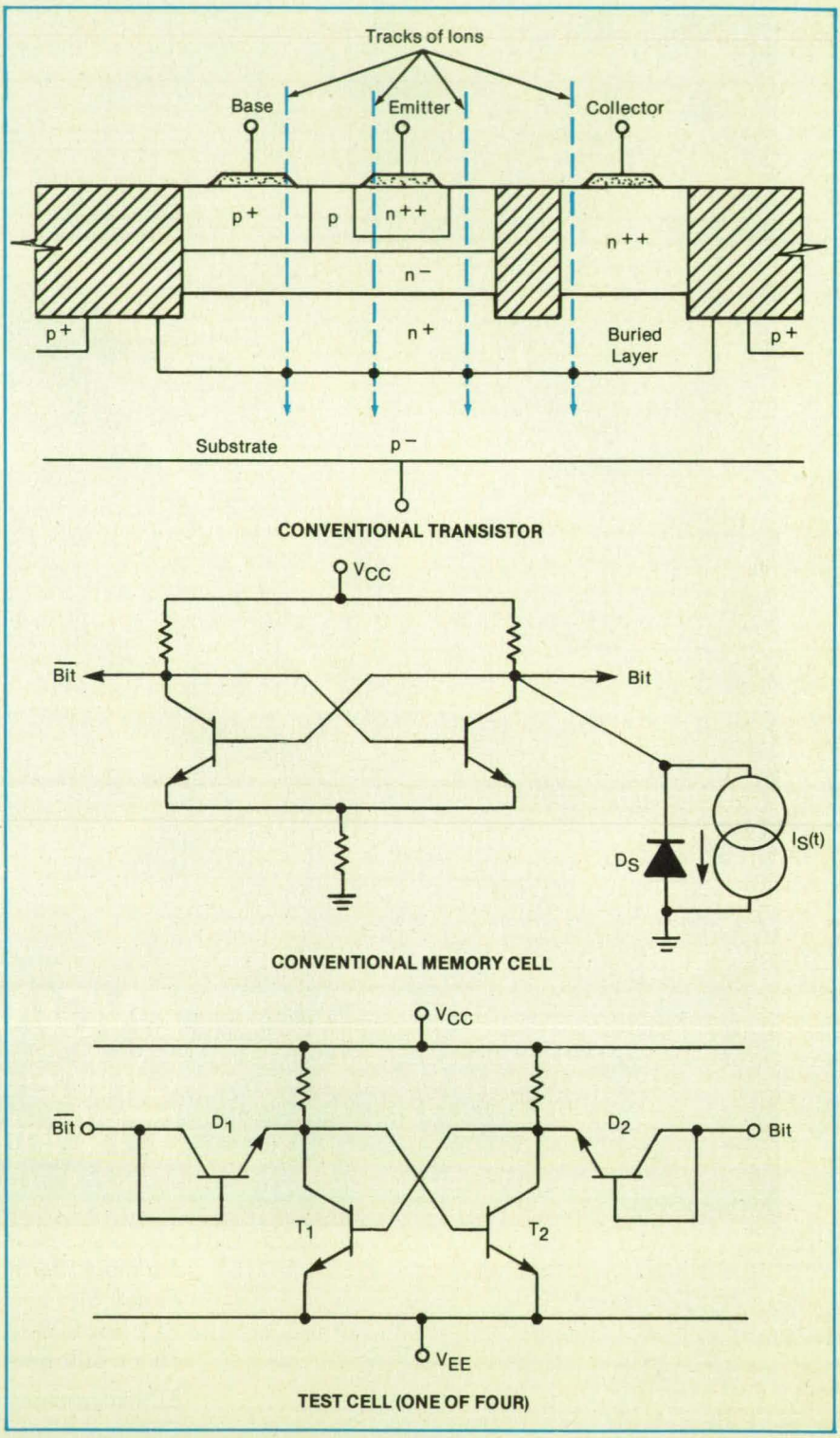

Figure 1. The **Conventional Silicon Bipolar Integrated-Circuit Transistor**, as part of a memory cell, is vulnerable to single-event upsets caused by energetic ions that penetrate through the buried layer into the substrate. The test cells provide for the application of forward bias to the buried-layer/substrate diodes of the transistors in these cells to reduce the susceptibility of these cells to single-event upsets.

After centuries of practice, mankind perfects engineering calculations: MathCAD.

Announcing MathCAD 2.5: The Dawn of a New Age.

What the historians will call it, only time will tell.

Perhaps the Century of Speed, or the Era of Ease. But whatever the name, this is the age of MathCAD 2.5, the only math package that looks and works the way you think.

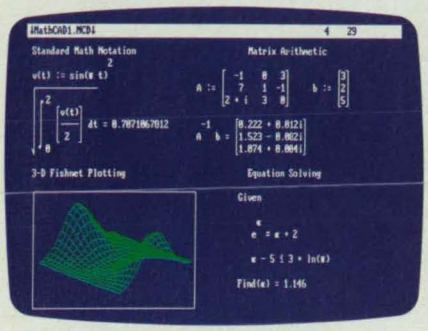

MathCAD 2.5 includes 3-D plotting, HPGL sketch import, and PostScript output.

MathCAD is far and away the best-selling math package in the world. Because it lets you perform engineering and scientific calculations in a way that's faster, more natural and less error-prone than the way you're doing them now—whether you're using a scratchpad, calculator, spreadsheet or program that you wrote yourself.

And now we've made the best even better. MathCAD 2.5 is a dramatically improved version that includes three-dimensional plotting, enhanced numerical analysis, and the ability to import HPGL files from most popular CAD programs, including AutoCAD.® And now you can print on PostScript® compatible printers.

And like before, MathCAD's live document interface™ lets you enter equations anywhere on the screen, add text to support your work, and graph the results. Then print your analysis in presentation-quality documents.

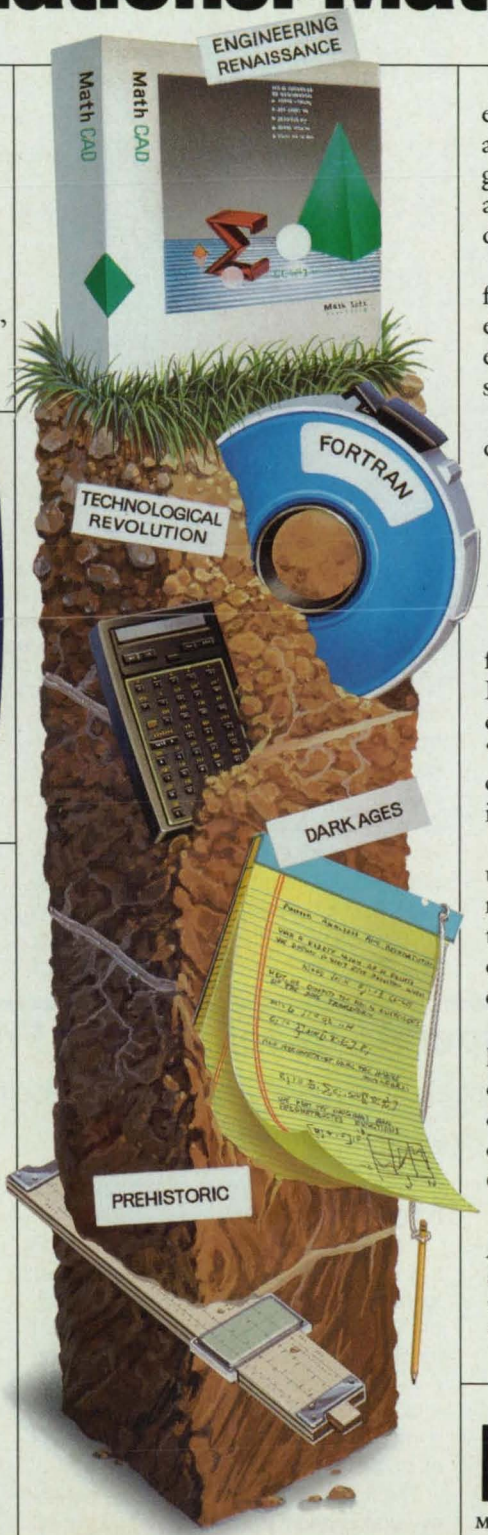

It has over 120 commonly used functions built right in, for handling equations and formulas, as well as exponentials, differentials, cubic splines, FFTs and matrices.

No matter what kind of math you do, MathCAD 2.5 has a solution for you. In fact, it's used by over 60,000 engineers and scientists, including electrical, industrial, and mechanical engineers, physicists, biologists, and economists.

But don't take our word for it; just ask the experts. PC Magazine recently described MathCAD as "everything you have ever dreamed of in a mathematical toolbox."

PC MAGAZINE EDITOR'S CHOICE
March 14, 1989 issue.
Best of '88
Best of '87

And for Macintosh® users, we present MathCAD 2.0, rewritten to take full advantage of the Macintosh interface. Entering operators and Greek letters into equations is pure simplicity!

Look for MathCAD 2.5 at your local software dealer, or give us a call. For more information, a free demo disk, or upgrade information, dial 1-800-MATHCAD (in MA, 617-577-1017).

Available for IBM® compatibles and Macintosh computers.

TM and ® signify manufacturer's trademark or manufacturer's registered trademark respectively.

MathCAD®

MathSoft, Inc. One Kendall Square, Cambridge, MA 02139

22

U.K.: Adept Scientific 0462-480055; **France:** ISE CEGOS 1-46092768; **Germany:** Softline 07802-4036; **Japan:** CRC 03-665-9768. *PE*

Circle Reader Action No. 682

the smaller cells were not decreased by forward bias. This was because the 50-μA operating current was chosen to suit the largest cell. The smaller cells should exhibit behavior similar to that of the largest cell when the proper current is applied.

This work was done by John A. Zoutendyk of Caltech for **NASA's Jet Propulsion Laboratory**. *For further information, Circle 55 on the TSP Request Card.*

This invention is owned by NASA, and a patent application has been filed. Inquiries concerning nonexclusive or exclusive license for its commercial development should be addressed to the Patent Counsel, NASA's Resident Office-JPL [see page 14]. Refer to NPO-17573

Exact Chord-Length Distribution for SEU Calculations

Computed rates of SEU's can now be more accurate.

NASA's Jet Propulsion Laboratory, Pasadena, California

The exact integral chord-length distribution has been derived for use in calculations of the rates of single-event upsets (SEU's) (changes in logic states) caused by the impingement of cosmic rays or other ionizing radiation on electronic logic circuits. The integral chord-length distribution $C(x)$ gives the fraction of all chords (representing paths of isotropically incident ionizing particles) through a rectangular parallelepiped that have length x or greater. The rectangular parallelepiped represents the SEU-sensitive volume of an electronic device. $C(x)$ is used in conjunction with the differential linear energy transfer (LET) spectrum of the ionizing radiation to calculate the rate of SEU in the device. One can also use the differential chord-length distribution with the integral LET spectrum.

The exact $C(x)$ is derived from Coleman's differential chord-length distribution $P\mu(x)$. The exact $C(x)$ is specified by a complicated set of equations that involve x and the dimensions a, b, and c of the parallelepiped. Each equation is applicable between certain limiting values of x that depend on the relative values of a, b, and c. The exact $C(x)$ has been used to evaluate other chord-length distributions — especially that of Bradford, which has been called "semi-exact" because it is exact only at $x \leqslant b$ (see figure).

In principle, it makes no difference whether one uses the integral chord-length distribution with the differential LET spectrum or the differential chord-length distribution with the integral LET spectrum to calculate the rate of SEU. It can be shown analytically that both yield the same result. However, each method has its advantages and disadvantages, depending on the available LET spectral data and computing capabilities. Now that the exact $C(x)$ has been found, one can choose the better of the two methods for the problem at hand without having to sacrifice accuracy in the calculated rate of SEU.

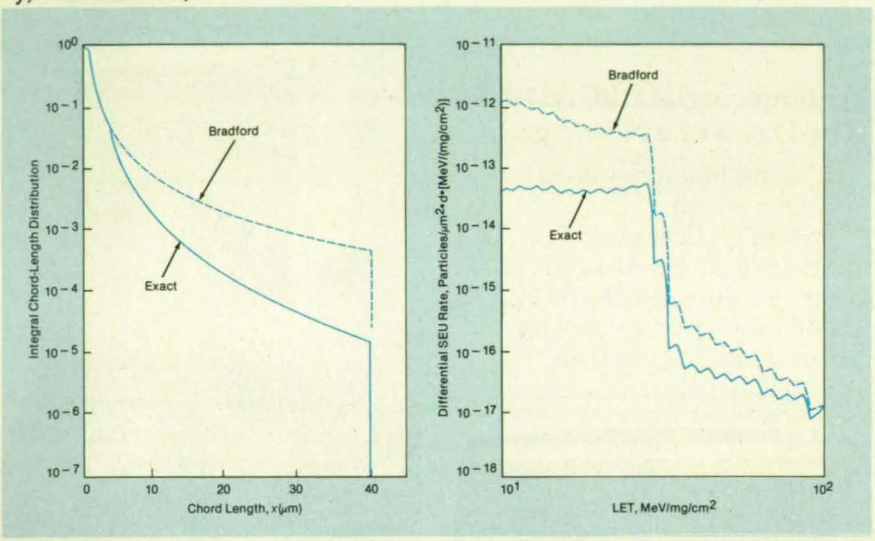

The **Integral Chord-Length Distribution C(x)** was calculated by the Bradford (semi-exact) equations and the exact equations for a parallelepiped of a = 1 μm, b = 4 μm, and c = 40 μm. The two distributions were used to calculate the differential SEU rate. The rates of SEU calculated with Bradford's equations are too high.

This work was done by Martin G. Buehler of Caltech and Keung L. Luke of California State University for **NASA's Jet Propulsion Laboratory**. *For further information, Circle 53 on the TSP Request Card. NPO-17657*

Crystal Oscillators Operate Beyond Rated Frequencies

Amplifiers with single-pole frequency responses are used in their "roll-off" regions.

Goddard Space Flight Center, Greenbelt, Maryland

A class of crystal oscillators is based on the use of negative-voltage-gain amplifiers at frequencies well into the "roll-off" frequency regions of their gain-versus-frequency curves. This defining characteristic helps keep the costs of these oscillators low in that it is not necessary to use the more expensive amplifiers that have flat frequency responses out to the desired operating frequencies. Operation in the "roll-off" region enables an amplifier to produce the phase shift necessary for oscillation, reducing the cost further by eliminating the need for some of the passive components that have to be included for this purpose in oscillators of more conventional design.

An oscillator of the new type can include a gate inverter operating as an amplifier (gate amplifier), an operational amplifier, or bipolar transistors. Several different feedback schemes are available to set the desired current and voltage biases and to enable the oscillator to operate at the fundamental frequency of the crystal or at one of its overtones.

The figure shows a fundamental-frequency version and two overtone versions, all containing gate amplifiers. In the fundamental-frequency version, the crystal is connected directly between the input and output terminals of the amplifier. A loading capacitor is connected between the input terminal and ground. A resistor between the input and output terminals is chosen to bias the input and output of the amplifier at about half the supply voltage. This arrangement makes the gate amplifier operate as a nearly linear amplifier (rather than as the on/off switch that it is nominally designed to be) so that the circuit can oscillate. The crystal exhibits inductive reactance when operating at its fundamental frequency. The combination of the crystal and the specified loading capacitance constitutes a resonant circuit at this frequency.

The first overtone version is similar to

or the ough jobs hey call Motorola.

e transmitting photo
a from Neptune after
years in space. Or
eband processors for
vanced Communications
chnology Satellites.
transmitting scientific
d photo data during
gellan's Venus Radar
pping Mission.

UGH JOBS
CAN DO FOR YOU.

ace Comm. Systems
equency Sources
&C Subsystems
/WB Microwave Comm.
/WB Secure Comm.
wer Converters
LS User Transponders
ep-Space Transponders
RSS User Transponders
LS User Transponders
ar-Earth Transponders
S User Receivers
gh-Data-Rate Modems
seband Processors
aceborne Radars
ace Station Comms.
ound Support Equipment

ll the pioneers
space communications
2/732-3015 or write to
x 2606, Scottsdale,
Z 85252.

MOTOROLA INC.
Government Electronics Group

the fundamental-frequency version except that an additional capacitor is inserted in series with the crystal. This capacitor is selected so that at the fundamental frequency of the crystal, the reactance of the branch appears capacitive. Thus, the capacitor prevents oscillation at the fundamental frequency. At the overtone frequency, the reactance of the capacitor is sufficiently small that the inductive reactance of the crystal predominates in the series combination and interacts with the loading capacitor to form a resonant circuit. Thus, the circuit can oscillate at the overtone frequency, even though it cannot oscillate at the fundamental frequency.

The second overtone version is similar to the fundamental-frequency version except that the value of the resistor is made much smaller. In this case, the component of inductive admittance due to the resistor is greater than the admittance of the loading capacitor at the fundamental frequency, thereby preventing oscillation at the fundamental frequency. On the other hand, the inductive admittance at the overtone is less than the admittance of the loading capacitor, enabling oscillation to take place at the overtone.

This work was done by Leonard L. Kleinberg of **Goddard Space Flight Center**. *For further information, Circle 7 on the TSP Request Card.*

This invention is owned by NASA, and a patent application has been filed. Inquiries concerning nonexclusive or exclusive license for its commercial development should be addressed to the Patent Counsel, Goddard Space Flight Center [see page 14]. Refer to GSC-13171

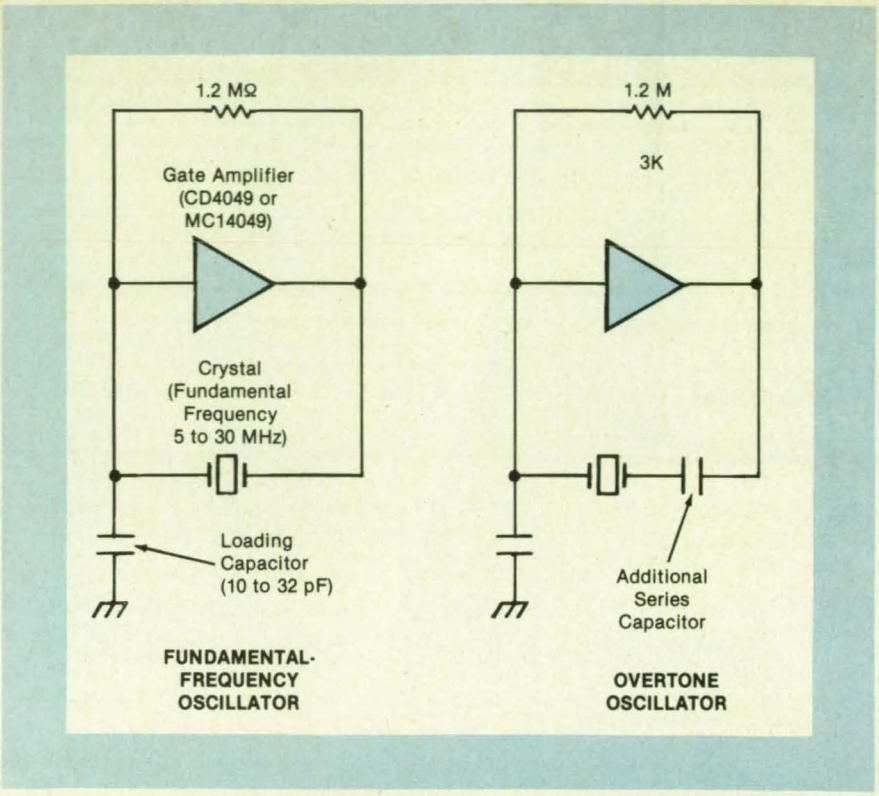

A **Fundamental-Frequency Oscillator and an Overtone Oscillator** are representative of the new type of crystal oscillator, which operates at a frequency well above the corner ("3-dB") frequency of the gain-versus-frequency curve of the amplifier. The values and type numbers of the components are given for example only: others can be used. The dashed lines indicate the second overtone version.

Thermal-Interaction Matrix for Resistive Test Structure

A simple linear model predicts small increases in temperature.

NASA's Jet Propulsion Laboratory, Pasadena, California

A linear mathematical model predicts the increase in temperature in each segment of a 15-segment resistive structure that is used to test electromigration. The assumption of linearity is based on the fact that the equations that govern the flow of heat are linear and that the coefficients in these equations (heat conductivities and capacities) depend only weakly on temperature and can, therefore, be considered constant over a limited range of temperature.

During a test, the structure is held in a chuck of known constant temperature and stressed by the application of known currents. The current through and voltage across each segment is measured and recorded as a function of time to monitor the drift in the resistance of each segment. The power P_j dissipated in each segment can be calculated from the measured current and voltage. Then the linear model predicts that, provided that currents, voltages, and temperatures change slowly, the temperature T_i of the ith segment is given by

$$T_i = \sum_{j=1}^{n} A_{ij} P_j + T_c$$

where n = the number of segments (in this case, 15), the coefficients A_{ij} constitute the thermal-interaction matrix, and T_c = the temperature of the chuck. The elements of the matrix have the dimensions of thermal resistance (temperature ÷ power).

The table shows two examples of the application of this technique. In the first example, current at a density of 2.2 MA/cm^2 was forced through all 15 segments of the test structure. In the second example, the current was forced through all segments except the eighth and ninth. The predictions of the linear model were within 1 K of the temperature determined by a resistance calibration procedure.

Example 1: All Segments Turned On															
Segments	1	2	3	4	5	6	7	8	9	10	11	12	13	14	15
A	181	184	186	188	188	190	190	189	191	189	189	189	187	185	183
B	182	185	187	188	189	189	190	190	190	189	189	188	187	186	184
Example 2: All Segments Except 8 and 9 (Simulating Two Adjacent Failed Segments) Turned On															
Segments	1	2	3	4	5	6	7	8	9	10	11	12	13	14	15
A	180	182	184	185	185	185	184			184	185	185	185	183	182
B	181	183	184	185	185	185	184			184	185	185	184	183	181

The **Temperatures of the Segments** in °C were determined by the linear model with the thermal-interaction matrix (A) and by a resistance calibration (B).

This work was done by Martin G. Buehler, Jaipal K. Dhiman, and Nasser Zamani of Caltech for **NASA's Jet Propulsion Laboratory**. *For further information, Circle 92 on the TSP Request Card.*
NPO-17673

TEAC.
BECAUSE IT TAKES ALL KINDS.

If you need to measure the bumps, the shakes, the beats, the pressure, or the heat, TEAC makes a data recorder in the right size and format to meet your needs. In fact, we make so many different kinds of data recorders you almost need a data recorder to keep track of them all.

We made the first, and we offer the most extensive line of VHS data recorders. For ease of operation, economy, and convenience of media, the VHS format is the best.

We make the world's smallest 9-channel portable Philips cassette data recorder.

And we make a comprehensive line of reel-to-reel data recorders with extended recording times and up to 28 channels available.

We offer the widest selection of cassette data recorders from 1- to 9-channel models, from pocket-sized to sturdy laboratory and field systems.

Our new portable data recorders incorporating DAT technology are the leading edge in instrumentation recorders.

If you can't find the data recorder in the format you need from TEAC, then it doesn't exist.

And if it doesn't exist it's because TEAC hasn't built it yet.

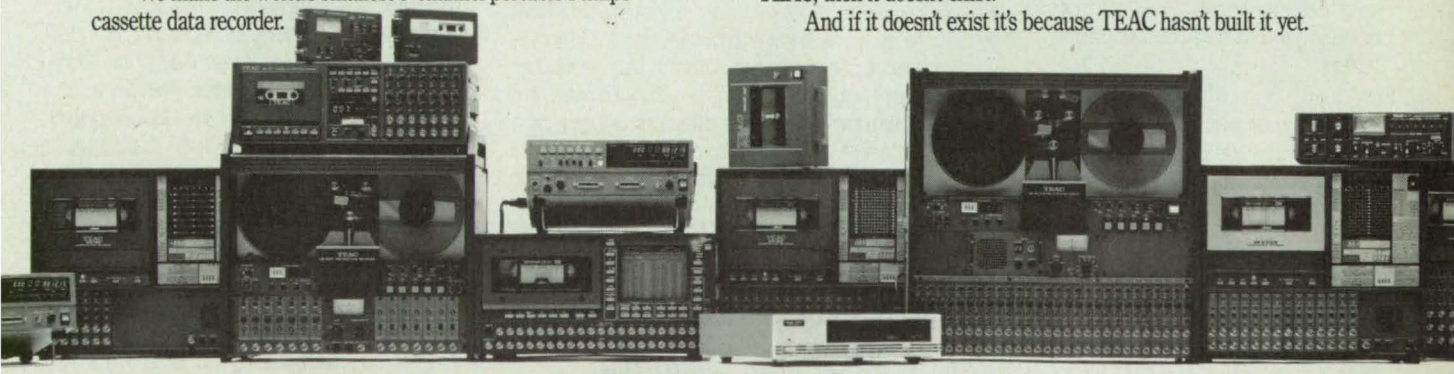

TEAC®

Instrumentation Data Recorder Division.

Circle Reader Action No. 344

Electronic Systems

Noise-Contamination Detector

Deviations in periods of output from a tracking filter are measured.

Marshall Space Flight Center, Alabama

A signal-analyzing system measures the degree to which a sinusoid is contaminated by noise. The system was developed to measure noise in the outputs of vibration sensors used to test bearings and other components of rotating machinery. Noise can indicate faulty bearings or faulty test equipment.

The signal from the sensor is fed through a tracking band-pass filter to a zero-crossing detector (see figure). The dither module, which is the remainder of the system following the zero-crossing detector, measures the deviations in the periods of the signal between the zero crossings. In particular, it computes the average of the absolute values

$$|\Delta T_i| = |T_{i+1} - T_i|$$

of the differences between consecutive periods of the signal. It then divides this average by the average period T to obtain A_d, the average fractional dither.

It has been found that A_d is related to the root-mean-square (rms) white-noise component N in the signal and to the rms value M of the signal (including sinusoid and noise) by the equation $kA_d = N/M$, where k is a constant of proportionality that must be determined for the equipment in question. From the fundamental properties of the sinusoid and the noise, $M^2 = N^2 + S^2$, where S = the rms amplitude of the sinusoid. Substituting $N = MkA_d$ from the first equation into the second equation, one obtains

$$S = M[1 - (kA_d)^2]^{1/2}$$

Thus, one can also use the fractional dither measured by the system and the rms amplitude of the noisy signal to estimate the rms amplitude of the sinusoid.

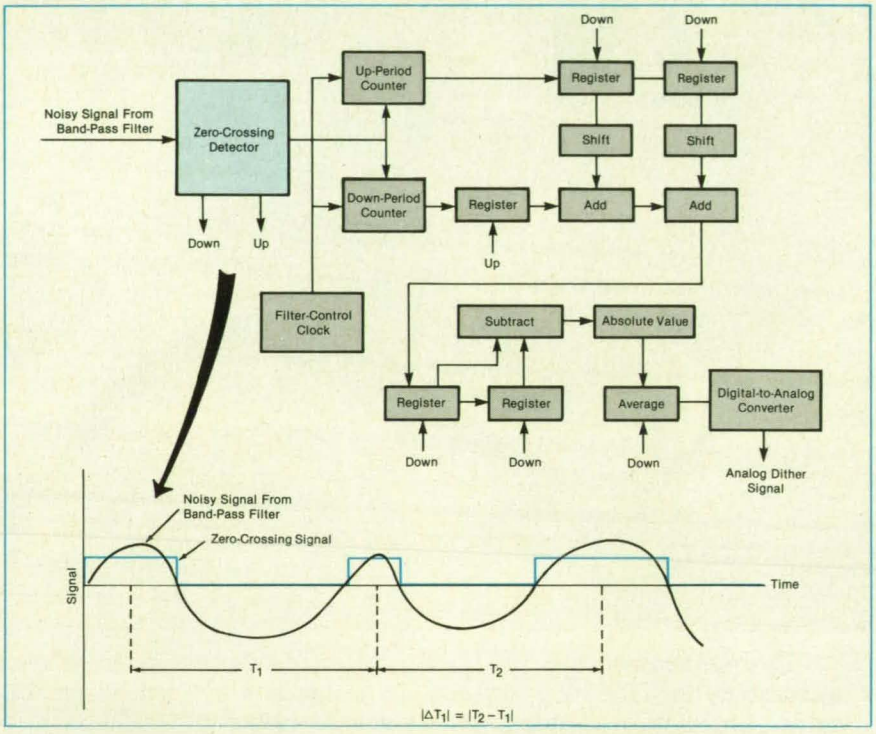

The **Noise-Contamination Detector** indirectly measures the noise in a noisy sinusoidal signal by measuring the average value of the fractional absolute dither in the period of the signal.

The system continually reports A_d to a computer that monitors its operation. If A_d exceeds a level that previous statistical tests have shown to be beyond the analytical capability of the system, the computer can trigger an alarm, possibly to alert the operator to select a different sensor or a different recording for analysis. As long as A_d remains within normal limits, it can be used to estimate continually the sinusoidal component (indicative of the amplitude of vibration in the particular passband) from the rms measurements of the noisy signal.

This work was done by Richard L. Randall of Rockwell International Corp. for **Marshall Space Flight Center**. *For further information, Circle 163 on the TSP Request Card.*

MFS-29537

Large-Constraint-Length, Fast Viterbi Decoder

A scheme for efficient interconnection makes VLSI design feasible.

NASA's Jet Propulsion Laboratory, Pasadena, California

A concept for a fast Viterbi decoder provides for the processing of convolutional codes of constraint length K up to 15 and rates of 1/2 to 1/6. A fully parallel (but bit-serial) architecture has been developed for a decoder of $K = 7$ to be implemented in a single dedicated very-large-scale integrated (VLSI) circuit chip. Such a chip can be used as a building block for decoders of larger K.

The number of states in a Viterbi decod-

complex problem

simple solution

Here's all the "tooling up" you need to build strong enclosures to your own specs: An ordinary mallet and a few wrenches. AMCO's 6061-T6 High Strength Aluminum framing system does the rest. You get extraordinarily strong enclosures, custom-made for your application, without long delays.

We can supply the pieces or build the whole enclosure.

Simple Hand-Mallet-Wrench assembly.
The system consists of extruded aluminum tubing, corner castings, locking pieces, and accessories. A relatively concise selection of standard pieces covers a very broad range of possible applications. Among other benefits, this cuts your waiting time to a minimum.

You decide the shapes and sizes.
Here is another big feature: You can build enclosures from 8″ to 20′ in any 90° plane. You can combine big compartments and small ones in any combination you need. You can use non-locking clips for prototyping or planned disassembly, or use locking clips for a tough permanent assembly. This enclosure framing system never boxes you in! Keep some in stock for those emergency needs.

Amazingly strong.
Our corner locking methods actually surpass the strength of welding—one of the reasons that this system offers you optimum weight/structural strength ratios. This system has withstood some very tough applications—like NASA Airborne, shipboard, ground support firing systems enclosures and missile launch systems, not to mention in house industrial use.

It's easy to check it out. Just phone for Catalog #203. Call **1-800-833-3156**. In Illinois, **1-312-671-6670**.

AMCO®

AMCO Engineering Co.
3801 N. Rose Street
Schiller Park, IL 60176-2190

AMCO's Heavy Duty Aluminum Structural System.

Circle Reader Action No. 500

er increases exponentially with K, and the number of interconnections increases in the same proportion. The partition of the De Bruijn graph that describes a Viterbi decoder involves, in general, many interconnecting wires. The problem is to find a partition that reduces the number of interconnections and, in addition, produces universal building blocks independent of the overall size of the decoder.

The design of the new chip and the circuit board on which the chips are mounted is based on a new, hierarchical partition of De Bruijn graphs, which reduces the number of external interconnections required to implement a Viterbi decoder. The partition is nested in the sense that a decoder of constraint length K can be obtained from two decoders of constraint length $K-1$. This partition is completely regular; i.e., it consists of identical building blocks at two distinct levels (chips and boards). This makes it possible to implement a Viterbi decoder of any K; of course, the amount of hardware increases exponentially with K.

The conceptual design for the $K = 15$ decoder (see figure) requires 16 identical circuit boards, each containing 16 identical chips. Each chip contains 32 butterfly processors, making a total of $16 \times 16 \times 32 = 8{,}192$ butterfly processors. The layout of each chip as well as the layout of a single board does not depend upon the size of the complete system: only the wiring between boards has to be modified to accommodate different constraint lengths.

The use of custom-made microcircuits is essential to the construction of the $K = 15$ decoder. Without the latest technology in application-specific integrated circuits, the decoder would be too large, too expensive, and too unreliable to be practical. The low-power complementary metal oxide semiconductor (CMOS) circuits envisioned for the 8,192 butterfly processors and supporting equipment are expected to consume less than 50 W when operating at full speed (> 1 Mb/s).

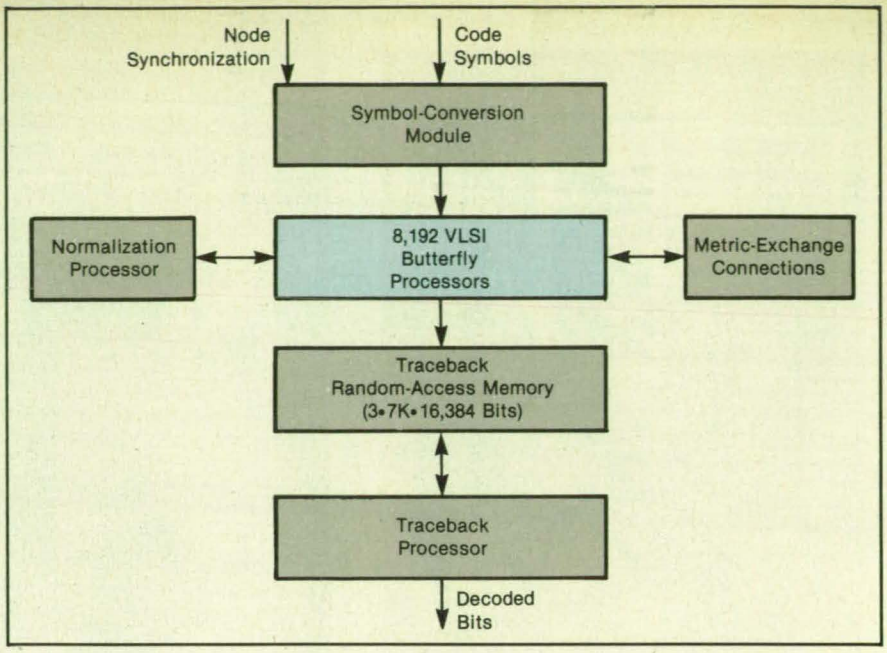

The **Large-Constraint-Length Viterbi Decoder** contains six major functional blocks. The VLSI circuits perform branch metric computations, add-compare-select operations, and then store the decisions in the traceback memory. The traceback processor then reads the appropriate memory locations and puts out decoded bits.

This work was done by O. Collins, S. Dolinar, In-Shek Hsu, F. Pollara, E. Olson, J. Statman, and G. Zimmerman of Caltech for **NASA's Jet Propulsion Laboratory**. *For further information, Circle 75 on the TSP Request Card.*

This invention is owned by NASA, and a patent application has been filed. Inquiries concerning nonexclusive or exclusive license for its commercial development should be addressed to the Patent Counsel, NASA's Resident Office-JPL [see page 14]. Refer to NPO-17639

Testing Microwave Landing Systems With Satellite Navigation

Less time and equipment are needed to perform tests.

John F. Kennedy Space Center, Florida

The satellite-based Global Positioning System (GPS) measures the accuracy of the microwave scanning-beam landing system (MSBLS) at airports used to support Shuttle landings. The GPS is especially suitable for this purpose in that it provides the time and three-dimensional information on the position and velocity with unprecedented accuracy. This same feature also makes it useful for testing other electronic navigation aids like LORAN, TACAN and microwave landing systems (MLS).

In a test of an MLS, an airplane is flown within the area of coverage, possibly along specified trajectories. The flight is tracked both by the MLS and by a reference system that is at least three times as accurate as the MLS is. A laser tracker can be used as the reference system, but it has several undesirable features. It is bulky, expensive, heavy, and susceptible to damage in shipment and requires about 4 weeks to ship and set up at the MLS site. These features are particularly disadvantageous if tests have to be conducted repeatedly at different airports to satisfy requirements for periodic calibration or certification.

When the GPS is the reference system, two commercially available GPS receivers are used in a differential mode to determine the relative position vector between the airplane and a reference location. The GPS reference-station antenna is set up above the MLS antennas, and the other GPS station is established aboard the airplane. The GPS reference station receives the L-Band signals bearing the coarse acquisition GPS code from at least four GPS satellites, uses these signals to calculate the distance to each satellite, calculates its position from these distances, compares this position to an initial reference position measured before the test, and calculates a correction based on this comparison.

Using a 408-MHz radio link, the reference station transmits the correction to the GPS receiver in the airplane once every second. The GPS receiver in the airplane uses the GPS signals it receives to calculate the position of the airplane in a manner similar to that of the reference station, then uses the correction transmitted by the reference station to eliminate common-mode errors. The position outputs from both the MLS and GPS receivers are fed to a computer, which compares them and provides a real-time display of angular errors during the flight. The position outputs are also recorded digitally for subsequent processing.

This work was done by John J. Kiriazes of **Kennedy Space Center**. *For further information, Circle 34 on the TSP Request Card.*

Inquiries concerning rights for the commercial use of this invention should be addressed to the Patent Counsel, Kennedy Space Center [see page 14]. Refer to KSC-11451

Ninety-five Percent Of What We Do, You Do. Which means that it's you, our suppliers, who are largely responsible for the continuing quality and reliability of our Atlas family of launch vehicles.

A & H TOOL ENGINEERING, CORP. A & M ENGINEERED AAMEC CORP. ABEX CORPORATION ACE CLEARWATER ENTERPRISES ACE TUBE BENDING ADEPT MFG., INC. ADVANCED COMPOSITE PRODUCTS ADVANCED COMPOSITE TECH. ADVANCED PRODUCTS CO. AEROCHEM INC. AEROFIT PRODUCTS, INC. AEROQUIP CORP. AEROSPACE TECHNOLOGIES, INC. AHF-DUCOMMUN, INC. AIRCRAFT ENGINEERING AIRCRAFT HINGE AIRDROME PARTS CO. AIRITE ALL FAB CORP. ALL POWER MFG. CO. ALLAN AIRCRAFT SUPPLY CO. ALLIED INDUSTRIES, INC. ALLIED SIGNAL AEROSPACE CO. ALLOY SPOT WELDERS ALUMINUM COMPANY OF AMERICA AM INDUSTRIES AMERICAN CYANAMID AMPHENOL CORP. AMRO FABRICATION CORP. ANDERSON, GREENWOOD & CO. APV MFG. & ENGR. INC. ARCTURUS MFG. CORP. ARDE, INC. ARDEN ENGINEERING CO. AREMAC ASSOCIATES AVE. ARWOOD CORP. ASI FABRICATION & MACHINE ASSOCIATED SPRING ASTRO SPAR INC. ASTROSPACE IND. AUTO AIR COMPOSITES AVX CORP. AYDIN AZURE INDUSTRIES INC. AZUSA PIPE & TUBE BABCOCK INC. BANDY, G.W., INC. BARRACUDA TECHNOLOGIES, INC. BAUER SPRINGS, INC. BAY CITY MARINE INC. BEALS CASTINGS, INC. BETTS SPRINGS, CO. BLAISDELL MFG. BOURNS INSTRUMENTS BOURNS SENSORS/CONTROLS INC. BOYD MFG. INC. BOZUNG, J.A. BREK MANUFACTURING BRICO ENGINEERING CO. BRUNSWICK CORP. BULOVA SYSTEMS & INSTRUMENTS BUNDY MFG., CO. BURRELLCO MANUFACTURING C & H MACHINE CALIFORNIA AERO DYNAMICS CALIFORNIA AVITRON CORP. CARDEN MACHINE SHOP CARLTON FORGE WORKS CASPIAN INC. CBA MACHINE CENTURY COMPOSITES CERTIFIED AEROSPACE CERTIFIED FABRICATORS INC. CERTIFIED SLINGS, INC. CHEMICAL DYNAMICS CORP. CHOMERICS CINCINNATI ELECTRONICS COAST METAL CRAFT COAST PRECISION ENTERPRISES COMPONENT RESEARCH CO. COMPOSITE TOOLING SPECIALISTS COMPUCRAFT INDUSTRIES INC. CONAX CORPORATION CONTROLLED PRECISION MFG. COULTER STEEL & FORGE CO. CRANE RESISTOFLEX CROWN COMPONENTS CORP. CRYENCO, INC. CTL AEROSPACE, INC. CUSTOM BOX AND PACKAGING CO. CVI INC. CYCLOPE INDUSTRIES, INC. DCX DEL AEROSPACE DEUTSCH ENGINEERED CONNECTING DEUTSCH METAL COMPONENTS DICKSON TESTING CO., INC. DIE CUT PRODUCTS DIVERSIFIED TECHNOLOGY DUKES, INC. DYE, R.E. DYNABIL INDUSTRIES, INC. EAGLE PICHER INDUSTRIES, INC. EAGLE PRECISION EARLE M. JORGENSEN CO. EATON CONSOLIDATED CONTROLS EDM SPECIALITIES, INC. EL-CO MACHINE PRODUCTS ELASTOMERIC SILICONE PROD. ELBIT COMPUTERS, LTD. ELECTRONIC ENGINEERING RESEARCH ELECTRONIC SPECIALTY CORP. ENCOTECH INC. ENDEVCO CORP. ENERGY CONTAINER CORPORATION ESTERLINE ANGUS INSTRUMENT EXTON METAL PRODUCTS, INC. F & B MANUFACTURING CO. FAIRCHILD CONTROL SYSTEMS FANSTEEL, ADVANCED STRUCTURES FLEXCO INC. FLEXFAB INC. FLEXONICS INC. FLUOROCARBON FONTANA MACHINE & ENGINEERING FORMING SPECIALTIES FRANKLIN'S INDUSTRIES FUTURECRAFT CORP. FUZAN CORP. G & H TECHNOLOGY, INC. GASKET MANUFACTURING COMPANY GEB INDUSTRIES, INC. GENERAL DYNAMICS ABILENE GENERAL DYNAMICS CONVAIR GENERAL DYNAMICS ELECTRONICS GENERAL DYNAMICS FORT WORTH GENERAL DYNAMICS SERVICES CO. GLOBE DYNAMICS INTERNATIONAL GOLD COAST ENGINEERING GOLDEN STATE CASTINGS GRAPHITE MACHINING GROVE VALVE & REGULATOR GST INDUSTRIES, INC. GULTON INDUSTRIES, INC. HAMBLIN INDUSTRIES HANSEN ENGINEERING CO. HBD INDUSTRIES, INC. HEARNE MACHINING INC. HEATH TECNA HEXCEL CORPORATION HEXCEL STRUCTURAL DIV. HI TEMP INSULATION HI-SHEAR TECHNOLOGY HI-TEMP FORMING CO. HIGH PRECISION GRINDING HOLLYWOOD ALLOY CASTING, CO. HONEYWELL SPACE AND STRATEGIC HONEYWELL, INC. HOOVER ELECTRIC CO. HUGHES BROS. AIRCRAFTERS HYATT DIECAST & ENG. CORP. HYDROFORM USA IMO DELAVAL INC. IMO INDUSTRIES

INDEPENDENT CONTRACTORS ENT. INDEPENDENT STEEL AEROSPACE CONTROLS ITT CANNON J & R LAMINATED PRODUCTS CORPORATION K-T CORPORATION KAI R. KUHL KEMET ELECTRONICS CORP. DIV. KENIG FORGE, INC. ENGINEERING CO. KIRKHILL RUBBER CO. KISTLER PACIFIC LANGLEY CORP. LEACH CORP. LEARJET CORP. LEE MANUFACTURING CO. LEMKE MANUFACTURING LEMON INDUSTRIES LOCKHEED AERONAUTICAL SYSTEMS LORAL MACHINE & TOOL M & R SHEETMETAL M & W SPECIALTIES MAGNA MILL PRODUCT INC. MANLEY ENGR CO. INC. MASTER MACHINE CORP. MEPCO MICROSEMI CORP. MIKOL MISSILE AIR MIL-R RUBBER & PLASTICS, INC. MILLER DIAL MILLER FLUID POWER MILLS, D. GRINDING & MACHINE MINNESOTA VALLEY ENGINEERING MISSION AEROSPACE CO. MOOG INC. MOORE INDUSTRIES MORRIS PRECISION PRODUCTS MORTAN IND. INC. MOTOROLA SEMICONDUCTOR MOTOROLA, INC. MUEHLEISEN MFG. MURATA ERIE OF NORTH AMERICA MURDOCK, INC. NATIONAL SEMICONDUCTOR NC DYNAMICS, INC. NEILL AIRCRAFT CO. NELSON AEROSPACE INC. NETWORKS ELECTRONIC CORP. NEW HAMPSHIRE BALL BEARINGS NORTHROP CORP. OCEANSIDE ENGINEERING & MFG. ODETICS INC. OMNI MANUFACTURING ONE-WAY MFG. INC. OPTIM ELECTRONICS CORP. ORLANDO PLATING OXWELL INC. PACIFIC AERO MFG. INC. PACIFIC COAST PRODUCTS PACIFIC SCIENTIFIC PACIFIC TERMINATIONS, INC. PANDJIRIS INC. PARKER BERTEA AEROSPACE GROUP PEACOCK PERFORMANCE PLASTICS INC. PETERSON AMERICA COMPANY PLAINVILLE ELECTROPLATING CO. PNEUDRAULICS, INC. PPC PRODUCTS CORP. PRECISE MACHINING & MFG., INC. PRECISION AEROSPACE CORP. PRECISION COIL SPRING CO. PRECISION DETAIL, INC. PRECISION MACHINING SHEETMETAL PRECISION TECHNOLOGY PRECISION TUBE BENDING PRECISION TUBEDRAW & MACHINE PROTOTYPE MODEL & MOLD CORP. PROTRONICS ENGR CORP. PTI TECHNOLOGIES, INC. PUCCIO METAL FAB. INC. PUROFLOW CORP. PYLE NATIONAL PYRONETICS DEVICES, INC. QMS MACHINING & TOOL CORP. QUALITY ALUMINUM FORGE QUINCY TECHNOLOGY RAH INDUSTRIES REINHOLD INDUSTRIES RICHLAR CO., INC. RICMAR ENGINEERING, INC. RITCHIE BROTHERS R & D ROCKET RESEARCH CO. ROCKWELL INTERNATIONAL ROGERS MACHINE ENG. SAAB SPACE AB SAFT SAN DIEGO STEEL SPECIALTIES SATURN MACHINE IND. SCHLOSSER FORGE COMPANY SCHLUMBERGER INDUSTRIES SCI TECHNOLOGY INC. SERVOTRONICS, INC. SHAMBAN W. S. CO. SHEET METAL SPECIALTIES SIEBELAIR SIERRACIN/HARRISON SINGER-GENERAL PRECISION SKYLINE ENGINEERING, INC. SMITH MFG. CO. SNAP-TITE, INC. SO CAL. METAL JOINING INC. SOLO ENTERPRISES CORP. SONFARREL INC. SORRENTO ELECTRONICS, INC. SOUTHWEST FABRICATORS SOUTHWESTERN COMPOSITES INC. SPACE FLEX COMPANY SPECIAL TOOLS & MACHINERY SPECIALTY ENGINEERING CO. SPECIALTY MANUFACTURING INC. SPIRA MFG. CORP. SPIROL INTERNATIONAL SPRAGUE ELECTRIC CO. SQUARE TOOL & MACHINE STAINLESS STEEL PRODUCTS STANDARD LOGIC, INC. STANDARD TOOL & DIE CO. STEMCO ENGINEERING STERER ENGINEERING & MGR. STILLMAN SEAL DIVISION STRATO-FLIGHT ENG. STRATOFLEX, INC. STRETCH FORMING CORP. STRUTHERS DUNN INC. SUNBANK ELECTRONICS, INC. SUNDSTRAND DATA CONTROL TALLEY DEFENSE SYSTEMS TAVIS CORP. TAYCO ENGINEERING, INC. TECHNETICS MILITARY ELECTR. TELEDYNE TELEDYNE CRYSTALONICS TELEDYNE INC. TELEDYNE RYAN AERO TEXTRON, H R INC. THERMECH ENGINEERING CORP. THIOKOL CORP. TITEFLEX CORP. TMP TOOL & MACHINE, INC. TRACOR AVIATION TRANSCO PRODUCTS, INC. TRI MODELS INC. TRONTECH, INC. TRU-CIRCLE MFG. INC. TRUE FORM INDUSTRIES, INC. TRW PRESSURE SYSTEMS, INC. TYEE AIRCRAFT, INC. UNIT ENGINEERING, CORP. UNITECH COMPOSITES INC. UNITED TECHNOLOGIES VAC-HYD CORP. VACCO INDUSTRIES VALCOR ENGINEERING CORP. VALLEY BOX CO. VALLEY FORGE, INC. VALLEY METALS, INC. VAN KNO TOOL & MFG., INC. VEGA PRECISION LABORATORIES VERSAFORM CORP. VICKERS INC. VOI-SHAN CORP. VOTAW PRECISION CORP. WARREN MACHINE & ENGR. WATKINS JOHNSON CO. WATSONS PROFILING CORP. WEBER METALS & SUPPLY CO. WELDMAC MFG. CO. WEST AMERICAN RUBBER CO. WEST COAST PACKING AND CRATING WESTERN FILTER CORP. WESTERN METHODS WESTERN MICROWAVE WHITTAKER ORDNANCE WHITTAKER-YARDNEY POWER SYST. WIL-JO MANUFACTURING, INC. WORLD AEROSPACE CORP. WYMAN-GORDON CO. ZERO WEST DIVISION ZIPCO HYDRAULICS, INC.

(As of 1/1/90)

To all of you who contribute so much, we offer our profound gratitude.

GENERAL DYNAMICS

Space Systems Division

Circle Reader Action No. 305

Array Feed To Compensate for Distortion in Antenna

An adaptive system partly restores the desired far-field radiation pattern.

NASA's Jet Propulsion Laboratory, Pasadena, California

An adaptive array feed for a paraboloidal-reflector antenna helps to compensate for the effects of slow changes in the shape of the reflecting surface; for example, changes caused by gradients of temperature or changes in orientation in the gravitational field. As the reflecting surface deviates from the ideal paraboloidal shape, the wave fronts also become distorted, causing a decrease in the on-axis amplitude and/or increases in the side-lobe amplitudes. The adaptive array feed counteracts the distortion by illuminating the reflector with wave fronts that have, in a sense, the "opposite" distortion.

For the purpose of numerical simulation, the far-field of a distorted reflector is first computed using a diffraction-analysis computer program. This computer program also incorporates the concept of conjugate field matching to generate complex excitation coefficients of the radiating elements in the array. These excitation coefficients can be chosen to compensate the distortion partly, either maximizing the directivity in the desired direction or reducing (or otherwise controlling) the side lobes. In practice, however, it is not necessary to measure the shape of the reflector directly. It suffices to measure the amplitude and the phase of the focal-plane field at a sufficient number of points for an incoming plane wave.

In an experiment to test the adaptive-array-feed concept, an offset paraboloidal reflector of 1.832-m focal length was deliberately machined with a shape representative of a typical thermal distortion. The reflector was fed by an array feed consisting of 19 cigar-shaped elements spaced 1.06 wavelength apart (at 8.45 GHz). Each element was fed through an analog phase shifter and a variable attenuator. The amplitude and phase of the reflection of an incoming plane wave were measured at each element and processed into excitation coefficients, which were used to adjust the phase shifters and attenuator (see figure).

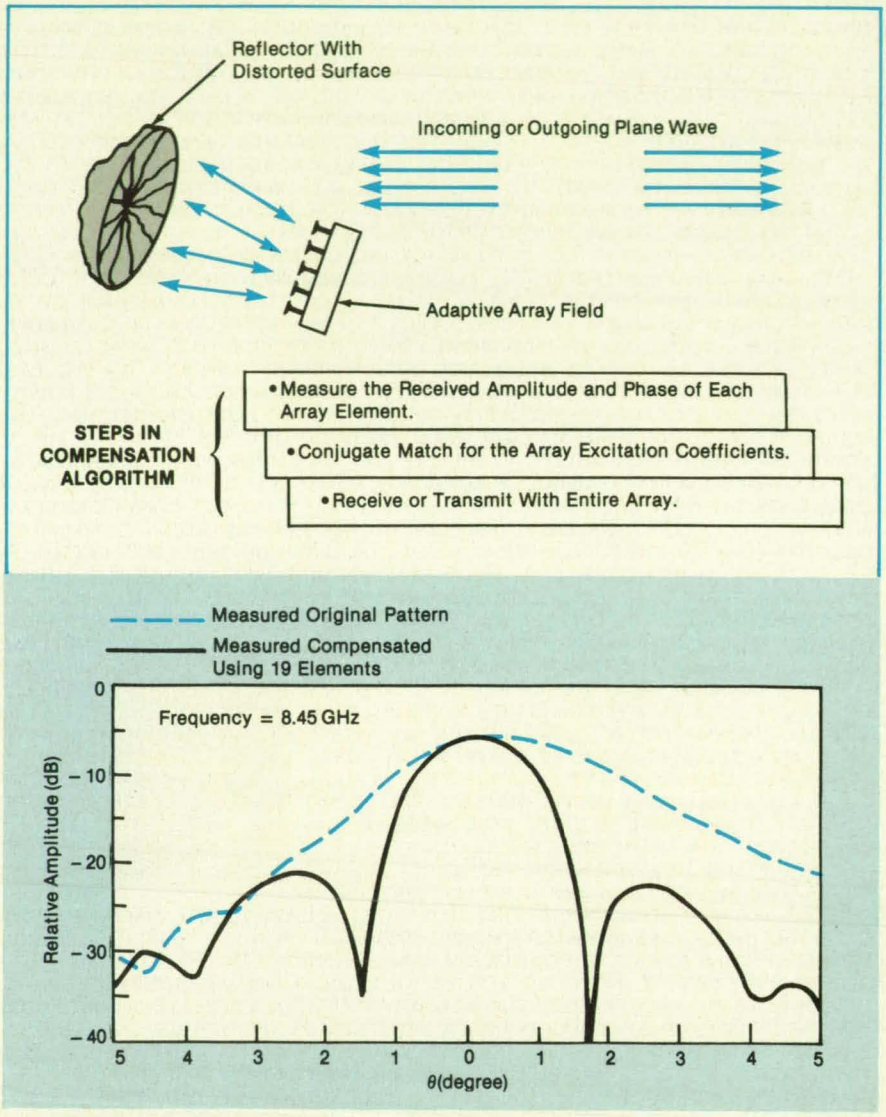

An **Adaptive Array Feed** implements an algorithm that compensates for the distortion in the radiation field caused by the distortion in the reflector.

The far-field pattern and the on-axis directivity were noticeably improved by the compensation. At the present time, the steps required in the adaptive design were implemented manually. It is planned to perform these steps automatically by performing a computer-controlled experiment.

This work was done by Y. Rahmat-Samii of Caltech for **NASA's Jet Propulsion Laboratory**. *For further information, Circle 86 on the TSP Request Card.*
NPO-17667

Acquisition of Spread-Spectrum Code

The effects of Doppler shift and data modulation are taken into account.

NASA's Jet Propulsion Laboratory, Pasadena, California

Two advanced schemes for the acquisition of direct-sequence spread-spectrum codes have been proposed. Both schemes take into account the slippage of code chips caused by severe Doppler shifts of the carrier and code frequencies. (As used here, "chips" means periods of time containing sequences of code bits, not small pieces of silicon containing integrated circuits.) In addition, one scheme takes account of data modulation.

Accurate and fast synchronization between the spreading (incoming) pseudo-noise code and the local despreading (receiver) code is necessary for the efficient

ANOTHER ASTRO-MED FIRST IN 8-CHANNEL RECORDERS

LASER PRINTER RESOLUTION!

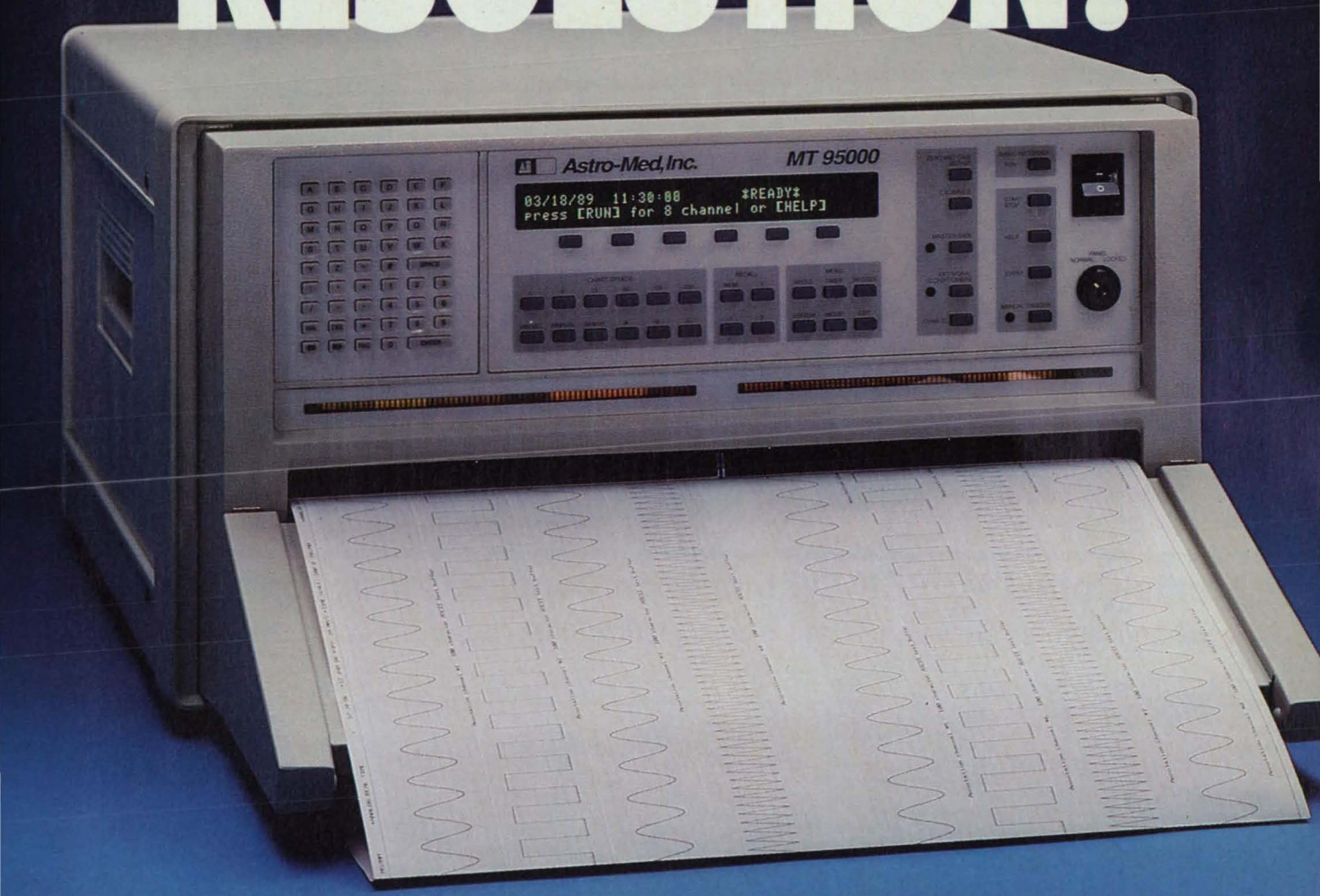

- **Laser Quality Writing–300 dpi**
- **20 kHz Frequency Response**
- **Automatic Self-Calibration–Traceable to NBS**
- **Expandable to 16 Channels**
- **Data Capture with 200 kHz Sample Rate Per Channel**
- **Built-In Programmable Signal Conditioners**

From its laser-sharp charts to its unparalleled frequency response, this remarkable new 8-channel recorder brings you the technology of the Twenty-First Century today! It outperforms even Astro-Med's MT-9500, which in 1987 was heralded as the first breakthrough in 8-channel recorders in 20 years. It has 50% more resolution, 4 times higher frequency response, and 8 times more memory than the MT-9500. With automatic self-calibration traceable to NBS, expandability to 16 channels, and a host of other important features. We call it the MT-95000, a product so unique that it is protected by U.S. Patent No. 4,739,344.

Phone, Fax or Write for details!

Astro-Med, Inc.®

Astro-Med Industrial Park, West Warwick Rhode Island 02893
Telephone (401) 828-4000 • Toll Free 800-343-4039
Telex No. 710-382-6409 • Fax (401) 822-2430

Circle Reader Action No. 405

utilization of any spread-spectrum system. Typically, the first step in synchronization is acquisition of the incoming code. This is a process of successive decisions wherein the ultimate goal is to bring the two codes into coarse time alignment within one code-chip interval.

In the proposed schemes (see figure), the uncertain carrier-frequency range and uncertain code-frequency range are partitioned into subbands. Within each subband, the code and carrier frequencies of the local reference signal are offset by quantized amounts that compensate as much as possible for the Doppler effect, thus limiting this effect in each subband during the correlation process. More subbands lead to better performance but require more correlators (i.e., higher cost).

More specifically, the scheme for Doppler shift only involves a coherent maximum-likelihood detector divided into strips, each of which does the processing at a different fractional offset $-\tau'_j$ in the code-chip time T_c (and thus, a corresponding offset in code frequency). Within each strip, samples are correlated at each of M_1 different time lags expressed as fractional code-phase offsets τ_j. The sampled correlation functions are processed via a fast-Fourier-transform algorithm.

Where there is no data modulation, the integration time can be arbitrarily long, but longer integration time results in finer carrier-frequency resolution, hence requiring more filters to cover the same uncertainty. Where there is data modulation, the integration time is limited by the data-bit time. Thus, the scheme for use with data modulation includes noncoherent detection to reduce the degradation of performance due to data modulation and to allow a long correlation time without necessitating a fast Fourier transform of a large number of points. The total correlation time is partitioned into subintervals, and the results of the integrations in the subintervals are square-law-noncoherently combined for detection.

These schemes have a highly parallel architecture that can be implemented with currently available technology. It might also be possible to use a hybrid parallel/serial architecture in which the acquisition time varies in inverse proportion to the number of correlators and fast-Fourier-transform processors.

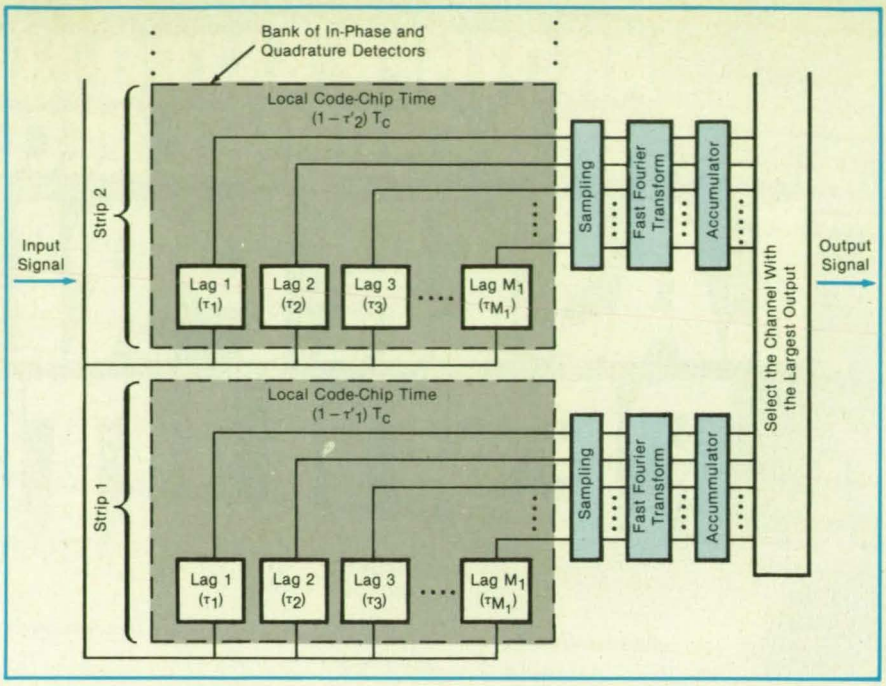

The **M_1-Lag Correlator** in each strip of the spread-spectrum-code detector operates at a different offset code-chip time. Each offset represents an assumed (tentative) Doppler shift.

This work was done by Unjeng Cheng, William J. Hurd, and Joseph I. Statman of Caltech for **NASA's Jet Propulsion Laboratory**. *For further information, Circle 46 on the TSP Request Card.*
NPO-17472

Trellis-Coded MDPSK System With Doppler Correction

Advanced features are incorporated in equipment for mobile/satellite communications.

NASA's Jet Propulsion Laboratory, Pasadena, California

A multiple-differential-phase-shift-keyed (MDPSK) microwave system is designed for communications between mobile and/or fixed terrestrial stations via satellite transponders (see Figure 1). Stations in the system could transmit and receive data or digitally-coded voice signals at rates up to 4.8 kb/s in channels only 5 kHz wide.

The system integrates advanced features, some of which have been described in previous issues of NASA Tech Briefs. These features include trellis-coded 8 DPSK modulation with finite interleaving and deinterleaving, differential encoding and decoding, root-raised-cosine pulse shaping at the transmitter and receiver (matched filtering for a dual-sample detection scheme), correction for Doppler shifts,

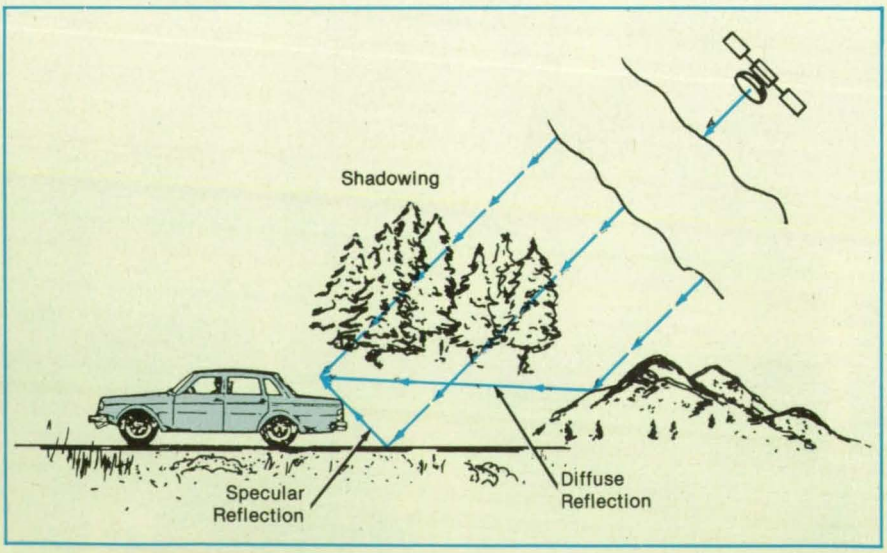

Figure 1. The **Mobile/Satellite Communication Channel** is subject to deep fades caused by shadowing, specular reflection, diffuse reflection, and motion. Motion also gives rise to a Doppler shift.

TECHNOLOGY 2000

November 27-28,1990

Washington Hilton Hotel, Washington, D.C.

The first national industrial conference and exposition spotlighting NASA technology and technology transfer

TECHNOLOGY 2000 will feature symposia and exhibits devoted to the commercial application of hot new technologies emerging from NASA R&D in such fields as:

- **software engineering**
- **materials science**
- **sensor technology**
- **robotics and artificial intelligence**
- **lasers/optoelectronics**
- **communications**
- **computational fluid dynamics**
- **bio-medicine**

Attendance at **TECHNOLOGY 2000** will enable you to:

- **meet top NASA researchers** and technology transfer experts;
- **tap into the vast storehouse** of technologies now available for license to industry;
- **explore cooperative R&D opportunities** with NASA and its contractors.

Circle Reader Action #693 for exhibit space or #695 for attendance.

Send **TECHNOLOGY 2000** information to us today.
We'd like to ☐ attend or ☐ exhibit .

Name_____ Title_____

Company_____

Phone_____

Address_____

City/State/Zip_____

Mail to: **Technology Utilization Foundation**
41 East 42 Street, Suite 921
New York, N.Y.10017
Phone (212) 490-3999 FAX (212) 986-7864

and synchronization of symbols (see Figure 2).

At the transmitting station, input bits at a speed of 4.8 kb/s are passed through a 16-state, rate-2/3 trellis encoder. The symbols put out by the encoder are interleaved into blocks of span 8 and depth 16 to break up burst errors caused by amplitude fades that last more than 1 symbol time.

The interleaved coded symbols are next differentially encoded and pulse-shaped by use of root-raised-cosine filters with 100-percent excess bandwidth to reduce adjacent-channel interference. The output of the pulse-shaping filters modulates quadrature radio-frequency carriers for transmission over the fading channel.

At the receiver, the faded, noise-corrupted signal is down-converted by sampling, then passed through "brick-wall" filters of bandwidth 2.6 kHz, which is the sum of the 8-PSK symbol rate (2,400 Hz) plus the maximum Doppler shift (200 Hz). The outputs of the "brick-wall" filters are provided to the Doppler-frequency estimator and to a pseudomatched filter, which consist of a "brick-wall" filter and a half-symbol-delay-and-add circuit. (In the absence of Doppler frequency shift, these pseudomatched filters are exactly root-raised-cosine filters.)

The differentially detected and Doppler-corrected samples are fed to the deinterleaver, then to the trellis decoder. At the trellis decoder, branch metrics are computed by use of a correlation (Gaussian-noise) metric, which is approximately optimum in the absence of information on the state of the channel. Each symbol time, branch metrics are provided to the Viterbi decoding algorithm via add/compare/select operations with state-metric normalization to prevent overflow from a buffer. The size of the buffer of the survivor path is chosen to be 32 symbols on the basis of computer simulations, which have shown that the difference in performance between a 32-symbol buffer and a 256-symbol buffer is a few tenths of a decibel.

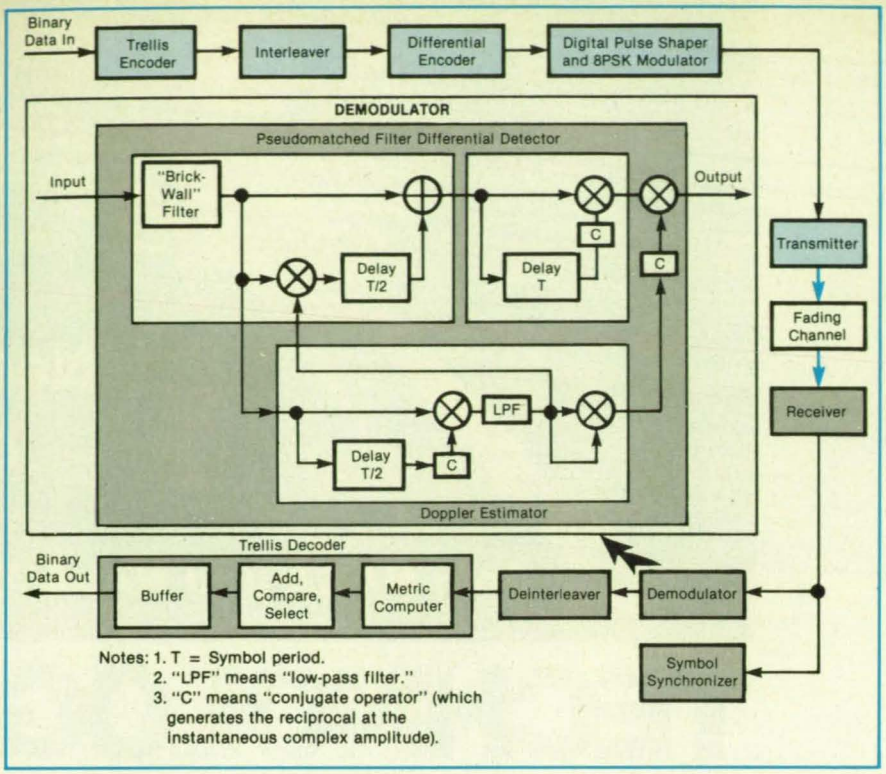

Figure 2. The **MDPSK Communication System** incorporates advanced encoding, decoding, modulation, and demodulation techniques to minimize the effects of error bursts. It also uses feedforward techniques for fast recovery from deep fades.

This work was done by D. Divsalar and M. K. Simon of Caltech for **NASA's Jet Propulsion Laboratory**. *For further information, Circle 14 on the TSP Request Card.*

In accordance with Public Law 96-517, the contractor has elected to retain title to this invention. Inquiries concerning rights for its commercial use should be addressed to

Edward Ansell
Director of Patents and Licensing
Mail Stop 305-6
California Institute of Technology
1201 East California Boulevard
Pasadena, CA 91125

Refer to NPO-17644, volume and number of this NASA Tech Briefs *issue, and the page number.*

Computer Assembles Mosaics of Satellite-SAR Imagery

Overlapping image frames are registered and blended automatically.

NASA's Jet Propulsion Laboratory, Pasadena, California

A digital image-processing system assembles maplike mosaic images of large areas of the Earth from overlapping images of smaller areas generated by spaceborne synthetic-aperture radar (SAR). The system automatically registers and blends the smaller images with each other. Thus, it eliminates the need for the time-consuming, tedious manual processing like that used to assemble mosaics of aerial photographs and images from airborne SAR. The system is modifiable to accept images from spaceborne optical sensors.

Before being fed to the system, the digitized SAR image data are preprocessed (NPO-17106): geometric distortions caused by interacting effects of the attitude of the radar beam and the altitude of the target are corrected, and the imagery is registered with digital models of the terrain obtained from existing topographical maps. The resulting images are relatively free of distortions, and the radar coordinates of the original images have been converted to geographic coordinates.

After selecting overlapping images, the system must determine the misregistration between them. This is because although the images are nominally registered with geographic coordinates, there are residual errors caused by uncertainties in the location of the radar platform, noise, and the

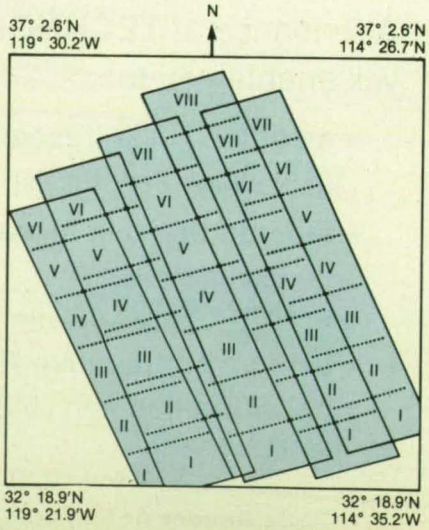

Figure 1. **Images Are Assembled onto a Map Grid** to obtain the large-scale mosaic image. First, images from the same along-track passes are connected side-by-side into long strips. Next, the adjacent strips are assembled to obtain the overall mosaic.

radiometric characteristics of terrain. The system measures the misregistration in either one of two ways: a procedure based on the correlation of the overlapping images; or, if cross correlation fails, a procedure based on the matching of contour features that are found by convolving the images with the Marr-Hildreth operator (the Laplacian of a smoothing Gaussian of specified width).

After correction for misregistration, the images are assembled (see example in Figure 1). Finally, radiometric disparities between the component images are reduced to smooth the transitions across the seams. This is done by a modified "feathering" technique in which the average intensities of the picture elements in the overlapping regions are used to rescale the intensities throughout the images. Figure 2 is an example of a "feathered" mosaic image.

The system includes a VAX-11785 general-purpose computer with 12 Mbytes of main memory, a Floating Point System (AP-5210) array processor, two 700-Mbyte disk drives for the manipulation of images and the storage of data, and a tape drive for off-line storage of data. The preprocessed images are loaded from the tape drive. The array processor is used mainly for the cross correlation of the component images. The coefficients used for the feathering scheme are calculated in the general-purpose computer.

The product mosaics are stored in quadrants of 6000 × 6000 picture elements each. From these quadrants, output products of different sizes and resolutions can be constructed. The generation of large, high-resolution mosaics is limited by existing laser-beam film recorders. The time required to construct one image quadrant is about 1 hour.

This work was done by R. Kwok, J. C. Curlander, and S. S. Pang of Caltech for **NASA's Jet Propulsion Laboratory**. *For further information, Circle 3 on the TSP Request Card.*

Inquiries concerning rights for the commercial use of this invention should be addressed to the Patent Counsel, NASA Resident Office-JPL *[see page 14].* *Refer to NPO-17683*

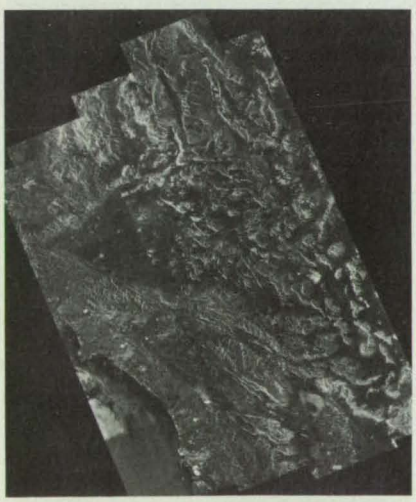

Figure 2. This **Mosaic Image of Southern California** was made from the 33 images shown in Figure 1. This mosaic covers an area of about 400 × 500 km from the Mexican border to the Sierra Nevadas.

Books and Reports

These reports, studies, handbooks are available from NASA as Technical Support Packages (TSP's) when a Request Card number is cited; otherwise they are available from the National Technical Information Service.

Controlling Shape and Vibration of Antennas

Sensors, control subsystems, and actuators would be integrated to maintain high performance.

A report discusses the application of advanced techniques to maintain a large wrap-rib, offset-feed spaceborne antenna reflector

in the precise shape required for high performance. The idea is to use an integrated system of sensors, a control processor, and actuators to measure and suppress both vibrations and static or slowly varying (e.g., thermal) deviations from the desired shape. The technology is also applicable to other elastically deformable structures.

For the type of antenna in question, it is required to provide knowledge of the static shape to an accuracy of 0.3 mm and to control the static component of deformations to an accuracy of 1.0 mm by use of rib-root actuators. The determination of shape involves the combination of mathematical modeling of deformations of the structure with optoelectronic sensing to estimate overall distortion. The control of shape to achieve the desired radiation pattern incorporates the estimated-distortion inputs and synsthesizes the predicted control function to correct for quasi-static elastic deformations.

It is required to correct for vibrations of the feed and reflector boom to stabilize, within 0.07°, the hub-to-feed line of sight of a 20-meter dish antenna operating at 1.61 GHz. To support such precise control, a characterization of the dynamics of the overall structure system, based on in situ measurements and processing methods for identification of the parameters of a mathematical model of the dynamics of the system, is integrated into the overall control system.

For the static component, the introduction of statistical model errors enables the treatment of effects that have been ignored in the modeling or that occur on too fine a scale to be modeled adequately. As a result, the observational data can be statistically referenced to a plant, and the estimates of distortion can be addressed in the mathematical framework that includes modeling errors and observational errors. This makes it possible to use a variety of mathematical models and sensing/actuating systems. The mathematical models may range from coarse geometric models that characterize overall features to fine-scale structural models that can resolve local features. The fine-scale models are represented by stiffness matrices or elliptic partial differential equations.

For the dynamic component, an accurate mathematical model of the structure is required. This, in turn, requires a multifaceted approach. The response to the firing of thrustors is analyzed first by Fourier methods to establish the integrity of the system and the existence of the major bending groups and to bound the frequencies and damping ratios of these groups. These results are used to develop an input sequence for precise identification of the parameters of the mathematical model of the dynamics of the system, which maximize the value of information returned by the sensors.

For excitation, proof-mass actuators (PMA's) are used. Accelerometers are distributed about the antenna and support structures in sufficient numbers to provide adequate observability of the major dynamic modes. Recursive-least-squares, maximum-likelihood-estimation, prediction-error, and other processing methods in the time domain are used to derive final parameter values.

The objective in the control of jitter in the hub-to-feed line of sight is to correct for static and dynamic motions that adversely affect the precision of the radiation pattern. Static errors are caused by mechanical bias errors and thermal loading. Dynamic motion is caused primarily by firing of thrustors or vibrations induced by control-moment gyros. The simplest strategy for the suppression of vibrations is to use proportional rate plus position feedback in the PMA's. For increased performance and suppression of higher frequencies, the linear quadratic Gaussian (LQG) methodology is used to suppress jitter in each major component of the structure independently. For highest precision, the measure of radio-frequency performance is maximized directly as the control objective, again using LQG methodology.

This work was done by E. Mettler, R. E. Scheid, and D. B. Eldred of Caltech for **NASA's Jet Propulsion Laboratory**. *To obtain a copy of the report, "Technologies for Antenna Shape and Vibration Control," Circle 15 on the TSP Request Card.*
NPO-17598

More About Fixed-Lag Smoothers for Tracking Carriers

Performance in the presence of fades can be improved.

A report amplifies and extends the subject matter of "Performances of Fixed-Lag Phase-Smoothing Algorithms" (NPO-17202), *NASA Tech Briefs*, Vol. 14, No. 1, page 73. Intended originally for use in the reception of weak phase-modulated signals in NASA's Deep Space Network, fixed-lag smoothers can also be used to mitigate the effects of short, deep fades, including multipath effects, in mobile or fixed terrestrial receivers of frequency- or phase-modulated signals.

The problem is to estimate the phase and frequency of a sinusoidal carrier signal in the presence of process noise (phase noise in the received signal generated by the transmitter or the propagation of the signal) and additive observation noise (unavoidable thermal noise generated by the receiver). In the receiver, raw estimates of the frequency and phase are produced by a phase-locked loop and refined by a post-loop correction filter, which, in this case, is a digitally-implemented fixed-lag smoothing filter. The general problem of optimal filtering and smoothing is nonlinear and intractable, but linear and nonlinear fixed-lag smoothers, which are suboptimal, can be designed to enhance the reception of weak signals.

The author presents the mathematical model of the signal and the equations of the suboptimum smoother, as derived from the stochastic optimization theory. With a minor modification, these equations are shown to be the linear Kalman filter equations for an appropriate linear-signal model applicable when the phase detector can be assumed to be linear. A simple finite-impulse-response-filter implementation of the smoother is presented: In the steady state, the coefficients of such a filter are constant and can be precomputed.

Next, the author discusses the transfer functions of first-, second-, and third-order filter/smoothers for a signal that includes zero-mean Gaussian white process noise and independent zero-mean, narrow-band white Gaussian observation noise. (These cases are commonly used in the mathematical modeling of the estimation of phase and frequency in communication and navigation systems.) Assuming the phase detector to be linear, closed-form expressions are derived for the transfer functions and the performance indices of the loop filter and the smoother.

The theoretical performances of receivers containing fixed-lag smoothers are compared with numerical simulations. When the phase detector is assumed to be linear, the performance predicted on the basis of optimal linear estimation theory is close to that of the numerical simulations. However, when the phase-locked loop is operating near the threshold signal-to-noise ratio, the phase detector cannot be assumed to be linear.

When the nonlinearity of the phase detector is taken into consideration and the receiver is operating at a high signal-to-noise ratio, the addition of the smoother decreases the effect of the phase- and the frequency-estimation errors by about 5.6 dB. However, as the signal-to-noise ratio is reduced, the corresponding improvement is also reduced. The reduction is more severe when the process noise is present than when only the observation noise is present. In the presence of both nonlinearity and process noise, the smoother exhibits a marked threshold behavior.

The results of the simulation also suggest that the performance of a loop-filter-and-smoother combination does not change significantly if the variance of the process noise is smaller than its design value. This is of interest because, in many practical cases, the statistics of the process noise are not known precisely and are therefore deliberately overestimated for conservative design.

This work was done by Rajendra Kumar of Caltech for **NASA's Jet Propulsion Laboratory**. *To obtain a copy of the report, "Optimum Filter and Smoother Design for Carrier Phase and Frequency Tracking," Circle 39 on the TSP Request Card.*
NPO-17389

Operation of the X-29A Digital Flight-Control System

Characteristics of the system and experience gained in tests are described.

A report reviews the program of testing and evaluation of the digital flight-control system for the X-29A airplane, with em-

phasis on operation during tests. Topics include the design of the system, special electronic testing equipment designed to aid in daily operations, and aspects of testing, including the detection of faults.

Because the X-29A is an aerodynamically unstable forward-swept-wing airplane, it requires a highly-augmented control system to maintain stable flight. The control system consists of triplex fly-by-wire digital flight-control computers (FCC's) with a triplex analog backup system. The FCC's obtain inputs from various sensors and provide outputs to hydraulic actuators on multiple control surfaces.

The digital flight-control system has proven to be very flexible. Many changes have been made since the first flight, including a major modification of the control system to enable the airplane to fly in an expanded range of velocities, altitudes, and accelerations; the addition of a flight-test mode that holds the flaps at a fixed position; and the addition of a remotely-augmented-vehicle system, which helps the pilot steer in a way that optimizes maneuvering trajectories and provides the capability to add signals to pilot or surface commands for the identification of aerodynamic parameters. Modifications were also made in the management of redundancy in data from air sensors (speed, altitude, etc.), in normal-mode gains, and in the built-in tests that can be initiated by the pilot.

The special electronic testing equipment was designed to examine the internal workings of the system. For the hardware-in-the-loop simulation, a breakout panel was built to make available a test point for every connection to the FCC's. This provides easy access to any combination of analog parameters that interact with the FCC's. The system-evaluation unit (SEU) serves as the interface to the internal workings of the FCC's.

The extended aircraft interrogation and display system (XAIDS), developed by NASA for use on several aircraft, is used here to present information on multiple parameters residing inside the FCC's. The XAIDS can display parameters in engineering units, perform tests on the data, and display results of the test. The combination of the SEU and the XAIDS provides the capability to read parameters from the FCC memory when the FCC's are not running or from the output bus of the FCC's when they are running.

The flight-test schedule limited the time available for disassembly and testing of the airplane on the ground, necessitating a simplified approach to testing on the ground; i.e., with only equipment that was easy to connect to the airplane. All instrumented signals were available from a hangar calibration system, which was used to monitor such slowly changing parameters as temperatures, voltages, and static values of such active parameters as positions of control surfaces and inputs from flight-control-system sensors. Breakout boxes were built to give access to analog signals.

During troubleshooting, it became evident that not all the signals of interest are available at connectors. To examine data inside the FCC's, a menu-operated personal computer was connected to the SEU through the same RS232 ports the XAIDS used in the simulation. Specific test programs were written for the FCC's to store data from the aircraft for a particular test. The data are then transferred to the personal computer where a spreadsheet program is used to evaluate the data for proper responses to the test.

This work was done by Vince Chacon and David McBride of **Ames Research Center**. *Further information may be found in NASA TM-100434 [N88-21152], "Operational Viewpoint of the X-29A Digital Flight Control System."*

Copies may be purchased [prepayment required] from the National Technical Information Service, Springfield, Virginia 22161, Telephone No. (703) 487-4650. Rush orders may be placed for an extra fee by calling (800) 336-4700.
ARC-12209

Physical Sciences

Acoustic Humidity Sensor

The speed of sound in air depends on the water content.

NASA's Jet Propulsion Laboratory, Pasadena, California

An industrial humidity sensor measures the volume fraction of water in the air via its effect on the speed of sound. The only portion of the sensor that has to be exposed to the sensed atmosphere is a pair of stainless-steel tubes (see Figure 1). The sensor is therefore rugged enough for use in harsh environments like those used to control the drying of paper in paper mills, where most humidity sensors do not survive.

From basic principles of thermodynamics and the kinetic theory of gases, it can be shown that the volume fraction, x, of water vapor in air is related to the speed of sound by

$$x \approx [11.312(C_m/C_d) - 10.611]^{1/2} - 0.837$$

where C_m is the speed of sound in the moist air and C_d is the speed of sound in a control sample of dry air at the same temperature as that of the moist air. This approximation is valid within 1 percent at temperatures from 330 to 1,000 K.

One of the stainless-steel tubes of the sensor is sealed and contains a charge of dry air; the other is perforated to a porosity of about 1 percent to admit the moist air. The objective is to measure the speed of sound in each tube in terms of the time between reflections of pulses of sound from a diametral stub and from an end wall.

The output of a pulse generator is fed to a pair of amplifiers, each of which feeds a transmitting and receiving transducer attached to one end of the tubes. Blocking diodes prevent the short circuiting of the return pulses by the pulse amplifiers and, together with terminating resistors, help prevent oscillations in the reverberant environments of the tubes. Counters measure the intervals between reflected pulses. Delay gates prevent the initial (transmitted) pulses from activating the counters.

Figure 2 shows a typical return signal from the perforated tube. The rumble between the two main reflection waveforms is caused by reflections from the perforations. The round-trip transit time of sound waves is determined from the interval between the first positive peaks in the two main reflection waveforms. One can increase the accuracy of the measurement by averaging over many pulses. Overall, the measurement of the intervals between pulses in the sealed and perforated tubes yields a value of water-vapor content that is correct to within 0.5 percent in the temperature range of interest.

This work was done by Parthasarathy Shakkottai, Eug Y. Kwack, and Shakkottai Venkateshan of Caltech for **NASA's Jet Propulsion Laboratory**. *For further information, Circle 91 on the TSP Request Card.*
NPO-17685

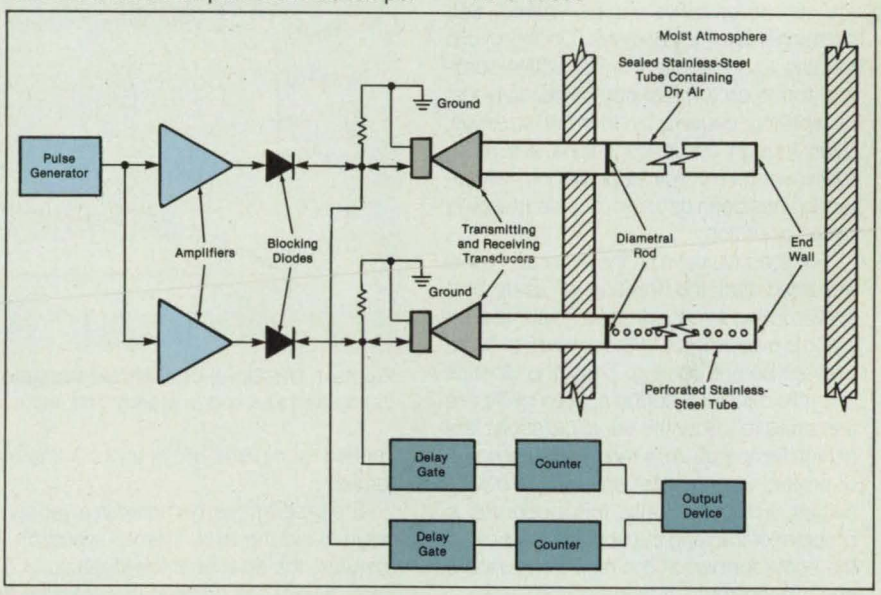

Figure 1. Pulses of Sound are generated and reflected in two tubes, one containing dry air and the other containing moist air. Counters measure the intervals between reflected pulses.

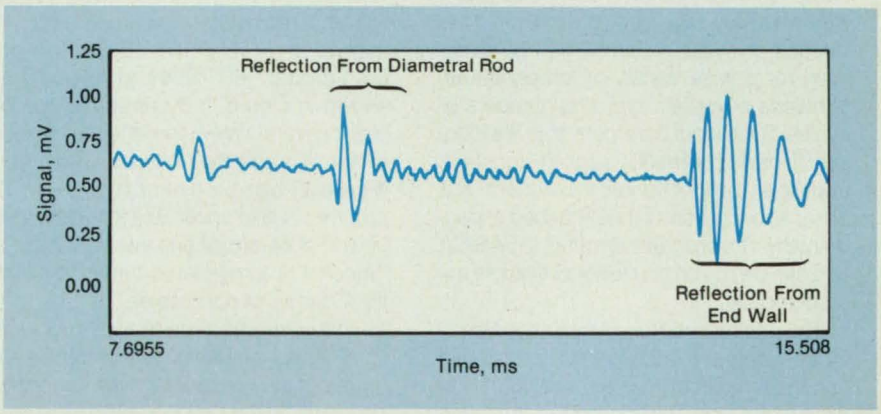

Figure 2. A **Typical Reflection Signal** from the perforated tube includes peaks that represent reflections from the diametral rod and the end wall. The speed of sound in the moist air is inversely proportional to the time between these two reflections.

Computer Simulation of Cyclic Oxidation

A program predicts oxidation kinetics for various durations and numbers of cycles.

Lewis Research Center, Cleveland, Ohio

A computer model has been developed to simulate the cyclic oxidation of metals. High-temperature gas/metal reactions, particularly oxidation, have been studied for many years. These studies have contributed to our basic understanding of oxidation mechanisms. Virtually all of the past studies have been performed in oxidizing environments at constant temperatures to follow reaction kinetics via changes in weight as functions of exposure time. However, in most real applications, exposure to high temperature is not isothermal but rather involves repeated heating and cooling.

For example, cyclic oxidation due to repeated start/stop operations is encountered in the heating elements of electric stoves, automobile-engine valves, and components of jet engines. During cyclic heating and cooling, the protective scale that forms on a metal can be partially lost by spalling caused by thermal stresses. Even though cyclic conditions are more representative of real applications, little attention has been devoted to understanding cyclic oxidation.

For the purposes of the simulation, it is assumed that the fraction of scale that spalls during cooling from a given heating cycle is proportional to the amount of scale present before cooling. Thus, the kinetics of cyclic oxidation during a given cycle are assumed to follow the usual parabolic law at high temperature, altered by the amount of protective scale lost during all previous cycles. Fundamentally, this becomes a problem of tracking the opposing effects of the scale formed at the high temperature and the scale lost during cooling.

Although this leads to rather complicated algebra, it can easily be handled by numerical methods on a computer. Thus, with relatively few input parameters, the kinetics of cyclic oxidation can be simulated for a wide variety of temperatures, durations of cycles, and total numbers of cycles. Such input parameters as the identity of oxide, parabolic scaling constant, and spall proportionality constant are either known or can be determined experimentally. The program is written in BASICA and can be run on any IBM-compatible microcomputer.

The original premise of the proportionality between the fraction of scale spalled and the amount of scale present has been experimentally demonstrated for both Cr_2O_3 formers and Al_2O_3 formers. The predictive abilities of the program have been verified for several alloys and coating materials.

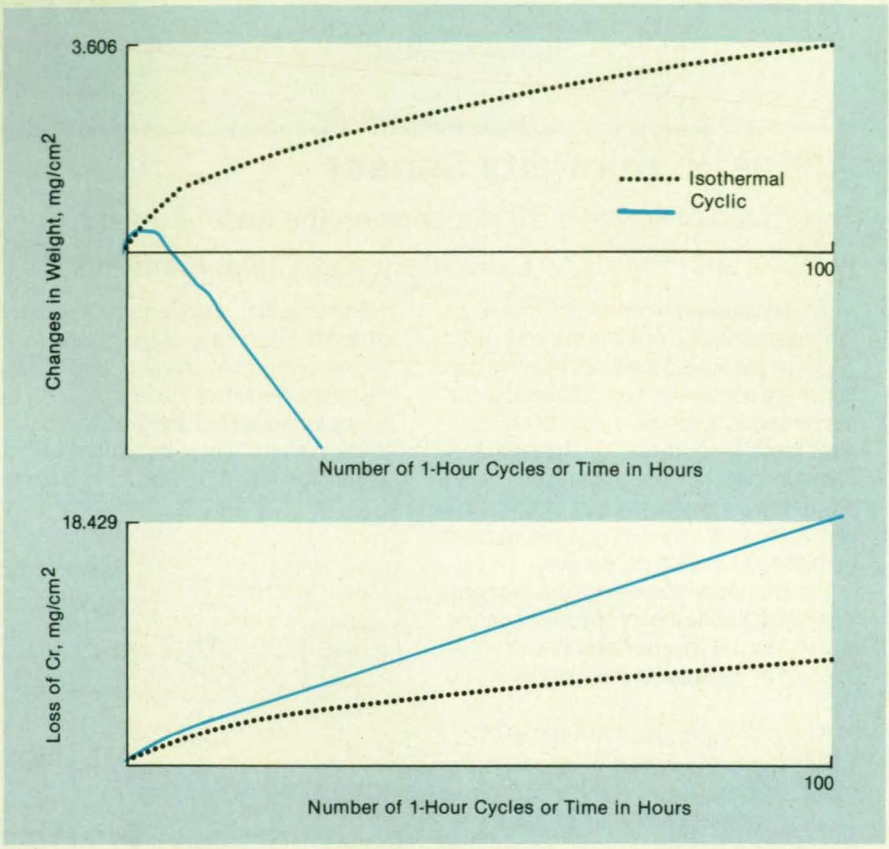

Figure 1. The **Simulation Shows the Gain or Loss** of weight of a sample of metal during oxidation and spalling in steady and cyclic heating.

The program can be used in a variety of ways to aid the experimental research. In minutes, the effects of the duration of the cycle and/or the number of cycles on the oxidation kinetics of a material can be surveyed. The output of the program provides plots of the weight of the sample and the amount of metal consumed in both isothermal and cyclic conditions. Such plots for Inconel* 601 alloy at 1,100 °C are shown in Figure 1. By rerunning the program several times, the effect of duration of the cycle on the consumption of metal (Figure 2) can be determined easily. The program is also applicable to the cyclic oxidation of ceramics and intermetallics.

*Inconel is a registered trademark of the INCO family of companies.

This work was done by H. B. Probst and C. E. Lowell of **Lewis Research Center**. *More detailed coverage of the concepts is contained in the October 1988 issue of the Journal of Metals, p. 18. The program may be obtained without charge by a written request to either author accompanied by a formatted 5-1/2" floppy diskette. Please state the density of the diskette, either high (1.2 Mb) or normal (320 Kb).*

LEW-14890

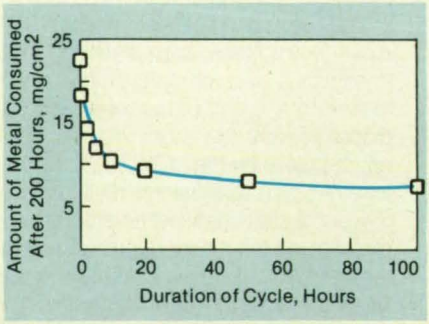

Figure 2. The **Effect of the Duration of the Cycle** on the loss of metal can be computed by rerunning the program several times.

Integrated Grating Spectrometer

An entire spectrometer would be fabricated on a silicon wafer.

NASA's Jet Propulsion Laboratory, Pasadena, California

The fabrication of a grating spectrometer as a monolithic, layered, waveguide structure on a silicon wafer rather than with conventional optical components could reduce volume and weight by a factor of over a thousand. Because it would be a monolithic structure, its alignment would be permanent. The proposed spectrometer would occupy an area of about 2 cm^2 on a wafer 0.4 mm thick. In contrast, a typical conventional spectrometer is 50 to 100 cm long and difficult to keep in alignment.

The proposed spectrometer (see Figure 1) would operate in the visible spectrum (wavelengths of 400 to 700 nm) and would be blazed to diffract in the first order. The 2-μm-thick SiO_2 lower cladding layer (refractive index 1.46) would be grown thermally on the silicon substrate. The 2-μm-thick Si_3N_4 waveguide layer (refractive index 2.05) and the 2-μm-thick SiO_2 upper cladding layer would be grown by chemical-vapor deposition.

The input light beam would be injected into the spectrometer by a multimode optical fiber. The output at a particular wavelength could be picked up with a second fiber or by a linear array of detectors that would provide a series of outputs over a range of wavelengths. An array of such spectrometers could be used to provide spectral analysis of a line image (see Figure 2).

The diffraction grating would be defined by electron-beam lithography and etched into the waveguide by reactive ion etching. This technique would enable continuous independent variation, along the grating, of the pitch, curvature, and blaze angle. The grating could thus be designed to have a large numerical aperture, zero aberration at two selected wavelengths, and very low aberration at intermediate wavelengths.

The length of the device has been chosen to be 20 mm, and the width must be 10 mm to provide the desired numerical aperture. The dispersion of the spectrometer has been chosen to be 10 nm of wavelength per 50 μm of lateral distance, a distance about the size of a single picture element in a typical array of detectors. The grating pitch (groove spacing) necessary to achieve this dispersion is about 1.95 μm — well within the capacity of an electron-beam lithography system that has a spot 8 nm wide.

This work was done by Robert J. Lang of Caltech for **NASA's Jet Propulsion Laboratory**. *For further information, Circle 140 on the TSP Request Card.*
NPO-17733

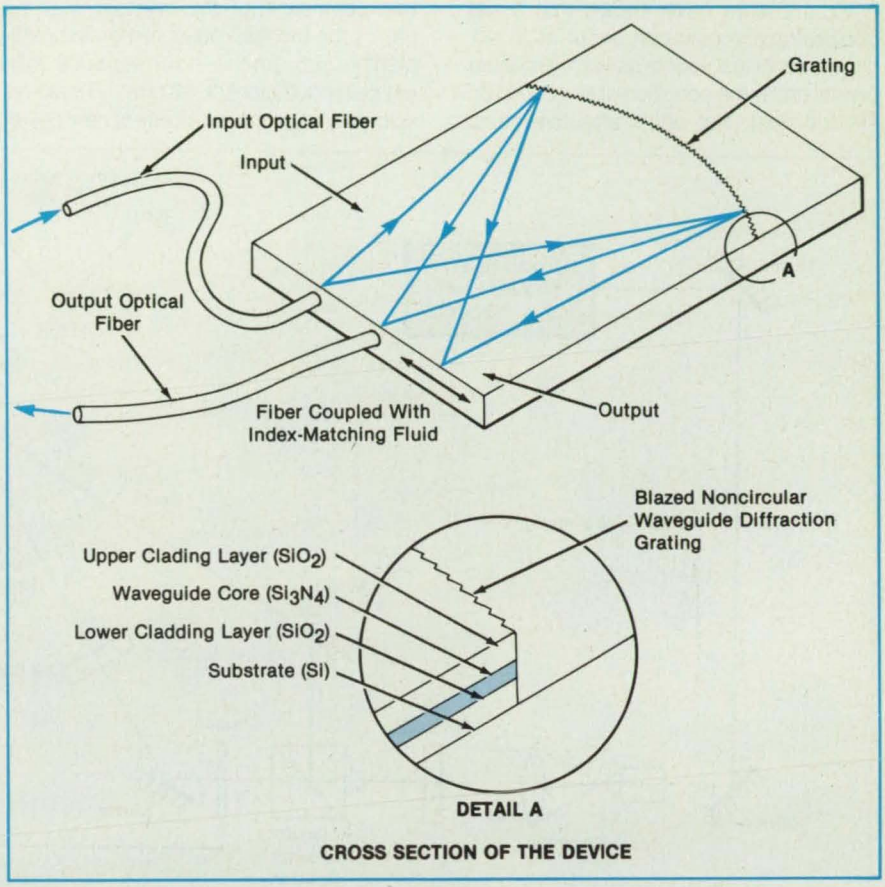

Figure 1. The **Proposed Integrated Grating Spectrometer** would be made in a waveguide layer on a silicon wafer.

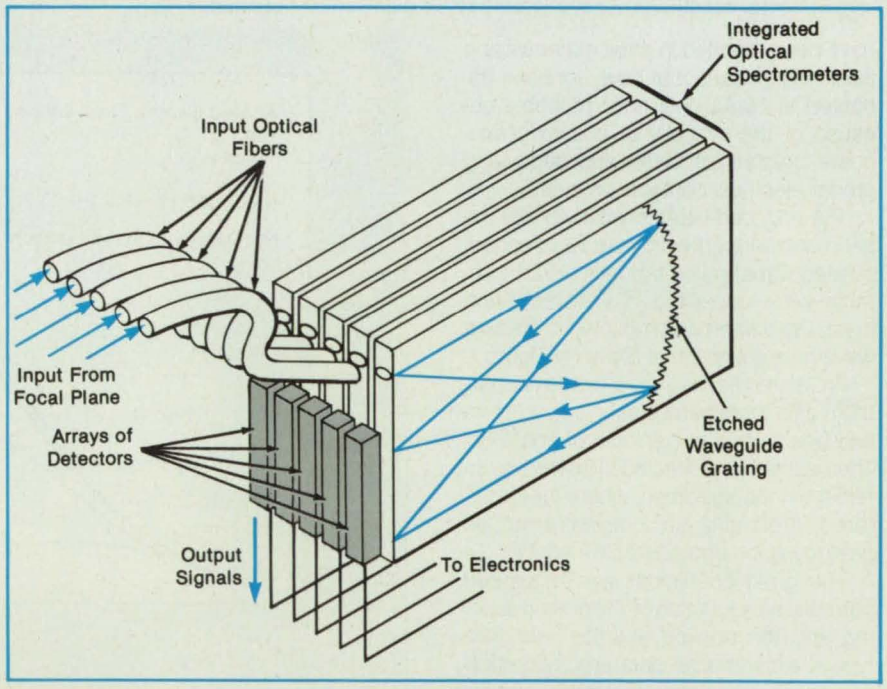

Figure 2. An **Array of Integrated Grating Spectrometers** would perform spectral analysis of the picture elements along a line. An optical fiber would couple the light from each picture element into a separate integrated spectrometer.

Net Photorefractive Gain in Gallium Arsenide

Prerequisite includes an applied electric field.

NASA's Jet Propulsion Laboratory, Pasadena, California

Experiments have shown that a net photorefractive gain can occur in an undoped semi-insulating gallium arsenide crystal under the condition of an applied dc electric field. Net photorefractive gains have been reported in other materials and predicted in GaAs, but have not been observed in GaAs until now, probably because of the difficulty of obtaining adequate crystals of GaAs and depositing proper electrical contacts on them.

The undoped GaAs crystals for the experiment were grown by the liquid-encapsulated Czochralski process. In/Zn contacts were deposited in vacuum. Each crystal specimen was mounted in the two-wave-mixing apparatus shown in Figure 1.

An infared beam from a neodymium:yttrium aluminum garnet laser was split into two beams in a power ratio of about 60. The beams were directed by mirrors to intersect in the specimen, where they interfered, producing an index-of-refraction grating via the photorefractive effect.

The grain coefficient was measured normally as a function of the grating spacing and the applied electric field. The typical experimental data and theoretical curves in Figure 2 show that the theoretical values of the grain coefficient have been attained. Because the measured absorption coefficient of the crystals was 1.3 cm^{-1}, the highest measured grain coefficient — 2.6 cm^{-1} — corresponds to a net gain coefficient of 1.3 cm^{-1}. These results may offer the possibility of new developments in real-time optical processing of signals by use of near-infrared lasers of low power.

This work was done by Tsuen-Hsi Liu and Li-Jen Cheng of Caltech for **NASA's Jet Propulsion Laboratory**. *For further information, Circle 47 on the TSP Request Card.*

NPO-17626

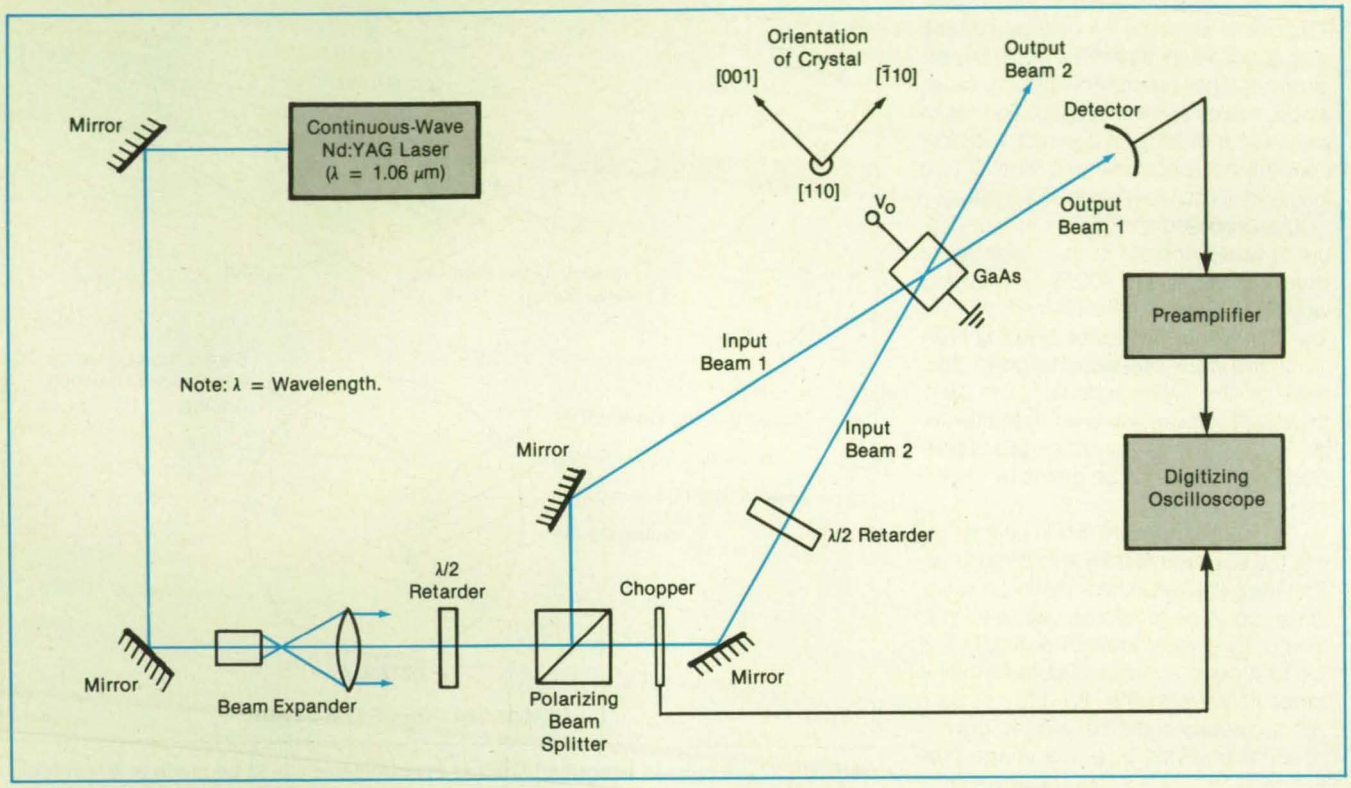

Figure 1. An **Electric Field Is Applied** to a GaAs crystal in which two infrared beams interfere. Depending on the quality of the sample and the experimental conditions, a net photorefractive gain can be obtained.

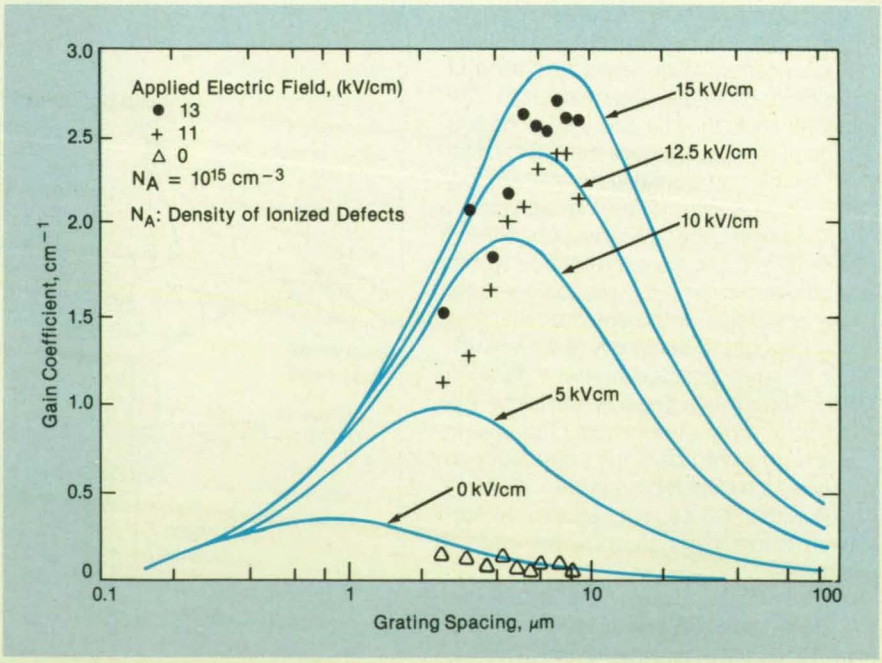

Figure 2. The **Gain Coefficient** as measured is compared with the theoretical coefficient at various applied fields, as a function of the spacing of the index-of-refraction grating (induced by intensity interference fringes at the intersection of the incoming laser beams).

Improved Liquid-Electrode/Solid-Electrolyte Cell

An organic liquid in the cathode may extend the working life.

NASA's Jet Propulsion Laboratory, Pasadena, California

A rechargeable solid-electrolyte electrochemical cell includes a novel mixture of organic and inorganic materials in a liquid cathode. As a consequence, the liquid cathode is more compatible with the β''-alumina solid electrolyte than are materials in such other types of liquid-electrode cells as sodium/sulfur. Moreover, the new cell operates at a temperature about 120 to 170 °C lower than that of sodium/sulfur cells. The new cell offers an energy density comparable to that of sodium/sulfur cells — about 150 Wh/kg — and thus is well suited to such applications as military systems and electric vehicles.

The liquid anode is molten sodium. The liquid cathode, tetracyanoethylene (TCNE), is mixed with sodium aluminum tetrachloride ($NaAlCl_4$). A tube of β'' alumina separates the liquid cathode from the liquid-sodium anode (see figure). The TCNE/$NaAlCl_4$ mixture attacks the alumina far less aggressively than does the molten sulfur used as the cathode material in previous cells of this general type. The lower operating temperature (230 °C vs. 350 to 400 °C in the Na/S version) reduces the deterioration of the alumina even further.

In tests of the new cell, the alumina separator appeared uncorroded and undamaged after six charge/discharge cycles. The open-circuit voltage proved to be a good indicator of the charge remaining in the battery. It decreased approximately linearly from about 3.5 V to about 1.9 V when the 45-mAh test cell was discharged by 30 mAh.

This work was done by Ratnakumar V. Bugga, Salvador DiStefano, Roger M. Williams, and Clyde P. Bankston of Caltech for **NASA's Jet Propulsion Laboratory.** *For further information, Circle 51 on the TSP Request Card.*
NPO-17604

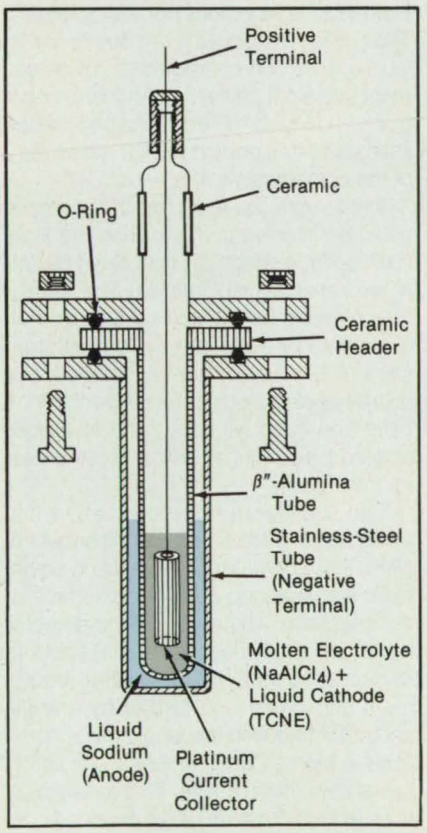

The **Tube of Solid Electrolyte** contains a novel liquid electrolyte mixture and a platinum wire grid current collector. A concentric outer tube holds the liquid-sodium anode.

X-Ray Fluorescence Surface-Contamination Detector

The x-ray spectrum of a contaminating element would reveal its presence.

Marshall Space Flight Center, Alabama

A proposed x-ray fluorescence spectrometer would be used to detect a thin layer of Conoco HD-2 (or equivalent) grease on D6-ac steel. Steels are frequently contaminated by greases, and during some manufacturing processes it is important to detect such contamination because it can adversely affect adhesive bonding, painting, and other surface treatments.

In x-ray fluorescence spectroscopy, one illuminates the specimen with x rays or low-energy γ rays and uses a suitable detector to monitor the spectrum of the resulting x-ray fluorescence emitted by the specimen. By a judicious choice of the source of radiation, one can limit the analysis to photon energies characteristic of a selected range of atomic species. One can also choose a detector and filters to reduce further the spectral contributions of background radiation, including that from elements that one does not wish to detect. Then if the detected x-ray spectrum includes a portion characteristic of an element that is part of the contaminant but not of the underlying material, one can use the intensity of that portion to infer the amount of the contaminant.

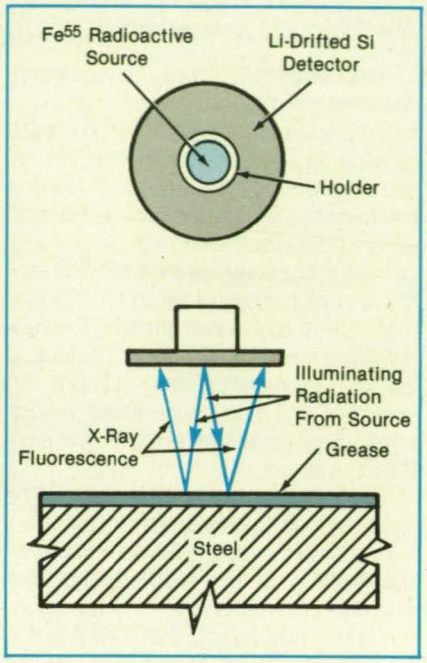

X-Ray Photons From the Fe^{55} Source would cause calcium in the grease to emit lower energy photons, some of which would strike the detector.

In this case, the thickness of the grease could be inferred by measuring the x-ray fluorescence spectrum near the 4.09-keV K_α excitation edge of calcium. The fluorescence would be excited by 5.9-keV and 6.5-keV x rays that result from electron capture in a radioactive Fe^{55} source. The source would be a disk mounted concentrically and flush with the face of a disk-shaped lithium-drifted silicon x-ray detector (see figure).

The source-and-detector assembly would be mounted on a remote manipulator with other contamination-detecting equipment and scanned across the surface of the specimen. The output of the detector would be fed through a coaxial cable to standard pulse-height-analyzing equipment and processed further by a small computer to obtain the x-ray energy spectrum. A Monte Carlo numerical simulation has shown that if a layer of grease 100 Å thick (about 10 mg/m^2) were illuminated by a 1-curie Fe^{55} source, it would produce a counting rate of 1 photon per second at the calcium peak. If the count could be prolonged for an hour, the precision of the measured calcium peak would be 1.7 percent.

This work was done by Hudson B. Eldridge of the University of Central Arkansas and Ralph Carruth of **Marshall Space Flight Center**. *For further information, Circle 105 on the TSP Request Card.*

Inquiries concerning rights for the commercial use of this invention should be addressed to the Patent Counsel, Marshall Space Flight Center [see page 14]. Refer to MFS-27222

Books and Reports

These reports, studies, handbooks are available from NASA as Technical Support Packages (TSP's) when a Request Card number is cited; otherwise they are available from the National Technical Information Service.

Processing of Multispectral Data for Identification of Rocks

Linear discriminant analysis and supervised classification are evaluated.

A report discusses the processing of multispectral remote-sensing imagery to identify kinds of sedimentary rocks by their spectral signatures in geological and geographical contexts. The raw image data are the spectra of picture elements in images of seven sedimentary rock units exposed on the margin of the Wind River Basin in Wyoming. The data were acquired by the Landsat Thematic Mapper (TM), the Thermal Infrared Multispectral Scanner (TIMS), and the NASA/JPL airborne synthetic-aperture radar (SAR).

To construct and analyze the extended spectral signature for each picture element, it was first necessary to register the three sets of data. This was accomplished by use of a "rubber-sheet stretch" based on tie points that appeared to be the same in all images and that were selected manually. All data were then resampled with picture elements of the same size as, and registered with, the TM picture elements. All images were normalized by use of a Gaussian contrast stretch because the data are not calibrated, and it was thought that the differences between the dynamic ranges of the different sensors might bias the analysis. In addition, a 5-by-5 median-value filter was applied to the SAR data to suppress the effects of speckle.

The resulting extended spectral signatures were analyzed by two techniques: linear discriminant analysis (LDA) and supervised classification. In LDA, areas of known rock types are selected as training areas, and means and standard deviations for each training area in each image are calculated. The LDA computer program then determines which image is best for discriminating among the training areas by computing the discriminant function for

each area and attempting to separate training areas into groups. Remaining images are then checked at the next step to find the next-most-useful image for separating the training areas into groups, and so on. In this way, images can be ranked in order of their utility for separating the training areas, and it is possible to determine which set of data contributes most to the discrimination between specific rock units.

This procedure provides only classification accuracies for the training areas themselves and may not necessarily represent the ability to classify areas outside the training areas. The results of LDA show that the use of the TM, TIMS, and SAR data (instead of one of these sets of data alone) increases the ability to differentiate training areas. However, it is also important to be able to map the extent of the lithologic units that were selected in the analysis. Moreover, in order to extend lithological information to poorly understood areas it is important to be able to use training areas from well-characterized test sites to classify other areas.

A supervised classification was performed both in the training areas of the original study area and at an adjacent site. A parallelepiped algorithm was used to determine a decision boundary of each spectral band. To be assigned to a class, a picture element had to fall within the N-dimensional decision boundary for that class. If the spectral signature of a picture element fell outside the decision boundary for all classes, the picture element was assigned to the unknown class. A picture element, the spectral signature of which fell within the decision boundary for more than one class, was considered ambiguous. This ambiguity was then resolved by use of the Bayes maximum-likelihood algorithm. Classification accuracies were determined by subtracting the supervised-classification maps from a digitized version of a photogeologic map obtained previously to determine errors of omission and commission.

The results of supervised classification show that while multisensor data provide an overall improvement in the accuracy of classification, some units may be better classified by use of data from an individual sensor. Thus, if an investigator is interested only in a particular type of sedimentary rock, a sensor can be optimized to search for a distinguishing characteristic. However, the classification of a variety of types of rock is more accurate when use is made of multisensor data that are sensitive to such different characteristics of rocks as mineralogy and surface roughness.

This work was done by Diane L. Evans of Caltech for **NASA's Jet Propulsion Laboratory**. *To obtain a copy of the report, "Supervised Classification of Sedimentary Rocks Using Extended Spectral Signatures," Circle 81 on the TSP Request Card. NPO-17581*

Materials

Hardware, Techniques, and Processes

Books and Reports

Advanced Reusable Foam Cryogenic Insulation

Specimens have been demonstrated in the temperature range of −420 to +400 °F (−251 to +204 °C).

Langley Research Center, Hampton, Virginia

Lightweight, reusable cryogenic containers are needed to reduce the costs of operation of advanced hypersonic airplanes and space launch vehicles. Such containers may also be useful on Earth in laboratories, factories, and transportation systems. One essential element of a reusable cryogenic tank is insulation that can repeatedly endure exposure to relatively high temperatures during entry into the atmosphere, and thus reduce the external thermal-protection system (TPS) mass. Studies have shown that an increase in the reuse temperature of the insulation from 175 to 400 °F (79 to 204 °C) can reduce the mass of the TPS by 20 to 50 percent, approximately 0.3 to 1.0 lb/sq ft (1.5 to 5 kg/m^2), and reduce the thickness of the TPS by about 50 percent, from 3.0 to 1.5 in. (7.6 to 3.8 cm).

A prototype reusable cryogenic foam insulation developed for this purpose has a maximum service temperature of 400 °F (204 °C). It consists of two discrete layers of closed-cell polymethacrylimide foam of density 6.9 lb/ft^3 (111 kg/m^3) bonded together with an epoxy adhesive. The bond line is additionally reinforced with a 0.003-in. (0.08-mm)-thick layer of fiberglass cloth. The resulting block of foam is wrapped with a precut and preformed vapor-barrier cover made of the non-permeable, high-temperature material, Kapton (or equivalent)/aluminum/Kapton (or equivalent) (KAK). The covered insulation blocks are externally bonded to the wall of the cryogenic tank.

Several specimens, each 2 in. (5 cm) thick and 10 in. (25 cm) square, bonded to an aluminum panel, have been fabricated to verify the manufacturing techniques. A specimen was successfully tested during 100 thermomechanical cycles, which consisted of cooling the surface of the metal to −323 °F (−197 °C) while heating the outer surface of the foam insulation with air at 400 °F (204 °C) to simulate aerodynamic heating. A tensile load of 15,000 lb (67 kN) was simultaneously applied in the aluminum panel to represent the internal pressure in the tank. In a similar test of another specimen, the insulation was exposed to the air at 400 °F (204 °C), while the metal surface of the tank was exposed to −420 °F (−251 °C) for 20 cycles.

In both tests, the foam suffered no apparent damage. Yet another specimen endured over 250 thermal cycles in which the cold surface was alternately cycled 9 times to −320 °F (−196 °C) followed by 1 cycle to −420 °F (−251 °C). Specimens made of materials of lower density [4.4 and 3.1 lb/ft^3 (70 and 50 kg/m^3, respectively)] have also been fabricated and tested. The conductivity and permeability of the cryogenic foam insulations will be determined over the range of environmental conditions anticipated during service in both external and internal applications. The initial data on conductivity were generated by use of a guarded-hot-plate calorimeter. A boiloff calorimeter is being rehabilitated to obtain data on conductivity at temperatures near that of liquid hydrogen.

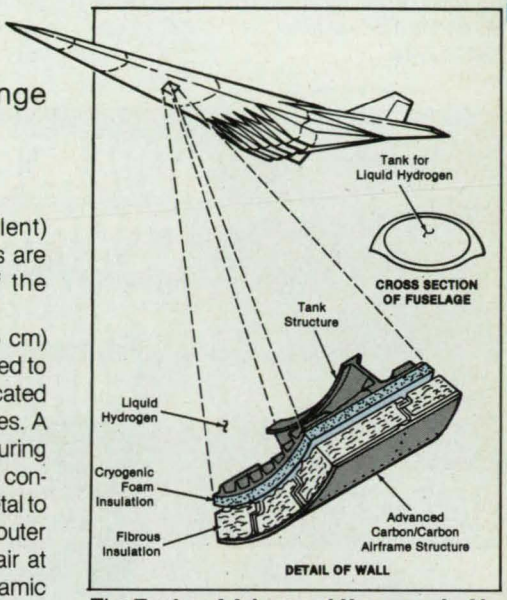

The **Tanks of Advanced Hypersonic Aircraft** or space launch vehicles might include reusable foam insulation to insulate the cryogenic propellants.

This work was done by Allan H. Taylor of **Langley Research Center**, *P. S. McAuliffe of Lockheed California Co., and L. L. Sparks of the National Bureau of Standards. For further information, Circle 67 on the TSP Request Card.*
LAR-14014

Books and Reports

These reports, studies, handbooks are available from NASA as Technical Support Packages (TSP's) when a Request Card number is cited; otherwise they are available from the National Technical Information Service.

Prototype V-Groove Radiator Heat Shield

A space-saving unit has been designed and tested.

A report describes design, fabrication, and testing of a heat radiator equipped with a multi-V-groove radiator heat shield. The device is a compact, efficient structure intended to remove heat from infrared detectors, gamma-ray detectors, and similar instruments aboard the Mars Observer spacecraft and radiate that heat into outer space. It is designed to maintain a detector for a gamma-ray spectrometer at a temperature of 80 K in a cold vacuum under a heat load of 80 mW.

The prototype multiple V-groove shields are made of aluminum, though the production shields would be made of aluminized sheets of polyethylene terephthalate. The shields surround the cold-stage radiator plate, protecting the stage from heat radiated toward it from the sides.

A thermal-analysis mathematical model was used to size the radiator, specify the types and quality of the thermal coatings and finishes, select the number of shields, and determine the thermal parameters for

the support system. The model was also used to predict the temperatures of the assembly in orbit about Mars. The assembly, including a 1.7 kg mockup of the detector assembly, was successfully vibration-tested to the Mars Observer orbit specifications.

This work was done by S. Walter Petrick and Steven Bard of Caltech for **NASA's Jet Propulsion Laboratory**. *To obtain a copy of the report, "Design, Fabrication, and Dynamic Testing of a V-Groove Radiator Mechanical Development Unit," Circle 90 on the TSP Request Card.*
NPO-17744

High-Temperature Materials for Stirling Engines

Heat-resistant piston rings and linings could increase engine efficiency.

A report discusses research on materials for piston rings and cylinder coatings in automotive Stirling engines. The materials will make it possible to place piston rings at the tops of pistons ("hot" piston rings) instead of at the cooler bottoms. Engine efficiency will thereby be increased by several percent.

Candidate materials were tested on a pin-on-disk machine, which measures wear and friction. The tests were performed in hydrogen at temperatures up to 760 °C to simulate the conditions in a typical automotive Stirling engine. The data from the tests show that a cobalt-based alloy, Stellite 6B, is a good choice for the piston rings and PS200, a plasma-sprayed metal-bonded chromium carbide matrix with dispersed solid lubricants, will function well as the cylinder coating.

An automotive Stirling engine was then modified by the incorporation of these materials into a "hot"-piston-ring structure. As a result, the specific fuel consumption of the engine was reduced by an average of 3 percent and by as much as 7 percent under some operating conditions, in comparison with that of the unmodified engine.

It was found that certain properties of materials indicate the likelihood that they will function as solid lubricants in a given temperature range. These properties are plasticity, low yield strength in shear, low hardness, and thermochemical stability in the environment of interest.

Some combinations of two or more solid lubricants can be incorporated into composites to lubricate over a broader temperature range than any single material can. The PS200 cylinder coating is an example. It includes silver and barium fluoride/calcium fluoride eutectic dispersed in the matrix of metal-bonded chromium carbide. Silver alone lubricates up to about 500 °C, and the fluoride lubricates from 400 to 900 °C. The combination lubricates from room temperature to 900 °C.

This work was done by Harold E. Silney of **Lewis Research Center**. *Further information may be found in NASA TM-100276 [N88-15872], "Hot Piston Ring/Cylinder Liner Materials — Selection and Evaluation."*

Copies may be purchased [prepayment required] from the National Technical Information Service, Springfield, Virginia 22161, Telephone No. (703) 487-4650. Rush orders may be placed for an extra fee by calling (800) 336-4700.

This invention is owned by NASA (U.S. Patent No. 4,728,448). Inquiries concerning nonexclusive or exclusive license for its commercial development should be addressed to the Patent Counsel, Lewis Research Center [see page 14]. Refer to LEW-14836

Is your subscription about to expire?

Check the expire date. If it is less than 6 months now is the time to fill out a new qualification form before your subscription expires.

CHOOSE INCO COATED PRODUCTS FOR HIGH PURITY AND PREDICTABLE PROPERTIES.

Nickel Coated Graphite Powders

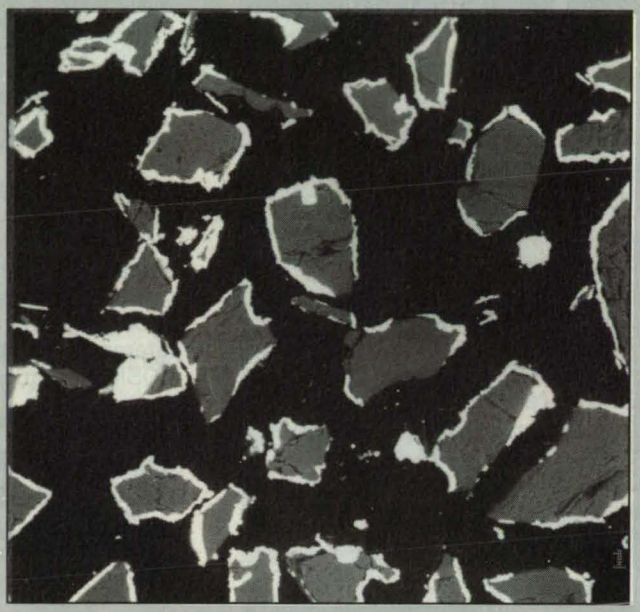

Nickel Coated Alumina

INCO Specialty Powder Products' development of the use of carbonyl gas coating allows deposition of nickel with very high purity and predictable properties and is uniquely suited for a variety of coated products and applications.

INCO SPP COATED PRODUCTS

Nickel combines a unique mixture of special physical, conducting and magnetic properties. The ability to deposit nickel on various substrates greatly extends the potential for the use of these properties. Coatings are being made, for example, on silica, graphite, alumina, tungsten carbide, clays and ceramics. INCO SPP has the capability to coat special substrates on a custom basis for individual users.

APPLICATIONS

New uses for INCO SPP Coated Products include conducting film technology, electronics packaging, EMI shielding, electronic detection devices, controlled heating systems, hard metals and powder metallurgy parts.

RESEARCH

INCO SPP research activities for this line of products include nickel carbonyl coated powders and other substrates. Applications include advanced products for EMI shielding, ESD, arc welding, powder metallurgy additives, and in battery technologies.

One highly interesting area of research is in the area of electronic detection. Coated products are being combined with paint for highway divider strips and as ink in bar codes for vehicle identification. This could provide an accurate measure of automobile speed on those highways. Another futuristic consideration is "computer trips for cars" using those strips and bar codes to program automotive travel and identification.

INCO SPP

INCO Specialty Powder Products is your unique resource for coated products. Our customer focused worldwide marketing service group is ready to help you with your current and future needs for coated products.

For more information write INCO Specialty Powder Products, Dept. 2-90, Park 80 West-Plaza Two, Saddle Brook, NJ 07662

INCO SPP

Park 80 West-Plaza Two, Saddle Brook, NJ 07662
Shin-Muromachi Building, 4-3 Nihonbashi-Muromachi 2-Chome, Chuo-ku, Tokyo 103 Japan
1-3 Grosvenor Place, London SW1X7EA England
15/Fl Wilson House, 19-27 Wyndham Street Central, Hong Kong

Circle Reader Action No. 452

Computer Programs

COSMIC: Transferring NASA Software

COSMIC, NASA's Computer Software Management and information Center, distributes software developed with NASA funding to industry, other government agencies and academia.

COSMIC's inventory is updated regularly; new programs are reported in *Tech Briefs*. For additional information on any of the programs described here, circle the appropriate TSP number.

If you don't find a program in this issue that meets your needs, call COSMIC directly for a free review of programs in your area of interest. You can also purchase the annual *COSMIC Software Catalog*, containing descriptions and ordering information for available software.

COSMIC is part of NASA's Technology Utilization Network

COSMIC® — *John A. Gibson, Director,*
(404) 542-3265
The University of Georgia, 382 East Broad Street, Athens, Georgia 30602

Computer Programs

These programs may be obtained at a very reasonable cost from COSMIC, a facility sponsored by NASA to make computer programs available to the public. For information on program price, size, and availability, circle the reference number on the TSP and COSMIC Request Card in this issue.

Mathematics and Information Sciences

Making Mosaics of SAR Imagery

Minimal intervention by the operator is required.

Spaceborne synthetic-aperture-radar (SAR) images are useful for the mapping of planets and investigations in the Earth sciences. However, the widths of SAR swaths rarely exceed 100 kilometers, and images must be patched together to create mosaics to enable the analysis of larger areas. The primary function of the MOSK computer program is to generate large digital mosaics of SAR imagery without manually marked tiepoints.

MOSK can produce a multiframe mosaic by combining images along the ground track, in adjacent cross-track swaths, or in ascending and descending passes. Images registered with geocoded maps such as the ones produced by MAPJTC (NPO-17718), are required as input. The output is a geocoded mosaic on a standard map grid, which enables easy registration with other geocoded sets of data.

Making a mosaic of geocoded SAR imagery involves three steps. First, a match point is selected at the center of the overlapping area, then an image patch around the match point is extracted from both images and cross-correlation is done on this area. Then images with their refined match points are merged together to form a mosaic. To handle the large volume of data from overlapping intermediate stages, large mosaics are divided into quadrants of equal size, with each quadrant cut from an intermediate mosaic. The full mosaic can then be assembled from the individual quadrants. Finally, radiometric disparities at the seams in the image are smoothed by a "feathering" technique.

The automatic mosaic system generates output with minimal interaction with operator. However, manual tiepointing is required in cases of a large errors in registration or of two images with smooth surfaces such as ocean images.

Mechanics

Measuring Changes in Dimensions of Turbine Blades

A mechanical fixture and electronic gauge probe the surface before and after fabrication processes.

Marshall Space Flight Center, Alabama

An assembly of commercially available devices measures changes in the dimensions of an irregularly shaped part. The assembly was developed specifically to measure the thickness of material added to or removed from the surface of a turbine blade during fabrication processes.

The part to be measured is clamped at a preset torque (by means of a torque wrench) in a vise on a rotary table and turned to face the mechanical probe of an electronic depth gauge (see figure). The probe is mounted on a three-axis translation stage, the translating micrometer of each axis of which has a precision of ± 0.0005 in. (± 13 μm). The translation stage is adjusted until the probe touches the surface of the part at the desired point. The operator records the angle of the rotary table, the settings of the translation-stage micrometers, and the reading of the electronic depth gauge. The operator repositions the probe to many different spots on the surface of the part, recording the readings at each spot.

The part is processed — with its clamping surfaces protected so that they are not coated or milled, then returned to the vise and clamped in place at the same preset torque. The operator sets the rotary table at its previous angles and returns the probe to each previously selected point on the surface of the part. Again, the operator records the indications of the electronic depth gauge. The difference between the second and first readings at each point reveals the change in thickness at each spot.

This work was done by William H. Woodford of Martin Marietta Corp. for **Marshall Space Flight Center**. *No further documentation is available.*
MFS-28338

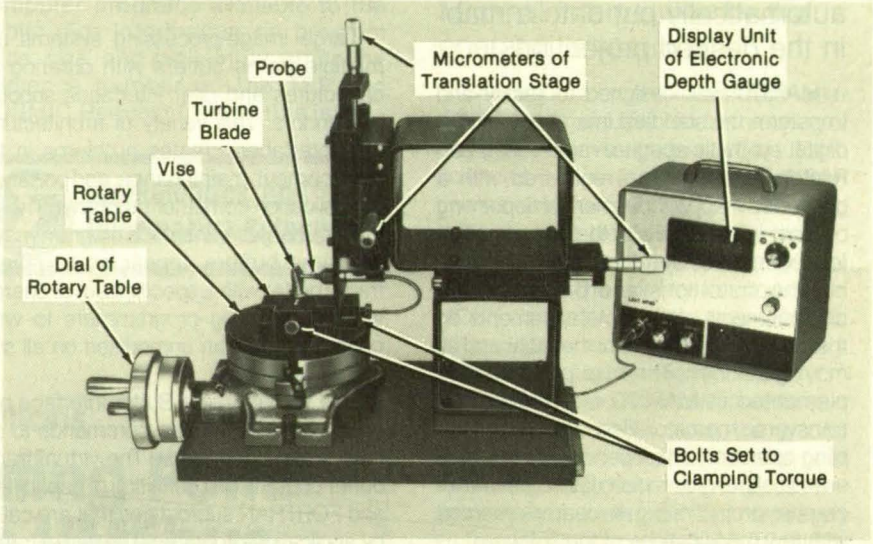

A **Turbine Blade Clamped on a Rotary Table** is touched by the probe of an electronic depth gauge. Positioned by the micrometers of a three-axis translation stage, the probe just touches the blade.

Steel Foil Improves Performance of Blasting Caps

Performance is five times that of standard blasting caps.

Langley Research Center, Hampton, Virginia

Blasting caps, which commonly include deep-drawn aluminum cups, can give significantly higher initiation performance by application of steel foils on the output faces. Past research sponsored at the NASA Langley Research Center on initiation of explosives across hermetically sealed interfaces was applied to common blasting caps to determine whether performance could be improved inexpensively. The explosive-transfer variables studied in that research are summarized in the figure.

The most significant variable was found to be the closure-fragment energy ($E = \frac{1}{2} mV^2$). The capability for initiation was assessed by increasing the airgap between the donor and acceptor. At gaps ap-

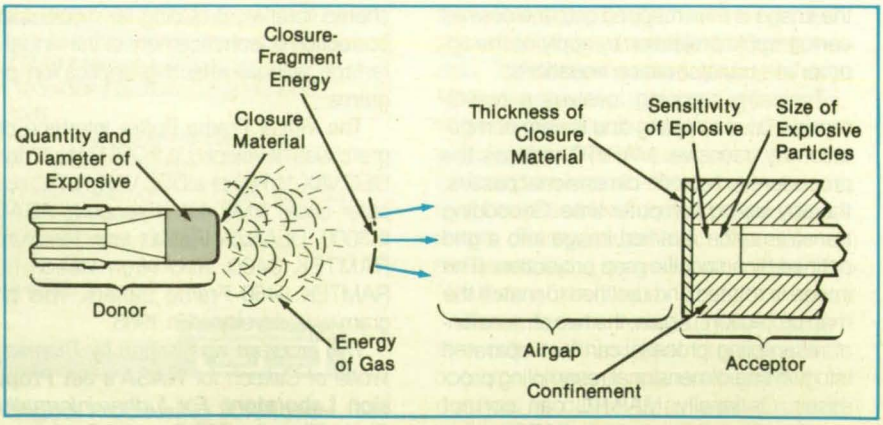

The **Most Significant Variable** is the closure-fragment energy.

MOSK is implemented on a DEC VAX 11/785 computer running VMS 4.5. Most subroutines are in FORTRAN, but three are in MAXL and one is in APAL. The program requires 1 Mb of memory and a Floating Point Systems AP-5210 array processor. The system memory usage is approximately 1,000 pages, and the requirement of page file size is 2,000 blocks. MOSK was developed in 1988.

This program was written by John C. Curlander, Ronald Kwok, Shirley S. Pang, and Amy A. Pang of Caltech for **NASA's Jet Propulsion Laboratory**. *For further information, Circle 33 on the TSP Request Card.*
NPO-17586

Extracting Geocoded Images From SAR Data

The SAR imagery is automatically put onto a map in the desired projection.

MAPJTC was designed to rectify and transform the standard image output of a digital synthetic-aperture-radar (SAR) correlator into an image registered with a geocoded map, without manual tiepointing or other interaction with the operator. This is accomplished by mathematically modeling the distortions and predicting the displacements of the picture elements on the basis of parameters of the radar and its moving platform. The map projection implemented in MAPJTC is the universal transverse mercator. Because the resampling operation is independent of the generation of transformation data, other cartographic projections can be implemented with few modifications of the software.

MAPJTC makes a precise determination of the geodetic location of an arbitrary picture element within the image frame based on the simultaneous solution of a set of Earth-model equations, SAR Doppler equations, and SAR range equations that identify the slant range from the sensor to the target at a specific picture element in the image. On the basis of a table of geodetic coordinates of the picture elements, the image is then mapped onto the desired cartographic projection by applying the appropriate transformation equations.

Typically, mapping involves a two-dimensional resampling and is very computationally intensive. MAPJTC reduces the procedure to two one-dimensional passes, thereby saving computer time. Geocoding transforms the rectified image into a grid defined by a specific map projection. (The image is rotated and rectified to match the map projection.) Again, the two-dimensional resampling process can be separated into two one-dimensional resampling processes. Optionally, MAPJTC can correct terrain-induced distortions in SAR imagery when a digital elevation map is available.

MAPJTC was developed on a DEC VAX 11/785 computer under VMS 4.5. The program is written in FORTRAN (84 percent), APAL (2 percent), and MAXL (14 percent). It requires 6 Mb of memory and a Floating Point Systems AP-5210 Array Processor equipped with 1 Mb of memory. MAPJTC can run interactively or as a batch job. MAPJTC was developed in 1987.

This program was written by John C. Curlander, Ronald Kwok, Shirley S. Pang and Amy A. Pang of **NASA's Jet Propulsion Laboratory**. *For further information, Circle 48 on the TSP Request Card.*
NPO-17418

Virtual Frame Buffer Interface Program

All frame buffers are made to appear as a generic frame buffer.

Large image-processing systems use multiple frame buffers with differing architectures and user interfaces supplied by vendors. This variety of architectures and interfaces creates problems in the development, maintenance, and portability of application computer programs. The Virtual Frame Buffer Interface program makes all frame buffers appear as a generic frame buffer with a specified set of characteristics, allowing programmers to write codes that will run unmodified on all supported hardware.

The Virtual Frame Buffer Interface program converts generic commands to actual device commands. The virtual frame buffer consists of a definition of capabilities and FORTRAN subroutines that are called by application programs. The virtual-frame-buffer routines may be treated as subroutines, logical functions, or integer functions by the application program. Some of the included routines allocate and manage such equipment as frame buffers, monitors, video switches, trackballs, tablets, and joysticks; give access to image-memory planes; and generate alphanumeric fonts or texts. The subroutines for the various "real" frame buffers are in separate VAX/VMS shared libraries, providing for modification, correction or enhancement of the virtual interface without affecting application programs.

The Virtual Frame Buffer Interface program was developed in FORTRAN 77 for a DEC VAX 11/780 or a DEC VAX 11/750 computer under VMS 4.X. It supports ADAGE IK3000, DEANZA IP8500, Low Resolution RAMTEK 9460, and High Resolution RAMTEK 9460 Frame Buffers. This program was developed in 1985.

This program was written by Thomas L. Wolfe of Caltech for **NASA's Jet Propulsion Laboratory**. *For further information, Circle 50 on the TSP Request Card.*
NPO-16713

proximately 0.25 in. (6.4 mm) or more, the gaseous energy is dissipated and does not contribute to initiation. Steel closures 0.005 in. (0.13 mm) thick proved to be more effective than aluminum ones were. The density of steel is about three times that of aluminum, and steel fragments are larger than those produced by aluminum cups. Aluminum cups disintegrate in explosions into very small particles.

Recently, experiments were conducted on an aluminum-shelled blasting cap (2-grain PETN output) to determine whether performance could be improved. Steel foils with a thickness of 0.005 in. (0.13 mm) were first bonded directly to the curved end of the blasting cap and then, to maintain a flat surface, across a port in an aluminum block containing the blasting cap. Performance was evaluated by measuring the velocities of the fragments produced, by obtaining patterns of fragments in transparent polymer witness blocks, and by determining the maximum gap at which the blasting cap could initiate an explosion in a 0.156-in. (3.96-mm)-diameter HNS explosive acceptor in a 0.005-in. (0.13-mm)-thick steel cup. The greater the gap, the greater the demonstrated initiation capability of the donor.

Experimental results showed that the unmodified blasting caps produced fragments with velocities of 14,000 ft/s (4.3 km/s) and very small, scattered impressions in the witness blocks. The blasting cap initiated an explosion of the acceptor explosive at a maximum gap of 0.25 in. (6.4 mm). The blasting caps with the directly bonded steel foil produced fragment velocities of 9,300 ft/s (2.8 km/s) with large craters and unpredictable patterns to such a degree that no attempts were made to initiate explosions.

The blasting caps bonded into aluminum blocks with flat steel foils on the output faces produced fragments with velocities of 10,500 ft/s (3.2 km/s) with large, predictably located craters. The maximum gap for initiation of an explosion in an acceptor was 1.25 in. (31.8 mm). Flat steel foil bonded to the face of a blasting cap perpendicular to its axis improves the performance of the cap by a factor of 5 over that of a standard blasting cap. This improved performance should be useful in military and aerospace applications and in such specialized industries as mining and exploration for oil.

This work was done by Laurence J. Bement of **Langley Research Center**, *Ronnie Perry of PRC Kentron, and Morry L. Schimmel of Schimmel Co. No further documentation is available.*

This invention is owned by NASA, and a patent application has been filed. Inquiries concerning nonexclusive or exclusive license for its commercial development should be addressed to the Patent Counsel, Langley Research Center [see page 14]. Refer to LAR-13832

Feeder System for Particle-Size Analyzer

Powder is metered evenly into flowing gas.

Marshall Space Flight Center, Alabama

A feeder system meters a precise stream of powder into a precise flow of gas. The system is used to feed a light-scattering particle-size analyzer that determines the distribution of sizes of particles in the powder. With the feeder system, dry analysis of a powder takes about one-third the time of conventional wet analysis and consumes less powder (~1 g compared to ~100 g). Furthermore, the feed rate is more precisely controllable, leading to more precision in the analysis. Yet another advantage is that, in dry analysis, there is no need to dispose of hazardous liquid waste.

The dry-analysis light-scattering technique has not been used extensively in the past because of difficulty in maintaining a constant, adjustable flow of powder in a given flow of gas and because the agglomeration of particles in a powder can distort the measurements. The new feeder system vibrates the powder to prevent agglo-

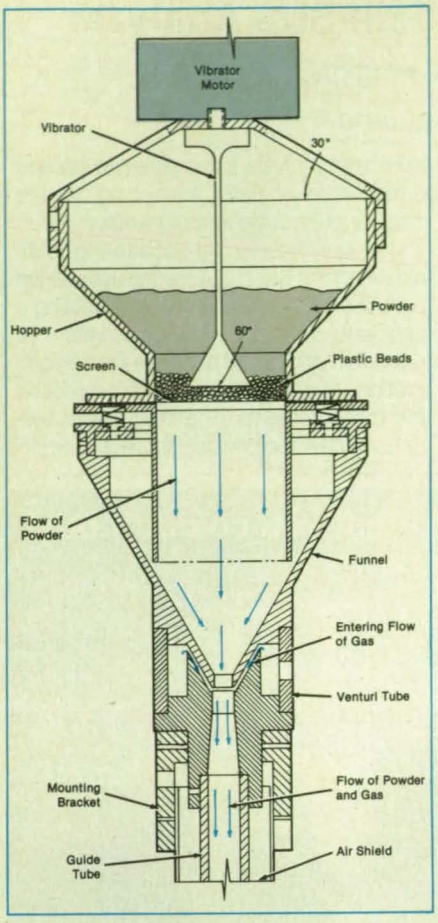

meration and feeds dry powder into a preset volumetric flow of gas.

The sample of powder is placed in a hopper (see figure). At the bottom of the hopper is a screen covered with plastic beads, which together act as a metering device that limits the flow of powder. A vibrator extends downward from the top of the hopper to a point above the screen; driven by a motor, it produces a vertical resonant vibration at the center of the sample. Thus, the sample is prevented from compacting and made to flow at a limited, even rate through the screen. A funnel under the screen directs the falling powder to a low-pressure venturi tube, which introduces gas to aerate and dilute the powder.

This work was done by Keith E. Ramsey of Morton Thiokol, Inc., for **Marshall Space Flight Center**. *For further information, Circle 111 on the TSP Request Card.*

Inquiries concerning rights for the commercial use of this invention should be addressed to the Patent Counsel, Marshall Space Flight Center [see page 14]. Refer to MFS-28326.

The **Feeder System** prevents the formation of clumps of powder and meters the powder into a flow of gas.

Books and Reports

These reports, studies, handbooks are available from NASA as Technical Support Packages (TSP's) when a Request Card number is cited; otherwise they are available from the National Technical Information Service.

Transport of Passive Scalars in a Turbulent Channel Flow

Computer simulation shows flow structures and statistical properties.

A computer simulation of the transport of passive scalars in a turbulent channel flow is described in a report. As used here, "passive scalars" means scalar quantities like fluctuations in temperature or concentrations of contaminants that do not disturb the flow appreciably. The transport of heat and contaminants in turbulent flows is important in engineering. Examples include the transport of heat in heat exchangers, gas turbines, and nuclear reactors and the dispersal of pollution in the atmosphere.

In general, a turbulent flow field causes fluctuations in a scalar field through turbulent convection, whereas the fluctuating scalar field influences the velocity field through mean gradients and changes in

density. However, for small differences in temperature or small concentrations of contaminants, the turbulent velocity field drives the scalar field, and the influence of the latter on the former is rather weak and can be neglected. In such a case, a passive scalar field can be determined independently by solving the conservation equation of the passive scalar for a given turbulent velocity field.

In this study, the three-dimensional Navier-Stokes equations of flow and the equations for the passive scalar fields were solved simultaneously by a finite-difference method on a grid of 128 points along the channel (x direction) and 129×128 points across the channel (y and z directions, respectively). The Reynolds numbers were 3,300, based on the mean velocity at the centerline and the half width of the channel, and 180, based on the wall shear velocity and the half width of the channel.

A spectral method — Fourier series in the x and y directions and Chebyshev polynomial expansion in the z direction — was used for spatial derivatives. The advancement in time was made by a semi-implicit method: the Crank-Nicolson scheme for viscous terms and the Adams-Bashforth method for the nonlinear terms. No subgrid-scale model was used inasmuch as the grid was fine enough to resolve all the essential turbulent scales. Once the velocity field was advanced for each time step, the corresponding scalar fields were obtained by integrating the equations of transport of the scalars, which include convective, diffusive, and source terms. The computations were carried out until the passive scalar fields reached statistically steady states. The initial velocity field was taken from a previous calculation in which the velocity field already had reached a statistically steady state.

The numerical simulation was carried out with three passive scalars at different molecular Prandtl numbers. Computed statistics including the turbulent Prandtl numbers were compared with experimental data. The computed fields were also examined to investigate the spatial structures of the scalar fields. The scalar fields were found to be highly correlated with the streamwise velocity: the coefficient of correlation between the temperature and the streamwise velocity was as high as 0.95 in the wall region. The joint probability distributions between the temperature and velocity fluctuations were also examined and were of a form that suggests that it might be possible mathematically to model the scalar fluxes in the wall region in a manner similar to that of the Reynolds stresses.

This work was done by John Kim and Parviz Moin of **Ames Research Center**. *To obtain a copy of the report, "Transport of Passive Scalars in a Turbulent Channel Flow," Circle 151 on the TSP Request Card.*
ARC-12109

Machinery

Hardware, Techniques, and Processes

Electromagnetic Meissner-Effect Launcher

Projectile coils and brush contacts would not be needed.

Marshall Space Flight Center, Alabama

A proposed electromagnetic Meissner-effect launching apparatus would differ from previous electromagnetic launchers in that there would be no need for an electromagnet coil on the projectile. As a result, there would be no need for brush contacts and high-voltage commutation equipment to supply current directly to the projectile coil, or for pulse circuitry to induce current in the projectile coil if brush contacts are not used.

In the electromagnetic Meissner-effect launcher, the projectile would be accelerated along the axis of a segmented solenoidal electromagnet (see figure). The projectile would consist of a forward section containing the payload, a middle (separation) section consisting of a bulkhead and insulation, and an aft (propulsion) section. The outside surface of the aft section would be covered by one of the newly discovered materials that becomes superconductive at and below the temperature of liquid nitrogen.

The segments of the electromagnet behind and surrounding the aft section would be activated in sequence as the projectile passes by. For this purpose, laser beams would be aimed at photodetectors across the gaps between the segments. The photodetectors would sense the axial position of the projectile via interruptions of laser beams, and the outputs of the photodetectors would thus serve as control signals for the segments.

The Meissner effect is the expulsion of a magnetic field from the interior of a superconductor. Because of the Meissner effect, the magnetic field would be compressed between the superconductive surface and the interior surface of the electromagnet. The resulting gradient of magnetic pressure on the cylindrical portion of the superconducting surface would provide a lateral magnetic restoring force that would help keep the projectile on axis, while the gradient of magnetic pressure on the conical portion would provide both the axial propulsive force and some additional centering force.

A supply of pressurized liquid nitrogen in the propulsion section would keep the superconductor cool immediately before and during launch. The liquid nitrogen would be forced out through a tube at the top of the tank, then down along a spiral channel in contact with the superconductor, and out through a hole at the rear end of the projectile. The width of the channel would increase gradually toward the rear end to allow for expansion of the nitrogen. A valve could be placed at the end to control the release of nitrogen before and during launch.

This work was done by Glen A. Robertson of **Marshall Space Flight Center**. *For further information, Circle 68 on the TSP Request Card.*

Inquiries concerning rights for the commercial use of this invention should be addressed to the Patent Counsel, Marshall Space Flight Center [see page 14]. Refer to MFS-28323

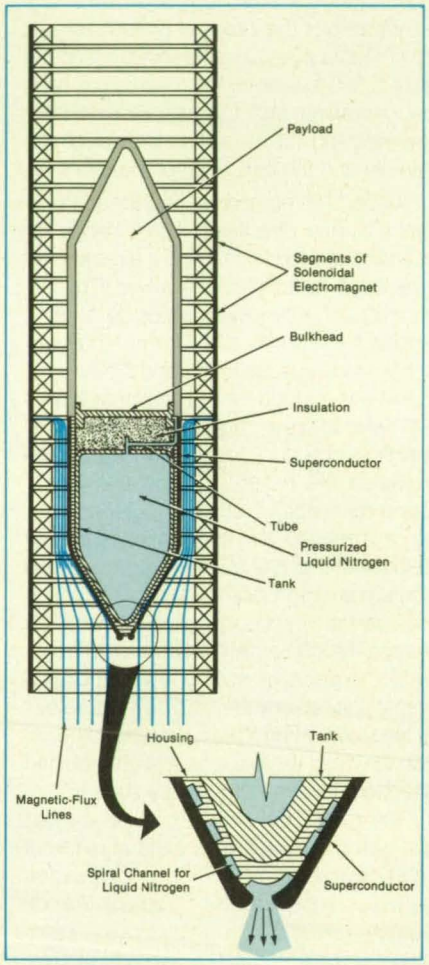

The **Meissner Effect** would compress the magnetic field surrounding the rear surface of the projectile, creating a gradient of magnetic pressure that would push the projectile forward.

Array of Rockets for Multicrewmember Evacuation

Crewmembers can hook up to tractor rockets and fire them unaided.

Lyndon B. Johnson Space Center, Houston, Texas

An emergency egress system undergoing development for aircraft and aerospace vehicles uses a fixed array of tractor rockets to eject crewmembers. It serves the same function as the ejection system described in the preceding article. That system, however, relies on a rocket magazine in which rockets drop in sequence into a tube for firing, one per crewmember. In the fixed-array system, in contrast, 8 to 10 rockets occupy fixed positions in individual firing tubes around the egress hatch (see figure).

The array of rockets is positioned as a unit in a ready-to-use orientation during flight operations. On the ground, it is swung out of the way. The rocket array can also be mounted under the exit hatch, where it serves as the egress ramp. Crewmembers would kneel on the array to go through the egress steps.

To use the system, a crewmember dons a parachute, lies on the egress ramp, pulls a tear-away tab to open a rocket package, hooks a lanyard from the rocket to the parachute pack, and depresses a safety lever to activate a trigger mechanism. The crewmember pulls the lanyard to fire the trigger. The two-step firing — first activating the trigger, then firing it — prevents the crewmember from operating the rocket prematurely.

As soon as the fired rocket has pulled the crewmember horizontally through the hatch, the next crewmember reclines on the ramp and performs the emergency exit procedure. The procedure is repeated until all the crewmembers have been evacuated.

The fixed array does not require a jumpmaster because the lanyard is easy to attach, and there is no danger of a magazine mechanism jamming and needing attention. Moreover, the fixed array is more reliable than the magazine system because the failure of one rocket or its mechanism does not prevent the use of the remaining rockets.

This work was done by Margaret A. Allen of Rockwell International Corp. for **Johnson Space Center**. *For further information, Circle 106 on the TSP Request Card.*

This invention is owned by NASA, and a patent application has been filed. Inquiries concerning nonexclusive or exclusive license for its commercial development should be addressed to the Patent Counsel, Johnson Space Center [see page 14] Refer to MSC-21332

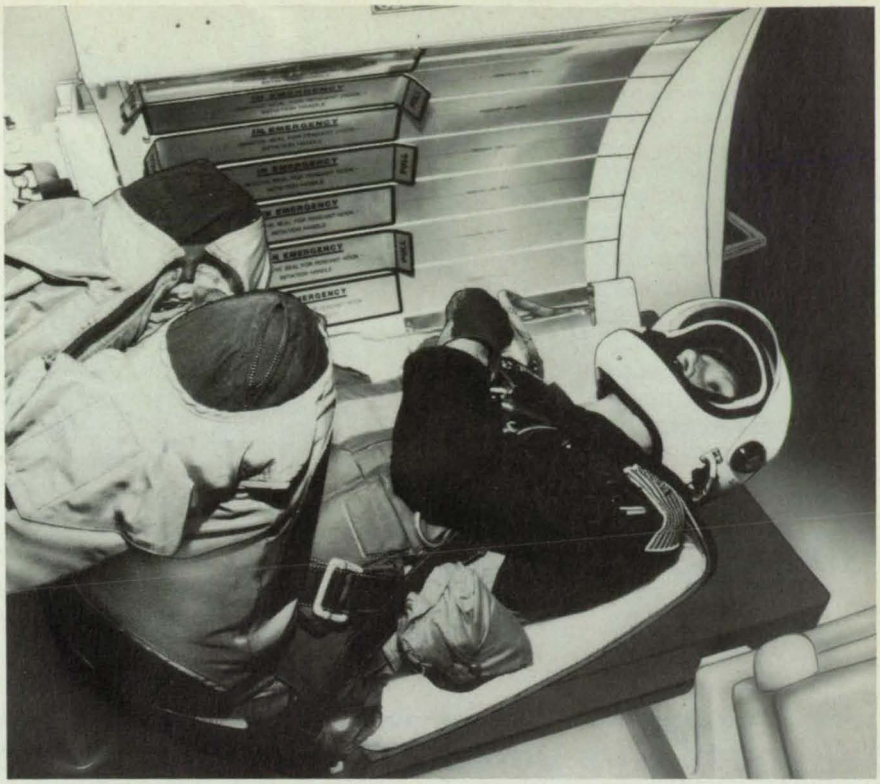

A **Crewmember Prepares** for ejection under an array of rockets. Another crewmember, left, waits to use the emergency egress system.

Serial Escape System for Aircraft Crews

A rocket ejection system enables an orderly evacuation.

Lyndon B. Johnson Space Center, Houston, Texas

An emergency escape system for aircraft and aerospace vehicles can eject up to seven crewmembers, one by one, within 120 s. The system is intended for emergencies in which a disabled craft is still in stable flight at no more than 220 kn (113 m/s) equivalent airspeed and sinking no faster than 110 ft/s (33.5 m/s) at altitudes up to 50,000 ft (15.2 km). The system provides an orderly, controlled exit and avoids ditching at sea or landing in rough terrain.

The crewmembers don parachutes and water survival gear before ejection. Supervised by a crewmember who has been trained as jumpmaster, the members in turn lie on an egress ramp and attach a pendant on the parachute harness to a small tractor rocket (see figure). When the jumpmaster pulls the ejection handle, a pair of gas cylinders ejects the attached rocket out the egress hatch. About 9 ft

Circle Reader Action No. 615

(2.7 m) from the launcher, just outside the hatch, the rocket fires and pulls the crewmember out the hatch. The crewmember's initial trajectory is horizontal and 5° to 10° forward of the sideways axis. This trajectory ensures that the crewmember clears the wings and tail.

As soon as a crewmember has been ejected, a new rocket rolls downward into the firing tube from a magazine. The ejection procedure is repeated until all crewmembers have left the craft.

The system differs from the system described in the next article in that rockets are fed from a magazine. Gravity and spring pressure force a stack of rockets downward so that the launcher reloads automatically.

This work was done by Kenneth E. Wood of Rockwell International Corp. for **Johnson Space Center**. *For further information, Circle 153 on the TSP Request Card.*
MSC-21310

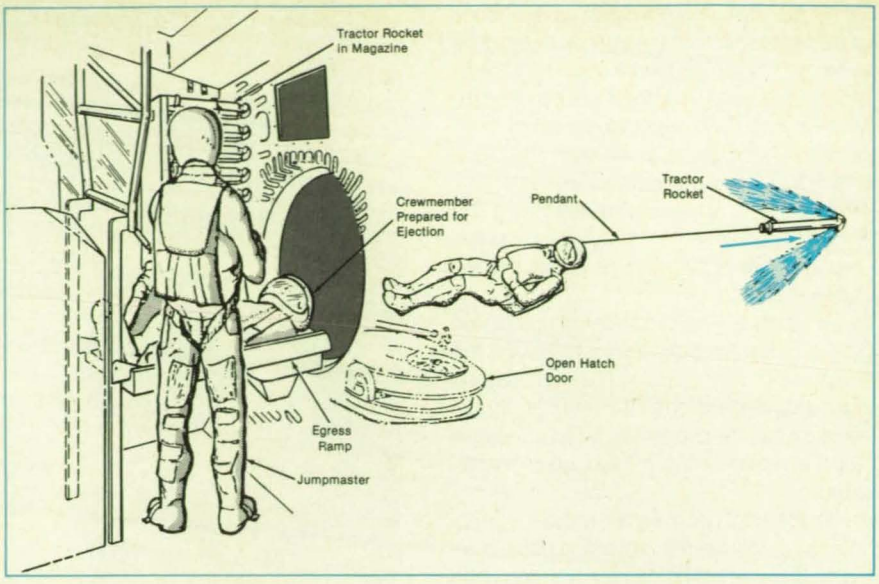

Ejection Rockets Load Themselves from a magazine after each crewmember is ejected. The jumpmaster queues the other crewmembers and helps them position themselves on the egress ramp. The rockets pull crewmembers clear of the aircraft structure.

Wrapped Wire Detects Rupture of Pressure Vessel

Breakage or burning of wire triggers a shutdown.

Lyndon B. Johnson Space Center, Houston, Texas

A simple and inexpensive technique helps to protect against damage caused by continuing operation of equipment after the rupture or burnout of a pressure vessel. Wire is wrapped over an area on the outside of the vessel where a breakthrough is

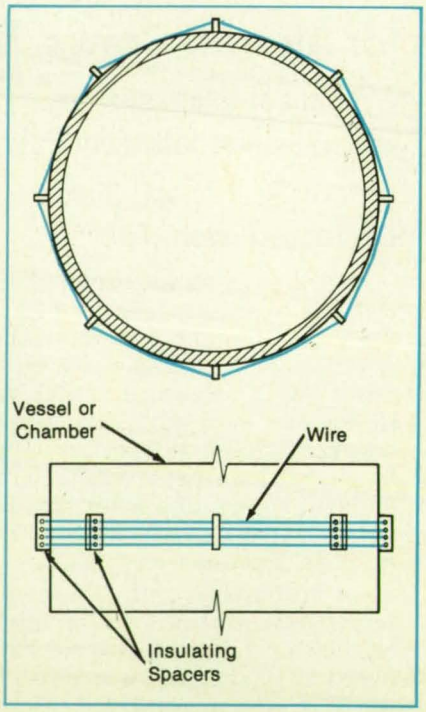

Loops of Wire encircle the outside of a pressure vessel or combustion chamber. If bursting or burnthrough occurs, the wire also is broken or burned, breaking the electrical connection and thus turning off the equipment.

Circle Reader Action No. 615

most likely (see figure). If the wall breaks or burns, so does the wire. Current passing through the wire then ceases, triggering a cutoff mechanism that stops flow in the vessel to prevent further damage.

The method, developed for Space Shuttle rocket engines, can be applied in other situations in which pipes or vessels can fail due to overpressure, overheating, or corrosion. In the rocket-engine application, lead wires for the propellant solenoid valves are wound around the outside of the combustion chamber. The wire is threaded through rigid insulating spacers, forming 14 loops with centers 0.115 in. (0.29 cm) apart in a band about 1.6 in. (4.1 cm) wide.

The band covers the region where exhaust gas as hot as 5,000 °F (2,800 °C) might burn through the wall during unstable combustion. The wires would then be burned too, cutting off power to the solenoids that control the fuel and oxidant valves, thereby shutting down the engine. The engine and surrounding equipment are thus protected from further damage.

This method was selected over other protection concepts because it is simple, provides positive shutdown, and functions independently of other instrumentation and equipment. The use of accelerometers or temperature sensors, for example, to detect instability of combustion was found to be overly complex and unreliable because the sensors themselves are subject to failure.

This work was done by James B. Hunt of Rockwell International Corp. for **Johnson Space Center**. *For further information, Circle 112 on the TSP Request Card.*
MSC-21449

Improved Stress Analysis of Multicomponent Rotors

Suitable formulation of a finite-element model speeds computation.

Lewis Research Center, Cleveland, Ohio

An improved method has been developed for the analysis of stress and of the compatibility of components in a multicomponent rotating assembly. In this method, a single finite-element mathematical model represents all of the components. This is made possible by the use of gap elements to represent contact surfaces between components.

The general problem is illustrated in simplified form in Figure 1, which shows a two-component rotor. In a typical multicomponent rotor, the concentricity of the components is maintained via tight fits of mating or pilot surfaces, and parts are often bolted together axially. The analysis must take account of contact and internal stresses as functions of temperature and speed of rotation, radial and axial expansions and contractions that loosen the parts, and transient complications of the foregoing and other effects.

The new method has been tested by application to a compressor rotor. A two-dimensional finite-element model of the entire compressor (see Figure 2) incorporates all of the components and simulates the effects of all contacting surfaces. The initial analysis, which uses the MARC finite-element computer program, was done in two parts. The first part was a heat-transfer analysis that determined the steady-state temperature distribution. The resulting temperatures of the elements were later incorporated into the stress/compatibility analysis.

A gap element can be defined with either a closure distance (that is, a gap) or an interference fit. When an interference fit is chosen, the MARC program simulates the pressure on the surfaces by forcing the two end nodes of the gap element (there is one node on each surface) to be displaced from each other an amount equal to the interference fit. As a result, interference fits on the model cause a stress distribution before any of the operating loading conditions are applied. In this analysis, only interference fits are used for the gap elements.

The stress/compatibility analysis of this system requires a nonlinear solution. Therefore, the equations must be solved

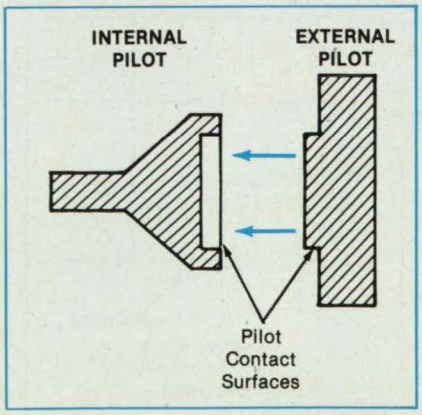

Figure 1. **Two Components** of a simple rotating assembly are joined at an external/internal pilot interface. A tight pilot interface (an interference fit) must be assured under all operating conditions to maintain concentricity.

Circle Reader Action No. 615

incrementally by the MARC finite-element program. The governing equations are expressed in an incremental form as

$$K\,du = df$$

where du and df are incremental displacement and force vectors, respectively, and K is the stiffness matrix. In the initial analysis, the model was loaded with nine successive equal increments. After the ninth increment of load was applied, the total load on the model was equivalent to the actual loads at the specified operating speed.

If a gap develops during one of the increments of load, the stiffness matrix changes and must be recalculated. The MARC program uses the full Newton-Raphson method to determine the new stiffness matrix. Within each increment of load, the program performs iterations, recalculating and refactorizing the stiffness matrix until the ratio of the maximum residual force to maximum reaction force is less than a given tolerance.

The previous method for the analysis of stress and compatibility, called the "flexibility-analysis" method, required significantly more computation. Consequently, to save time, analyses were often performed only at maximum operating speeds, and important information on trends in contact forces and displacements of pilot surfaces at lower speeds were not available. The new method makes it easier to identify these trends and to determine the effects of changes in design.

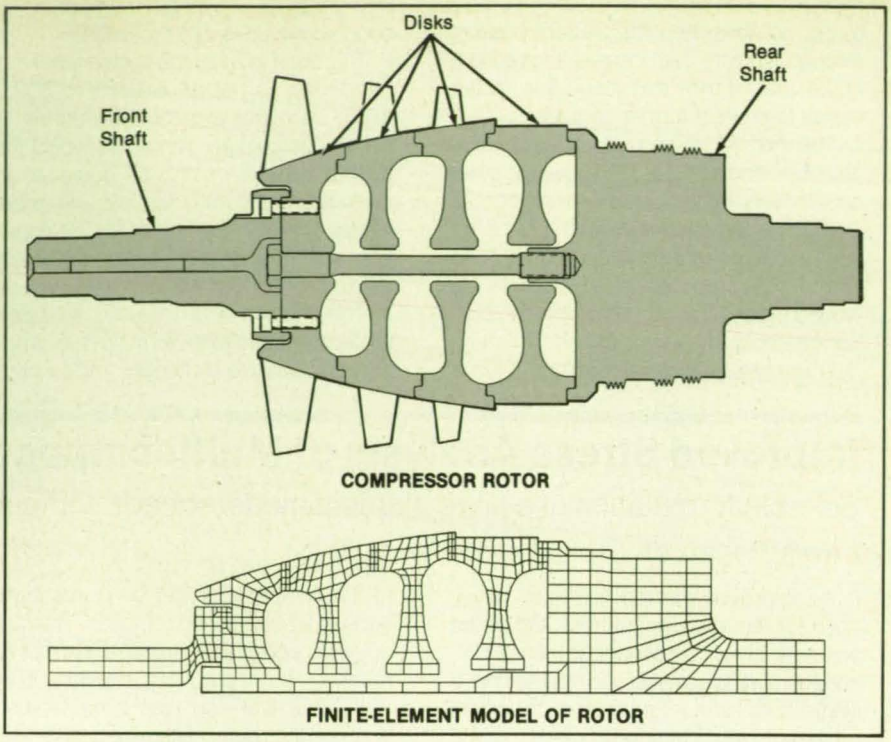

Figure 2. The **Rotor of a Compressor** is represented by a two-dimensional mathematical model that contains 371 eight-node quadrilateral axisymmetric elements.

This work was done by Gerald A. Carek of **Lewis Research Center**. *Further information may be found in NASA TM-100884 [N88-25935], "Improved Method for Stress and Compatibility Analysis of Multicomponent Rotating Systems."*

Copies may be purchased [prepayment required] from the National Technical Information Service, Springfield, Virginia 22161, Telephone No. (703) 487-4650. Rush orders may be placed for an extra fee by calling (800) 336-4700. LEW-14838

Two-Phase Accumulator

Liquid and vapor are used to regulate temperature and pressure.

Lyndon B. Johnson Space Center, Houston, Texas

A two-phase accumulator maintains the pressure and temperature in a thermal-bus system within a predetermined range during variations in the heat load on the system. The thermal-bus system can be used to dispose of waste heat, such as that from electronic equipment or a powerplant.

If the heat load decreases, the accumulator increases the level of liquid in a heat-rejection condenser, reducing the contact area for vapor and thereby also reducing the thermal conductance of the condenser and the amount of heat it transfers from the system. Conversely, if the heat load increases, the accumulator withdraws liquid from the condenser, increasing its contact area for vapor, its conductance, and its heat-transfer rate. The accumulator thus stabilizes the temperature and pressure within the system.

In a demonstration system in which ammonia is the working fluid (see figure), any set-point temperature between 31 and 104 °F (−0.6 and +40 °C) can be entered

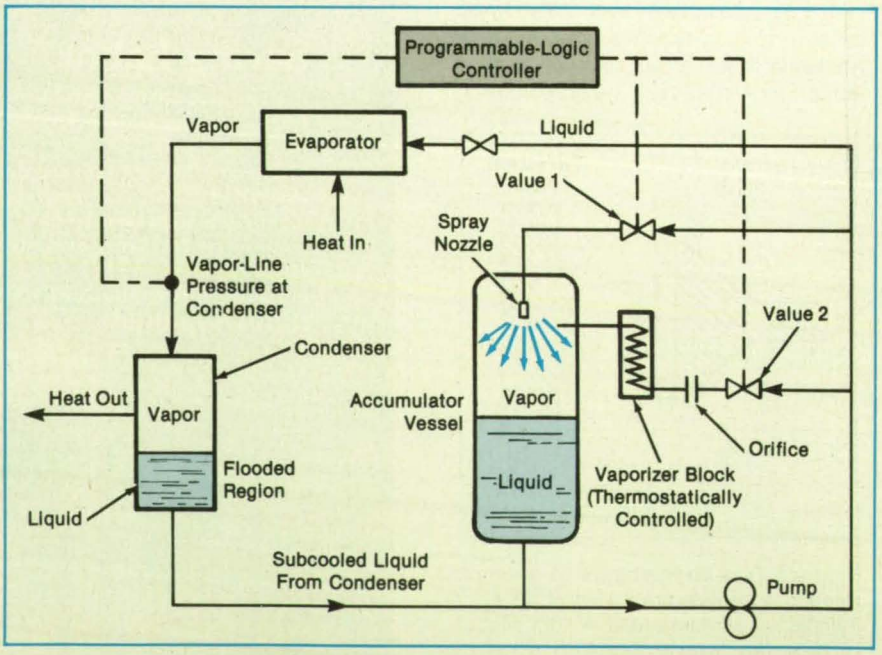

The **Accumulator Stores Liquid and Vapor Ammonia**. It exchanges liquid ammonia with the condenser to adjust the level of liquid in the condenser. The prototype accumulator has a capacity of 13 gallons (49 liters).

CONTROLLING CHANGE

Lock Into Dynamic Design, Material And Processing Creativity With GE.

Total solutions from a single source. A spectrum of resin technologies. Advanced alloys, composites, copolymers. Leading-edge process development and expertise. The exclusive Engineering Design Database—unique design and analysis tools in a total system for plastics engineering.

The innovative Intelligent Automation Series from Foxboro. Enclosures of injection-molded LEXAN® resin. Cell brackets of foam-molded LEXAN resin. Internals of NORYL® and VALOX® resins. Over 300 parts in all.

Diverse technologies and application development resources—only from GE.

For more information call:
(800) 845-0600

GE Plastics

® Registered Trademarks of General Electric Company.

Circle Reader Action No. 615

into a programmable-logic controller. By monitoring the pressure at the vapor inlet to the condenser and sending either subcooled ammonia liquid or vapor to the accumulator, depending on whether the pressure is high or low, the controller gets the accumulator to withdraw liquid from, or add liquid to, the condenser. It thus keeps the temperature of the vapor within ±4.5 °F (±2.5 °C) of the set-point temperature.

When the temperature rises above the deadband allowance, as indicated by a corresponding rise in the monitored pressure, the controller opens a solenoid valve (valve 1 in the figure) to spray subcooled liquid from the condenser into the vapor in the accumulator. Because the liquid drops are cooler than the vapor, the vapor condenses on them, creating a partial vacuum that draws liquid into the accumulator from the condenser. Although some liquid also flows out of the accumulator to make room for the inflowing liquid, the condensation results in a net inflow.

When the monitored pressure drops below the allowable deadband, the controller opens valve 2, admitting liquid to a vaporizer block. The block heats the liquid, vaporizing it as it flows into the accumulator. Vapor pressure builds up in the accumulator, forcing liquid out of it and into the condenser.

The two-phase accumulator offers important advantages over other proposed systems. For example, an accumulator in which a metal bellows ejects or draws in the ammonia on demand may be subject to leakage of its nitrogen pressurizing gas and to failure of the bellows. An electromechanical accumulator, in which an electric motor actuates a piston to drive the liquid, is likely to be mechanically complex and potentially unreliable.

The two-phase accumulator is simple and highly reliable. The only moving parts are the two solenoid valves, which could be combined into a single three-way solenoid valve. The two-phase accumulator responds quickly, restoring pressure and temperature to the proper values within minutes. It is low in cost and requires little further development.

This work was done by Charles E. Kalb, Robert L. Kosson, Joseph P. Alario, Richard F. Brown, and Fred Edlestein of Grumman Corp. for **Johnson Space Center**. *For further information, Circle 146 on the TSP Request Card.*
MSC-21464

Books and Reports

These reports, studies, handbooks are available from NASA as Technical Support Packages (TSP's) when a Request Card number is cited; otherwise they are available from the National Technical Information Service.

Hard Contact With a Force-Reflecting Teleoperator

Force feedback should be adjusted to provide stability without sluggish and fatiguing operation.

A paper reports on experiments with a single-axis force-reflecting teleoperator that made contact with a hard, immovable object. The experiments showed, among other things, that the dynamics of the human operator affect the stability of the response of the control system.

In the experiments, a human operator used a hand controller to move a model robot arm in a space containing a rigidly mounted obstacle. The following parameters of the teleoperator system were adjustable: robot position gain, robot rate gain, forward position ratio, coordinating position gain, forward delay, backward delay, hand-controller position gain, hand-controller rate gain, force gain, and force-filter time constant. Operation was also simulated on a computer with the SPICE electronic-circuit-simulation program. In the simulations, the parameters of the human operator and the coordinating and damping torques were varied. The simulations compared one-finger operation with full-hand operation.

The experiments showed that one of the effects of a stronger grip on the hand controller is to stabilize the system during a hard-contact task, much as local damping feedback of the hand controller does. An added effect of the damping, however, is to change the subjective feel of the system from "responsive" and "tight" to "sluggish" and "fatiguing."

The results of the experiments suggest a new control architecture in which the mechanical impedance of the human operator is continuously estimated and only the minimum necessary amount of damping is supplied by the system. This scheme could be implemented in any of three ways:

- The operator adjusts damping for optimum performance with stable operation.
- A contact sensor (such as a capacitance or infrared sensor) is used to determine whether the strength of the grasp is sufficient, in which case the control system reduces damping to a preset level.
- The control system continuously estimates the impedance of the human operator from force, torque, and displacement readings and continuously adjusts the damping accordingly.

This work was done by Blake Hannaford of Caltech and Robert Anderson of the University of Illinois for **NASA's Jet Propulsion Laboratory**. *To obtain a copy of the report, "Experimental and Simulation Studies of Hard Contact in Force Reflecting Teleoperation," Circle 60 on the TSP Request Card. NPO-17549*

Vibrations Caused by Cracked Turbopump Bearing Race

Expansion gives rise to eccentricity.

A brief report presents an analysis of the dynamic effects caused by the cracking of the inner race of a ball bearing in a turbopump. The crack had manifested itself via an increase in vibrations synchronous with the rotation and a smaller increase at twice the frequency of rotation. The analysis was conducted to verify that these increases were caused solely by the crack and to understand the implications for future such cracks.

It was postulated that centrifugal expansion of the cracked inner race would cause the race to become eccentric with respect to the rotating shaft and that the eccentricity would give rise to unbalance and consequent vibrations. The vibrations would be small or nonexistent at low speeds of rotation, at which compressive axial loads, ball loads, and shrink fits would exert restoring forces that would counteract the centrifugal force. With increased speed, the centrifugal force would increasingly overcome these restoring forces, expanding the cracked inner race outward.

Because one of the loads resisting expansion would be friction on the axial faces between the inner race and the bearing nut and spacer, the expansion would occur in frictional steps, locking at each successive step as the speed increased. The expansion with increasing speed would continue in steps up to the limit of the internal clearance of the bearing. Expansion at higher speeds would increase the loads on the outer race, which would then help to resist expansion by applying restoring forces through the balls.

These hypotheses were tested by computer simulation, using a mathematical model of the dynamics of the pump rotor with various amounts of eccentricity. Although this simulation predicted vibrations similar to those observed, it was considered inconclusive because of inadequacy of the part of the model that represented the pump housing. Therefore, experiments were conducted and correlated with the results of the simulation. The experimental plots of vibration amplitude with speed showed the effects of the postulated step-by-step expansion, and the observed increase in vibration amplitude with speed was approximately equal to that of the simulation for a realistic range of eccentricity of the inner race.

This work was done by David G. Goggin and Robert A. Dweck of Rockwell International Corp. for **Marshall Space Flight Center**. *To obtain a copy of the report, "SSME HPOTP — Cracked Bearing Inner Race Rotordynamic Model," Circle 160 on the TSP Request Card. MFS-29656*

Fabrication Technology

Hardware, Techniques, and Processes

Optical Arc-Length Sensor for TIG Welding

The length of the arc would be measured instead of inferred from voltage.

Marshall Space Flight Center, Alabama

A proposed subsystem of a tungsten/inert-gas (TIG) welding system would measure the length of the welding arc optically. At present, the length of the arc is inferred from the arc voltage, which depends on the welding current, the content (including contamination) of the purging gas, and the condition of the tip of the welding electrode. It is necessary to measure the arc length to control it and thereby assure the quality of the weld. Thus, in present systems, contamination and variations in welding currents and the flow of purging gases are common causes of flaws in welds.

In the proposed subsystem, a video camera would view the welding arc, which would be identifiable in the image by its extreme brightness or by its emission of discrete spectral lines and continuum radiation. The image would be brought to the video camera by a bundle of optical fibers or by mirrors along an oblique line of sight through or past the edge of the gas cup of the torch (see figure). A signal related to the length of the arc would be obtained from the video image by a simple optical processing technique developed for the recognition of images. The true length of the arc could be calculated from this signal and a knowledge of the lenses, angles, and distances of the optical train.

This work was done by Matthew A. Smith of Rockwell International Corp. for **Marshall Space Flight Center**. *No further documentation is available. MFS-29497*

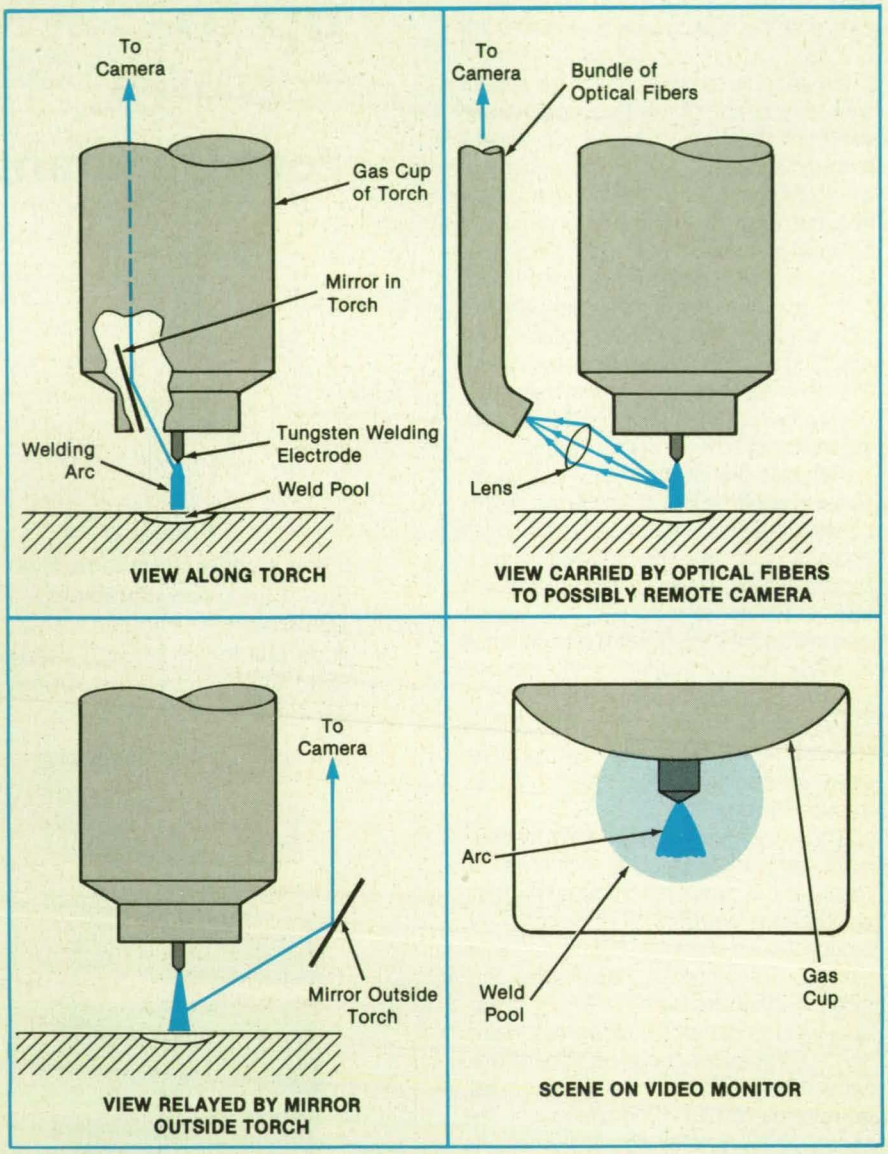

The Welding Arc Would Be Viewed by a video camera, in one of three alternative optical configurations.

Calibration Fixture for Welding Robot

This compact, lightweight device can be used in any position or orientation.

Marshall Space Flight Center, Alabama

A calibration fixture has been designed for use on a robotic gas/tungsten-arc welding torch equipped with a vision-based seam-tracking system. Through optics in the hollow torch cylinder, a video camera obtains an image of the weld, viewing along a line of sight coaxial with the welding electrode. The calibration fixture is needed because each time the welding configuration is changed and a different type of seam is to be tracked, the vision system must be recalibrated.

The calibration procedure involves finding the location of the electrode in the image, determining the magnification of the image, and refocusing the optics to the appropriate distance. The calibration fixture is a compact, lightweight device that can be used to perform calibration while the torch is in any position or orientation. It accommodates a standard focusing range

from 1/8 in. (3 mm) below to 3/4 in. (19 mm) above the outer end of the electrode and is adaptable to nonstandard cup sizes and electrode lengths.

The calibration fixture (see figure) includes inner and outer collars and an extension tube. A plastic retaining clip holds a ground-glass disk and a glass reticle with a 1-mm grid in position in the extension tube. The extension tube snaps into the outer collar with ball plungers so that it can rotate in the outer collar. The ground glass and reticle are illuminated from below by a fiber-optic light guide from a 150-W variable-intensity halogen-lamp microscope illuminator. A setscrew holds the light guide in the lower end of the extension tube.

Before using the calibration fixture, the

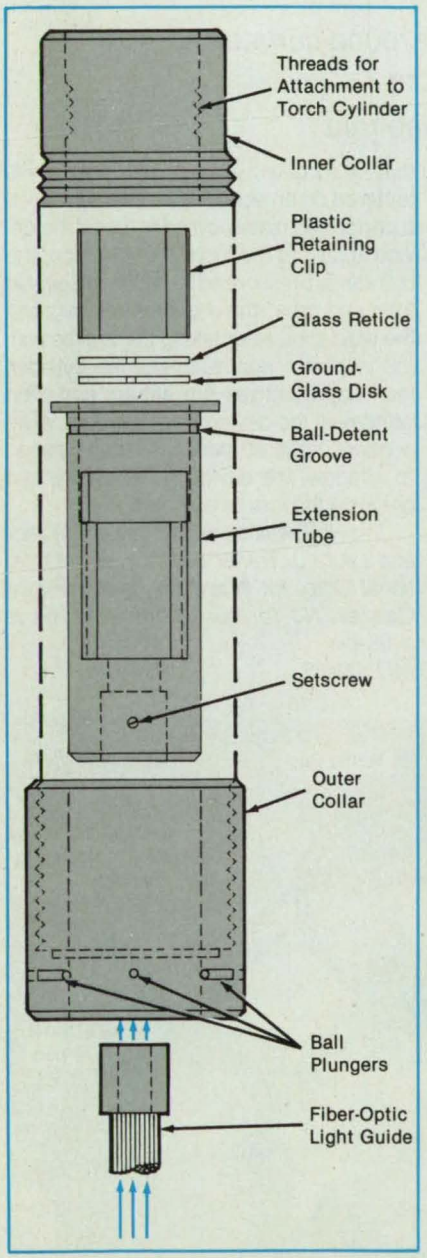

The **Calibration Fixture** is attached to the welding-torch cylinder in place of the gas cup that would normally be attached in use. By use of a longer or shorter extension tube, the fixture can accommodate a welding electrode of unusual length.

gas cup must be removed from the torch cylinder. Then, in place of the gas cup, the fixture is attached to the torch cylinder by the threaded inner surface of the inner collar. The welding electrode protrudes through coaxial holes in the reticle and ground glass. A rectangular hole in the side of the extension tube exposes the electrode so that the location of the end of the electrode can be measured with respect to the reticle. This hole also enables the technician to rotate the reticle by pushing on its edge.

With the inner and outer collars threaded together, the outer collar is turned to adjust the distance between the reticle and the tip of the electrode. An exceptionally long electrode may require the use of a longer extension tube with standard inner and outer collars.

This work was done by Krisztina J. Holly of Rockwell International Corp. for **Marshall Space Flight Center**. *For further information, Circle 149 on the TSP Request Card.*

Inquiries concerning rights for the commercial use of this invention should be addressed to the Patent Counsel, Marshall Space Flight Center [see page 14].Refer to MFS-29548

Borescope Device Takes Impressions in Ducts

The device can be maneuvered around curves and used in otherwise inaccessible locations.

Marshall Space Flight Center, Alabama

A maneuverable device built around a borescope is equipped to make impression molds of welded joints in the interior surfaces of ducts. The molds are then examined to determine the degrees of mismatch in the welds. The use of the device is fairly easy and requires little training.

The device (see figure) is inserted in a duct, and color-coded handles on the ends of cables can be used to articulate the head to maneuver around corners. Viewing the inner wall of the duct through the borescope, the technician aligns the device with the weld joint to be inspected. An airbag wrapped around the head is inflated to expand it against the interior surface of the duct and hold the device in place.

Before insertion, the mold material — a plastic material that has a consistency like that of modeling clay or stiff putty — is tethered on an elastic tube that surrounds a perforated platen cylinder. Once the device is held at the inspection position, the cylinder is pressurized to inflate the elastic tube and press the mold material against the weld joint. After taking the impression, the inspector depressurizes the cylinder, then depressurizes the airbag, and then withdraws the device from the duct. A redundant, tethered steel cable can be used to withdraw the device, if necessary, and prevents the loss of any part.

This work was done by Richard F. Walter and Laura J. Turner of Rockwell International Corp. for **Marshall Space Flight Center**. *No further documentation is available.*
MFS-29483

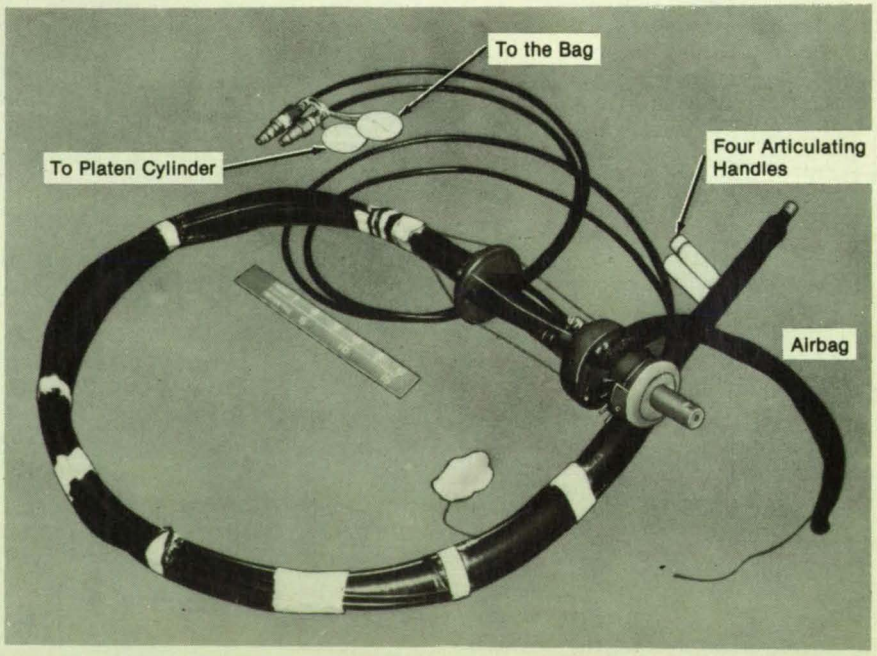

The Borescope and the Articulating Cables enable the inspector to identify the surface to be inspected and to maneuver the head around corners to reach the inspection position.

Internal Filler-Wire Feed for Arc Welding

The tungsten electrode holds and protects the filler wire.

Marshall Space Flight Center, Alabama

A tungsten electrode for gas/tungsten arc welding contains a lengthwise channel for feeding filler wire to the weld joint. The channel makes it unnecessary to feed the wire through guides outside the electrode and thus conserves valuable space near the weld and protects the wire from deformation by contact with other parts in the vicinity of the weld — a feature especially helpful in robotic or automatic welding.

The wire is fed along the inside of a ceramic liner in the channel in the electrode (see figure). The liner insulates the wire electrically from the electrode. Heat from the rod nevertheless passes through the liner to the wire, preheating the wire so that it can be fed more rapidly to the weld puddle. Welding can thus proceed faster than it can with externally fed wire. Moreover, the wire does not oxidize in the hot environment because it is always protected from air by the liner and by the shielding inert gas at the weld puddle.

This work was done by Gene E. Morgan and Gerald E. Dyer of Rockwell International Corp. for **Marshall Space Flight Center**. *For further information, Circle 5 on the TSP Request Card.*

This invention is owned by NASA, and a

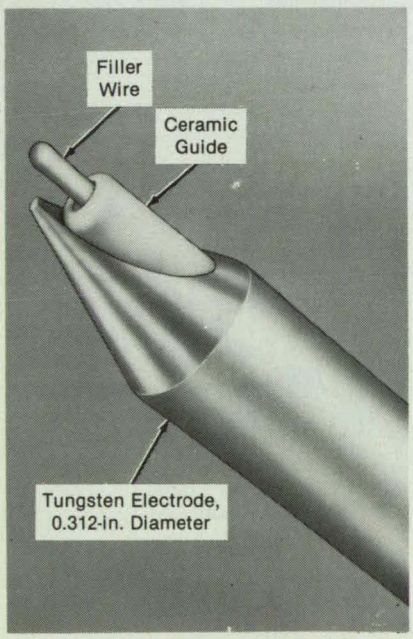

The **Hollow-Core Tungsten Rod** guides the filler wire to a weld joint. The ceramic liner insulates the wire electrically from the electrode so that the welding arc extends only from the electrode to the workpiece.

patent application has been filed. Inquiries concerning nonexclusive or exclusive license for its commercial development should be addressed to the Patent Counsel, Marshall Space Flight Center [see page 14]. Refer to MFS-29491.

Internal Wire Guide for Gas/Tungsten-Arc Welding

The wire is kept in the shielding gas, preventing oxidation.

Marshall Space Flight Center, Alabama

A guide inside the gas cup of a gas/tungsten-arc welding torch feeds the filler wire to the weld pool along a line parallel to the axis of the torch. The guide eliminates the problem of how to place and orient the torch to provide clearance for an external wire guide.

As shown in the figure, the guide is placed adjacent and parallel to the tungsten welding electrode. The guide keeps the wire within the shielding gas at all times during welding, thereby preventing oxidation of the wire.

This work was done by Gene E. Morgan and Gerald E. Dyer of Rockwell International Corp. for **Marshall Space Flight Center**. *No further documentation is available.*

Inquiries concerning rights for the commercial use of this invention should be addressed to the Patent Counsel, Marshall Space Flight Center [see page 14]. Refer to MFS-29489

Simplified Models Speed Electroforming Tests

Two-dimensional models are easier to construct than are fully-machined three-dimensional models.

Marshall Space Flight Center, Alabama

A method of evaluating the configurations of electroforming shields reduces the cost of evaluation. The method is applicable to electroformed parts that have axes of symmetry. The method involves electroforming material onto a two-dimen-

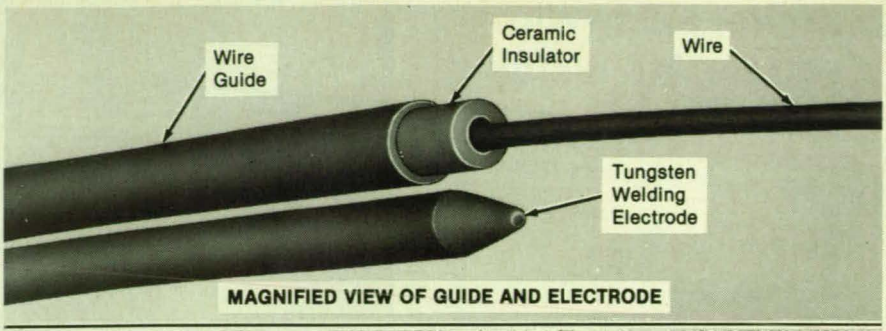

MAGNIFIED VIEW OF GUIDE AND ELECTRODE

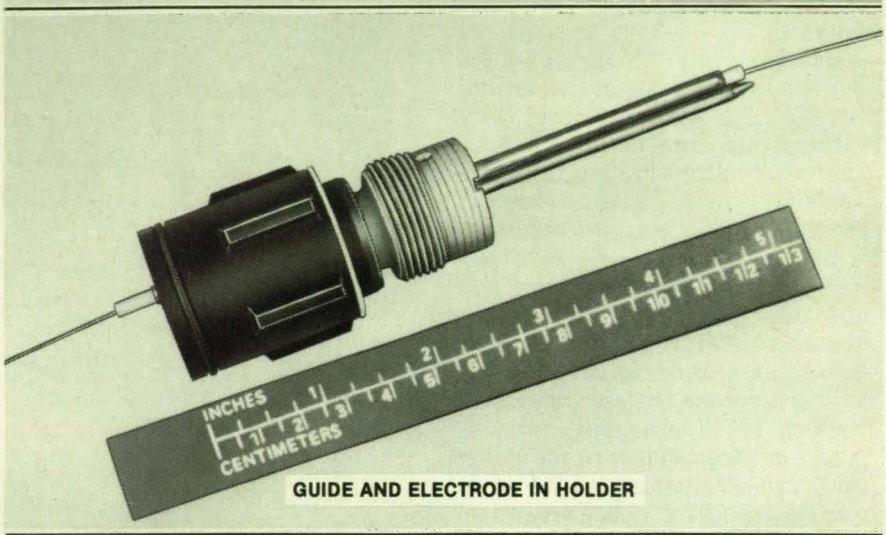

GUIDE AND ELECTRODE IN HOLDER

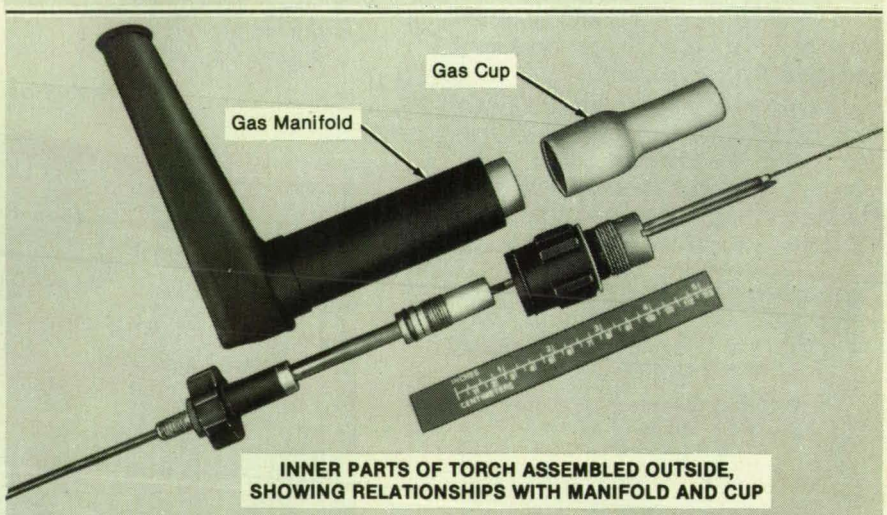

INNER PARTS OF TORCH ASSEMBLED OUTSIDE, SHOWING RELATIONSHIPS WITH MANIFOLD AND CUP

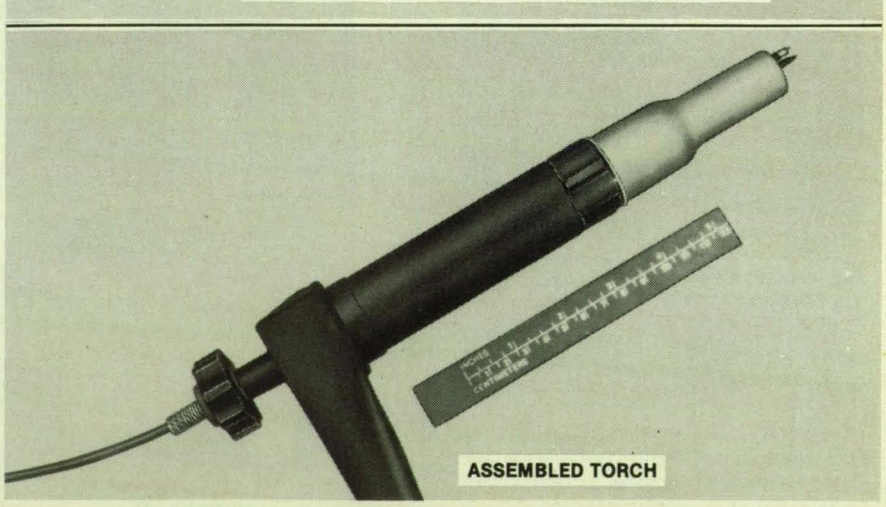
ASSEMBLED TORCH

The **Wire Guide and Tungsten Welding Electrode** are inserted in the torch side by side.

sional approximation of the part in question (see figure), using the side shields to be evaluated. After deposition, cross sections of the electrodeposited material are taken from critical locations and examined. Often, an important objective in the evaluation is minimization or postponement of the growth of nodules on the electroformed part. Nodules not only waste material but

ORIGINAL CONTOUR AFTER 105 HOURS OF ELECTROFORMING, SHOWING SOME NODULES

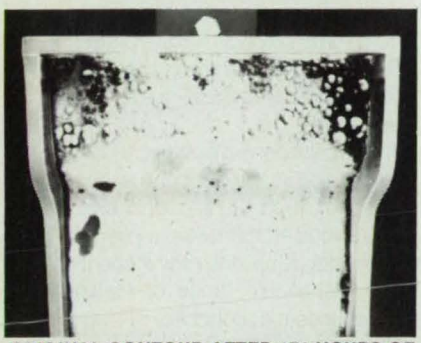

ORIGINAL CONTOUR AFTER 171 HOURS OF ELECTROFORMING, SHOWING FURTHER GROWTH OF NODULES

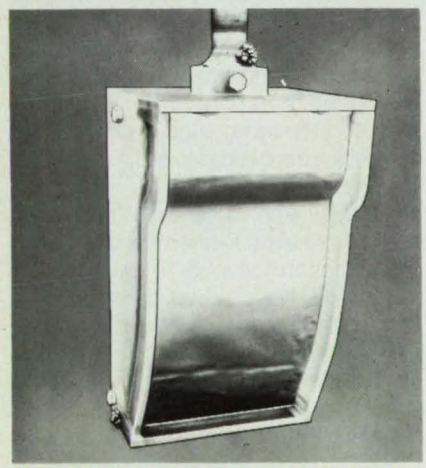

MODIFIED CONTOUR AFTER 172 HOURS OF ELECTROFORMING, SHOWING MINIMAL GROWTH OF NODULES

An **Electroformed Specimen** of nickel on a bent-sheet approximation of a three-dimensional axisymmetric part helps developers evaluate the conditions in the plating process as well as the configuration of the electroforming shields. Changes, if necessary, can then be made quickly.

also result in waste of time in that the electroforming process must sometimes be interrupted while nodules are ground off.

Previously, shields for a part to be electroformed were evaluated on a complete three-dimensional, fully machined model of the part. The new method not only eliminates the expense of constructing a full three-dimensional model but also makes it possible to perform the evaluation almost immediately.

A sheet of copper is bent to the outline of the part as it appears in a plane containing the axis of symmetry. The sheet is fitted with typical side shields and masked as required. It is then plated with nickel, for example, for the time required to build the thickness of the actual part (in some cases, more than 170 hours). The specimen is then sectioned, and the rates of deposition are determined.

At selected intervals during plating, the nickel can be interrupted with thin marker deposits of another metal — typically, copper. The thin deposits are visible as lines in the cross section and help in the evaluation of the deposition process.

This work was done by Ronnald Bodemeijer and Steven Filkin of Rockwell International Corp. for **Marshall Space Flight Center**. *No further documentation is available.*
MFS-29505

Prepenetrant Etchant for Incoloy* 903 Weld Overlays

The new etchant causes less damage.

Marshall Space Flight Center, Alabama

An etching solution has been developed for use prior to type-IVc penetrant inspection of Incoloy* 903 weld overlays. The previous prepenetrant etchant — a mixture of 50 percent hydrochloric acid and 50 percent hydrogen peroxide — tended to cause pitting and to give rise to an excessive fluorescent background, necessitating rework of the workpieces thus overetched.

The new etching solution is formulated as follows:

- 80 g ferric chloride hexahydrate,
- 300 mL reagent-grade hydrochloric acid,
- 25 mL food- or reagent-grade phosphoric acid, and
- 100 mL ethylene glycol.

This solution is applied to the surface to be etched for 90 to 120 seconds. In contrast, the previous etchant was applied for 15 to 30 seconds. Thus, the new etchant gives a more reasonable range of etching time and reduces the probability of overetching and resulting damage.

The new etchant does not pit or erode the surface of the workpiece. It reveals the microstructure of Incoloy* 903 without removing the constituents around the dendrites and grain boundaries and without attacking the grain boundaries. It does not produce etch-background anomalies that complicate the evaluation of the penetrant-inspection results.

The new etchant can be stored indefinitely. It is safe to use when standard safety procedures are followed. To avoid errors in formulation, it should be prepared by a trained technician in a laboratory, rather than in the shop where it is to be used.

*"Incoloy" is a registered trademark of the INCO family of companies.

This work was done by Joseph E. O'Tousa, Clark S. Thomas, and Robert E. Foster of Rockwell International Corp. for **Marshall Space Flight Center**. *No further documentation is available.*

Inquiries concerning rights for the commercial use of this invention should be addressed to the Patent Counsel, Marshall Space Flight Center [see page 14]. Refer to MFS-29576

Mathematics and Information Sciences

Differential Sampling for Fast Acquisition of Frequency

The amount of computation increases only linearly with the number of measurements.

NASA's Jet Propulsion Laboratory, Pasadena, California

An algorithm rapidly estimates the frequency of a sinusoidal signal corrupted by zero-mean, additive, white Gaussian noise. It incorporates a differential mathematical model of the signal, cyclic sampling of the signal, and a least-squares best-estimate criterion. Because it is recursive in the measurements, the algorithm can adapt to a changing signal frequency (see figure). The amount of computation required to obtain the estimate increases only linearly with the number of successive measurements to be processed.

Provided that the Nyquist sampling criterion is met at any signal frequency to be encountered, the signal and noise can be sampled at uniform or nonuniform intervals. At any given time, the N most-recent in-phase and N most-recent quadrature (with phase determined on the basis of the evolving estimated frequency) samples of signal plus noise are retained.

In the differential model, each in-phase and quadrature sample is expressed as the first n terms of a Taylor series expanded around the immediately-preceding in-phase and quadrature samples, respectively. The equations of the model can be put in a matrix•vector form that includes (a) an n-dimensional state vector derived from the measurements and (b) an n-dimensional parameter vector, the components of which are the frequency coefficients of the Taylor series. A standard least-squares procedure is then applied to obtain a recursive or nonrecursive expression for the parameter vector in terms of the measurements.

Because the noise component becomes colored in the differential model, the estimated parameter vector could attain a bias at low to medium signal-to-noise ratios. This bias is eliminated by use of an extended least-squares procedure that modifies the measurement to effectively whiten the noise. The result is a recursive extended least-squares algorithm with exponential measurement-weighting factors.

The dimension n of the state and parameter vectors does not depend on the number of measurements $2N$ and can be quite small; e.g., four is a typical value. Because smaller n means less computation, this is an advantage in comparison with previous algorithms in which n increases monotonically with the product of the uncertainty in frequency and the observation period. Although such a simplification can cause some loss of optimality, appropriate sampling procedures can make the loss in optimality insignificant. The reported work also presents an extension of the basic algorithm for the estimation of various derivatives of the frequency when this is desirable.

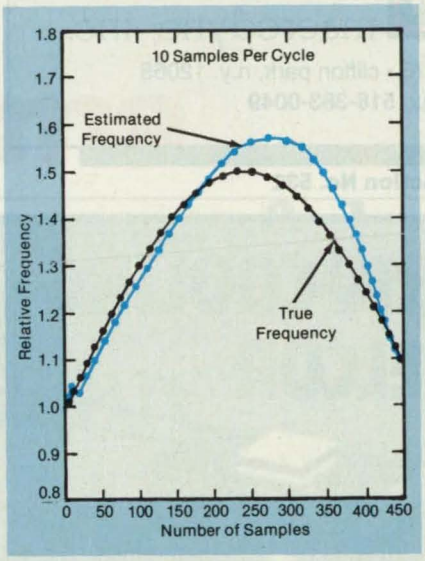

The **Estimated Frequency Adjusts Rapidly** to a changing true frequency.

This work was done by Rajendra Kumar of Caltech for **NASA's Jet Propulsion Laboratory**. *For further information, Circle 9 on the TSP Request Card.*

NPO-17358

Optimal Allocation of Tasks in Hypercube Computers

Uniform tasks should be distributed uniformly or else assigned to one processor.

NASA's Jet Propulsion Laboratory, Pasadena, California

An investigation in the theory of scheduling has yielded an optimal scheme for the allocation of tasks among digital data processors in a hypercube ensemble. The scheme applies to tasks that require equal times to execute, that can be performed in any order, and between any two of which equal amounts of communication are required.

Parallel-processing systems like hypercube ensembles (see figure) have the potential to reduce overall processing time for a given set of computational tasks. To realize all or part of this potential, it is necessary to distribute the tasks among the available processors in such a way that the overhead cost in communication time among tasks does not exceed the time saved by executing tasks in parallel.

The optimal-allocation problem is to allocate m independent tasks among n processors in such a way that the completion time or schedule length, S, has the smallest possible value. The completion time of the ensemble is the execution time plus communication time of whichever processor takes the longest time to complete its assigned sequence of tasks. In the general case, where some tasks may have to be completed before others are begun and various amounts of intertask communication are required,

$$S = \max_{1 \le j \le n} \left\{ \sum_{i=1}^{m} \sum_{k=1}^{m} \sum_{r=1}^{n} (e_{ij} x_{ij} + c_{ik} d_{jr} x_{ij} x_{kr}) \right\}$$

where e_{ij} = the execution time of task i on

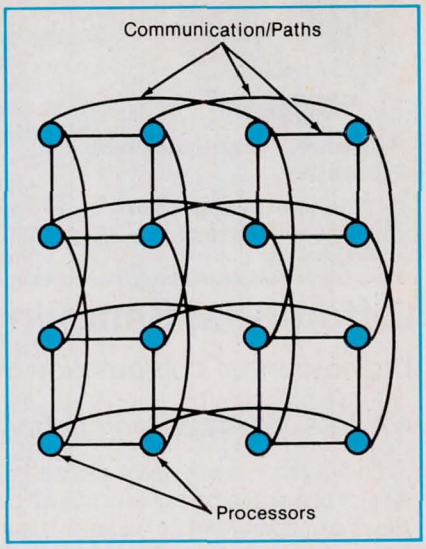

This **Hypercube Ensemble** of 16 data processors could, in principle, perform a computation 16 times as fast as could 1 of the processors, if not burdened by communication among the processors. The problem is to allocate the tasks among the processors to minimize the overall processing time.

processor j; c_{ik} = the time required for communication from task i to task k; d_{jr} = the cost per unit of communication sent from processor j to processor r; and $x_{ij} = 1$ when task i is assigned to processor j, and 0 otherwise.

In the general case, the minimization of S is an intractable problem. However, in the special case of uniform execution and communication times, the equation for S provides relatively-simple algebraic expressions for the times required for completion when the tasks are allocated to one processor, to all processors, and to various intermediate subhypercube combinations of processors. These expressions reveal that whenever the ratio of the uniform execution time for each task to the uniform communication time for each pair of tasks is less than a factor that depends on the particular hypercube configuration and on m, then the cost of interprocessor communication is so high that it is better to perform all tasks on a single processor. If the execution-time/communication-time ratio exceeds the given factor, then S is minimized by distributing the tasks evenly over all processors.

This work was done by Moktar A. Salama of Caltech and Camille C. Price of Stephen S. Austin State University for **NASA's Jet Propulsion Laboratory**. *For further information, Circle 13 on the TSP Request Card.*

Inquiries concerning rights for the commercial use of this invention should be addressed to the Patent Counsel, NASA Resident Office-JPL *[see page 14].* *Refer to NPO-17215.*

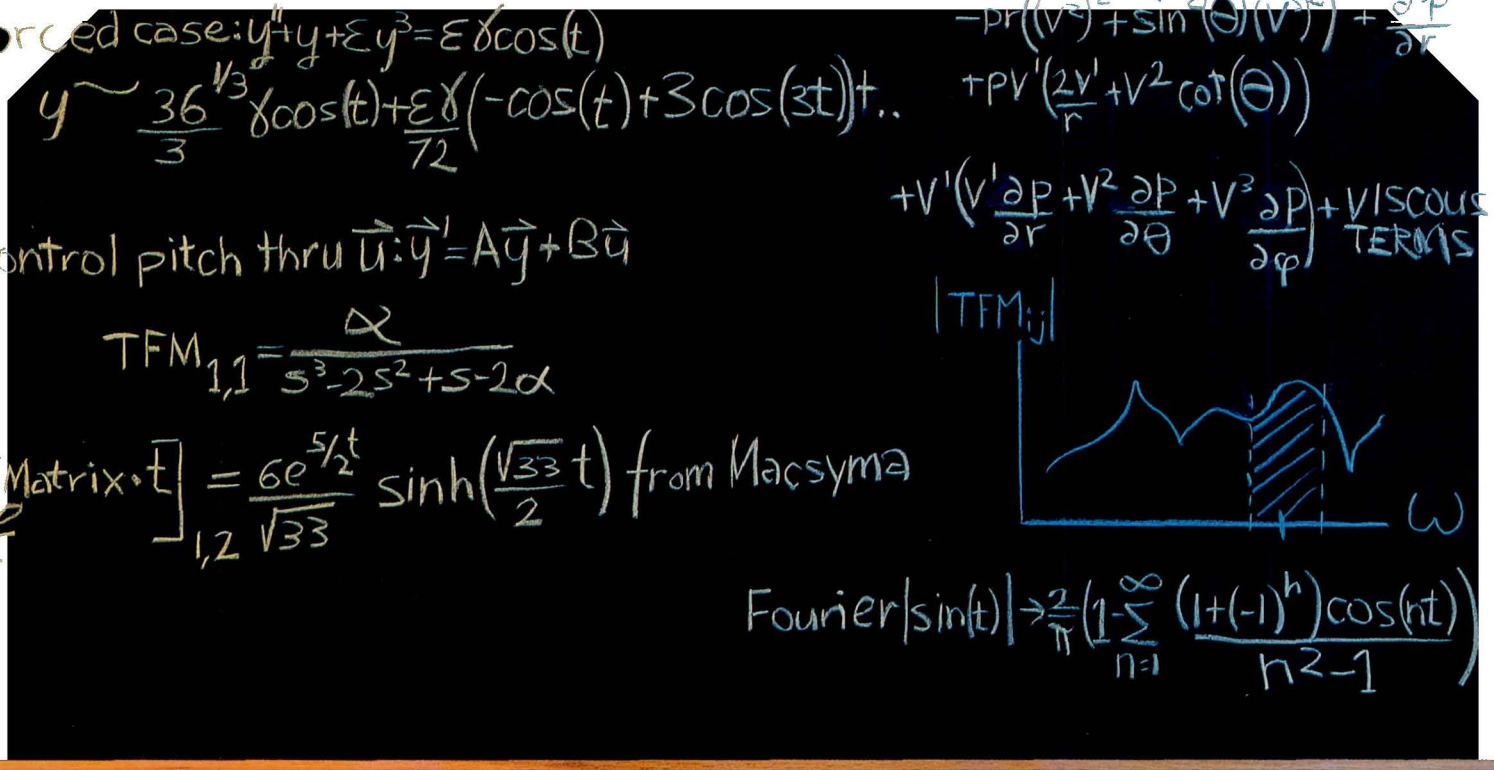

Macsyma®...

the most powerful math software in the world of workstations, mainframes, *and* PCs*

Now available on SPARC-stations

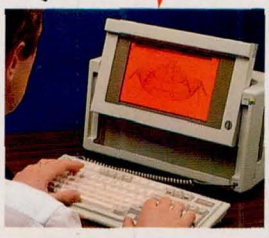

When it comes to solving complex symbolic and numerical math problems, there's no substitute for power. Other math packages claim they have it, but when it comes to the crunching they can't do much more than pretty graphics.

MACSYMA has the power you need.

With MACSYMA, you can easily tackle math modeling problems that other packages just sit and stare at. You can perform complex symbolic, numerical, and graphical calculations automatically — in applications ranging from plasma physics to aeronautics, from economics to fluid mechanics and more — right at your desk. Calculations such as differential and integral equations, Laplace and Fourier transforms, vector and tensor calculus...with greater depth and accuracy than any other software.

And MACSYMA is getting more powerful all the time, with dozens of new features to simplify even the most complex math.

But there's one thing about MACSYMA that isn't complex — using it. You can get right to work using our On-line Help and Quick Reference Card — without even opening a book.

Call 1-800-622-7962 (in Massachusetts, 617-221-1250.)

MACSYMA is a registered trademark of Symbolics, Inc.

symbolics Inc.

Macsyma Division

8 New England Executive Park East
Burlington, MA 01803 USA

*including Sun-4, Sun-3, Symbolics and Apollo workstations, VAXes and 100% IBM-compatible 386/DOS-based PCs.

SEE US AT ELECTRO/90, BOOTH #1016
HYNES AUDITORIUM, BOSTON, MAY 9-11

Circle Reader Action No. 524

Computer-Access-Code Matrices

Authorized users can respond to changing challenges with changing passwords.

NASA's Jet Propulsion Laboratory, Pasadena, California

A scheme for controlling access to computers defeats eavesdroppers and "hackers." The scheme is based on a password system of challenge and password or of sign, challenge, and countersign correlated with random alphanumeric codes in matrices of two or more dimensions. The codes are stored on a floppy disk or plug-in card and are changed frequently.

The host computer to which access is sought and the terminal from which access is attempted possess identical code matrices. In a two-dimensional version that could be used for identification (see Figure 1), the host computer transmits a challenge in the form of the alphanumeric codes at two corners (not in the same row or column) of a rectangle within the matrix. The terminal seeking access responds by sending the codes for the opposite corners of the same rectangle. If the codes are correct, the host computer grants access.

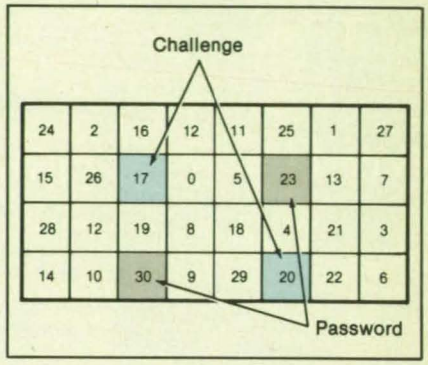

Figure 1. **Random Numerical Codes** that constitute challenges and passwords are arranged in matrix. For example, the challenge 17, 20 is answered with the password 23, 30.

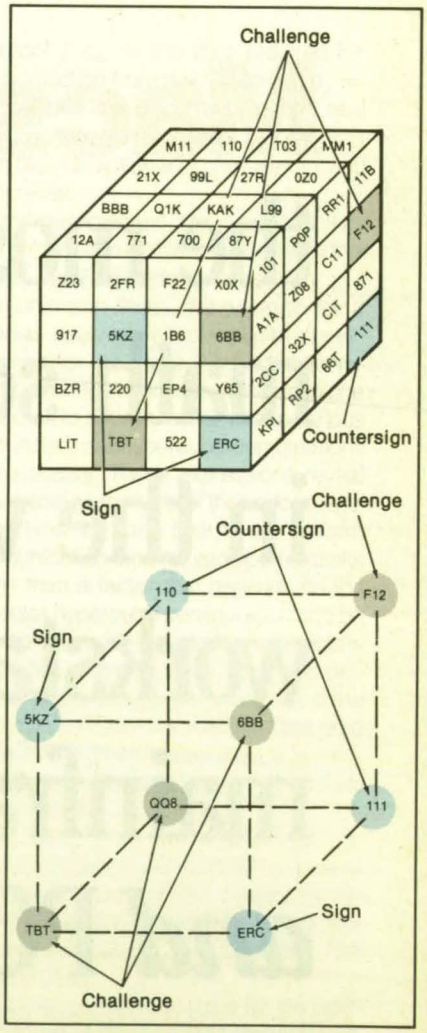

Figure 2. A **Three-Dimensional Matrix** — actually interrelated subsets of codes stored in memory — gives a caller and a host a great variety of choices in establishing a link with each other.

rect, access is granted.

The system discards codes used in a successful attempt at access and requires new codes for each new attempt. Thus, an eavesdropper cannot gain access by repeating the code sequence entered by an authorized user. Similarly, a hacker who tries a series of automatically generated passwords will find that the probability of gaining access is very low at the outset and diminishes rapidly thereafter.

Figure 2 illustrates a three-dimensional version for sign, challenge, and countersign. To gain access to the host, the caller sends two codes representing points on the same face of the matrix but not in the same row or column. For the example in the figure, the caller might choose 5KZ and ERC. The caller can choose the codes at random but must not repeat those already chosen.

The host responds by sending codes for points that complete a rectangle on the face — in this case, TBT and 6BB. (Receipt of the proper combination assures the caller that the proper host has been reached.) In addition, the host sends codes for two corners of a parallelepiped based on the rectangle just established — in this case, F12 and QQ8. The caller must now respond by sending the codes for the corners that complete the rectangle — 111 and 110. This sequence of codes cannot be used any more.

Any caller attempting a preset number of erroneous responses can be disconnected. If the caller tries to reconnect, the challenge from the host is different. Thus, the probability that a hacker can generate a correct response is minuscule. Of course, the code matrix must be changed often to provide an adequate number of choices for authorized users. For even higher security, matrices of four or more dimensions can be used, just as cubes are compounded into hypercubes in concurrent processing.

This work was done by Earl R. Collins, Jr., of Caltech for **NASA's Jet Propulsion Laboratory**. *For further information, Circle 85 on the TSP Request Card.*

This invention is owned by NASA, and a patent application has been filed. Inquiries concerning nonexclusive or exclusive license for its commercial development should be addressed to the Patent Counsel, NASA's Resident Office-JPL [see page 14]. Refer to NPO-17525

New Books, Posters and Videotapes

A free brochure describes the complete line of books, posters, and videotapes from NASA Tech Briefs. **Circle Number 700** for your free copy.

Determining Sense of Motion in Robotic Vision

Image-processing algorithms are based partly on natural visual/mental processes.

NASA's Jet Propulsion Laboratory, Pasadena, California

A proposed digital image-processing scheme (see figure) would determine the sense of motion of an object in an image along one coordinate axis (left to right or right to left) with respect to the background in the image. The image would be encoded by passing it through spatiotemporal filters, including a nonlinear contrast function with a threshold. The nonlinear response to the sums and differences of imagery processed through even and odd spatial filters would indicate the sense of motion.

In essence, the problem is to obtain a numerical indication of whether and how far a spatial pattern in the image has moved during the temporal interval between two observations or image frames. For this purpose, the image would first be processed through even (E) and odd (O) Gabor filters; namely,

$$F_E(f, x, x_o, \sigma) = \cos(2\pi f x)\exp[-(x-x_o)^2/2\sigma^2]$$

and

$$F_O(f, x, x_o, \sigma) = \sin(2\pi f x)\exp[-(x-x_o)^2/2\sigma^2]$$

where f is the spatial frequency of interest, x is the horizontal position being examined, x_o is the observer's point of fixation, and σ is an effective width of a spatially-localized smoothing function.

Gabor filters are chosen because they imitate some of the behavior of the visual cortex and optimize resolution on a linear scale in the spatial-position and spatial-frequency domains. The sine and cosine functions of the Gabor filters act like oriented 1 ½ octave bandpass spatial-frequency functions that extract the contrasts at each position. An even filter computes the smoothed contrast at each position, whereas an odd filter computes the corresponding contrast difference or spatial gradient.

In the proposed scheme, the sense of motion of a pattern in an image relative to the background in the image at two different times would be discriminated whenever the output from computations that involve the difference and sum of paired odd and even band-pass channels pooled across the background frame of reference exceeds the threshold. The following model is proposed to predict the visibility of shifts in the sense of motion of a test pattern (detected by F_O) relative to a multifrequency background (detected by F_E) between time t_1 and time t_2:

$$\frac{\delta}{\delta t}(F_E \pm F_O) = \left[\sum_{x=x_o-\frac{\beta}{2}}^{x=x_o+\frac{\beta}{2}} \left(\frac{k_j\, C_b^n}{C_b^n + C_o} F_E \pm \frac{k_i\, C_t^n}{C_t^n + C_o} F_O\right)^m\right]_{t_2}^{o} -$$

$$\left[\sum_{x=x_o-\frac{\beta}{2}}^{x=x_o+\frac{\beta}{2}} \left(\frac{k_j\, C_b^n}{C_b^n + C_o} F_E \pm \frac{k_i\, C_t^n}{C_t^n + C_o} F_O\right)^m\right]_{t_1}^{o}$$

where C_t corresponds to the contrast of the test pattern, C_b corresponds to the contrast of the the background pattern, C_o is a threshold expressed as a constant that corresponds to the signal-to-noise ratio used when detecting left-to-right movement of a test pattern relative to the background, n corresponds to the slope of the contrast response function (usually n is approximately 2), m is usually 1, sometimes $= 2$, $m \times o = 1$, β corresponds to the spatial period of the background frame of reference, and k_i and k_j are constants for the gain of the contrast sensitivity that is changed by feedback.

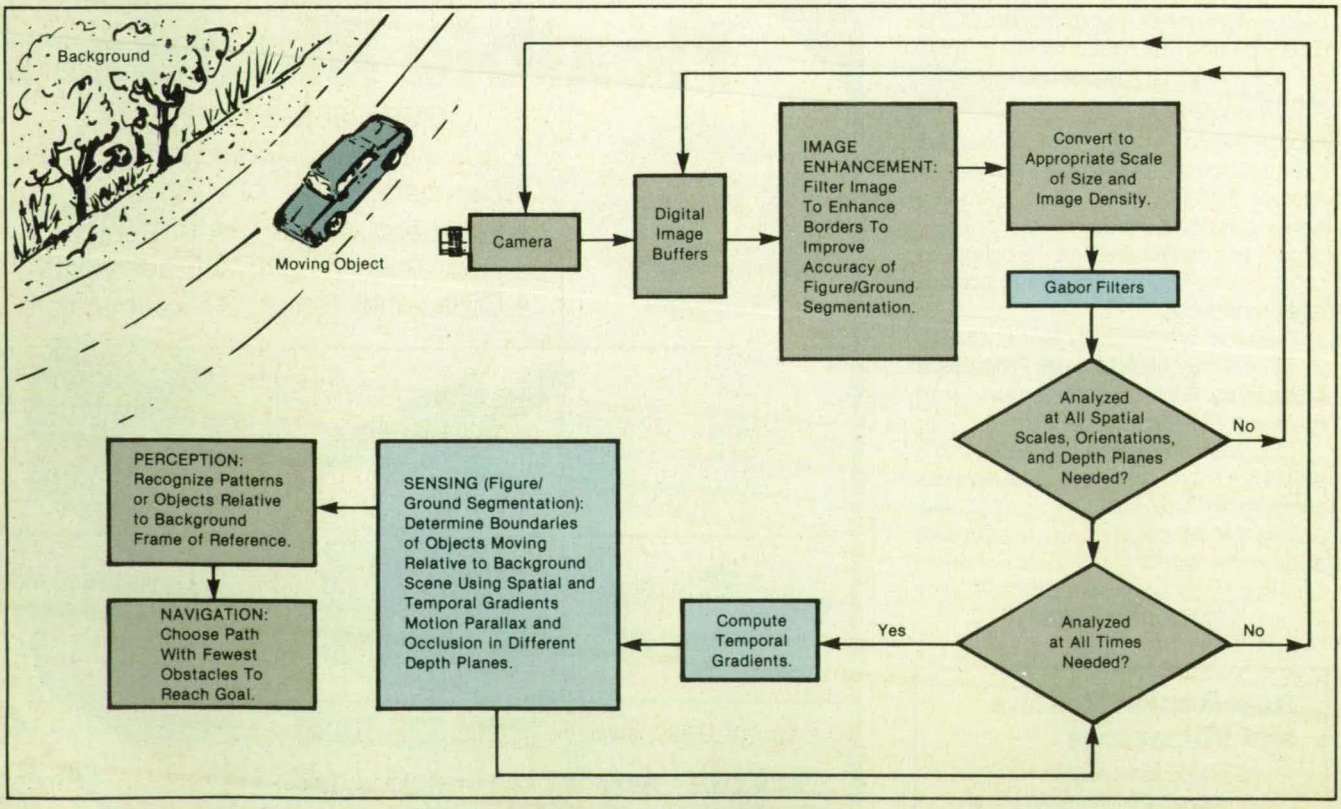

A Robotic Vision System could include a computing subsystem that would detect motion according to the proposed scheme. The processing of image data to detect motion might be performed by a neural-network computer in accordance with nonlinear Gabor-function algorithms.

Leftward movement is signaled by the difference between the outputs of paired odd and even filters, whereas rightward movement is signaled by the sum of the outputs of paired odd and even filters. Left-to-right movement at one spatial position would be discriminated when the difference of paired even and odd filters at time t_1 differs significantly from the sum at time t_2. The sign of the temporal gradient would determine whether the test pattern moved to the right or left of the peak luminance of the background.

This work was done by Teri B. Lawton of Caltech for **NASA's Jet Propulsion Laboratory**. *For further information, Circle 76 on the TSP Request Card.*
NPO-17552

Finding Optimal Gains in Linear-Quadratic Control Problems

Approximate gains are obtained for infinite-dimensional systems.

NASA's Jet Propulsion Laboratory, Pasadena, California

An analytical method based on Volterra factorization leads to new approximations for the optimal control gains in the finite-time linear-quadratic control problem of a system that has an infinite number of dimensions. The new method should involve less computation than does the prior method based on the numerical solution of Riccati equations.

The objective is to compute the optimal feedback control law for the following regulator problem:

$$\min_{u,x} J(u, x) = \int_0^{t_f} [\langle x(t), Q(t)x(t)\rangle + |u(t)|^2]dt$$

subject to the constraint

$$x(t) = S(t, 0)x(0) + \int_0^t S(t, \sigma)B(\sigma)u(\sigma)d\sigma$$

where J is a criterion function; the symbols $\langle\bullet, \bullet\rangle$ represent the inner product; t represents time in general; t_f represents the interval during which the system is measured; u represents the control and is R^m-valued; x represents the state of the system and is H-valued (H is a real separable Hilbert space); Q and B are strongly-measurable essentially-bounded $B(H)$- and $B(R^m, H)$-valued functions, respectively, with $Q(t) \geq 0$; and S is an essentially-bounded, jointly strongly continuous evolution operator on H. The standard approach, based on the approximation of the entire semigroup that characterizes the dynamics of the system, leads to a sequence of Riccati equations for the approximate control gains. The convergence of the approximate gains is established, but in general no a priori estimates of errors are derived.

The new approach circumvents the need to analyze and solve Riccati equations and provides a more transparent connection between the dynamics of the system and the optimal gain. Essential to this approach is a theorem that provides approximate explicit expressions for the optimal control law in terms of a compact manifold of solutions of the underlying infinite-dimensional system together with a solution to an associated problem of Volterra factorization of terms related to those in the regulator problem. Regularity conditions for the approximation of this manifold combine with regularity conditions for the approximation of the solution to the factorization problem to give asymptotically valid estimates for the errors in the approximate gains.

This work was done by Mark H. Milman and Robert E. Scheid, Jr., of Caltech for **NASA's Jet Propulsion Laboratory**. *For further information, Circle 107 on the TSP Request Card.*
NPO-17011

Computer Simulation for Multilevel Optimization of Design

Simple mathematical functions are substituted for complex engineering analyses.

Langley Research Center, Hampton, Virginia

Complex engineering systems are usually amenable to decompositions in which the wholes are treated as assemblies of smaller parts. Traditionally, engineers have used this technique to break large design tasks into smaller subtasks executed concurrently, thereby developing a broad workfront and speeding the design process. Methods for the application of formal optimization techniques to decomposed system-design problems are highly desirable and are currently under development.

Unfortunately, because of the mathematical complexity of the design subproblems, the experimentation with, and validation of, these methods becomes very expensive. As a consequence, tests of some of the new methods have had to be quite restricted in scope. However, a new simulator for multilevel optimization of complex hierarchical systems greatly reduces the cost of analysis in experimentation with multilevel design-optimization algorithms.

The simulator is a computer program that mimics the qualitative behavior and data couplings that occur among the subsystems of a complex engineering system, such as a car, an aircraft, or a building. The decomposition may be regarded as a pyramid of hierarchically related modules, in which each module corresponds to a design subtask. The subtasks may correlate with physical subsystems or with engineering disciplines that contribute to the design of the system. For the purposes of management, the modules may be groups of people.

Each module represents an algorithm that converts input into output. The algorithm may include both analysis and optimization. The overall procedure takes the form of a multilevel optimization, the purpose of which is to satisfy constraints and improve the performance of the whole system.

The simulator eliminates the engineering analyses in the subsystems by replacing them with judiciously-chosen analytical functions. The cost of analysis having thus been eliminated, the simulator is used for experimentation with a large variety of candidate algorithms for methodologies for the multilevel optimization of design to choose the best ones for the application. Thus, the simulator serves as a tool for the development of strategy for the multilevel optimization of design.

Experience with the simulator to date showed the following: agreement of the results of multilevel optimization with benchmark results produced without decomposition, acceptable rates of convergence for the multilevel optimization algorithms tested, and a slightly reduced rate of convergence of multilevel optimization when the strength and complexity of the couplings among subtasks were increased. In summary, the simulator confirmed the viability of the multilevel optimization algorithms tested and has proved to be a valuable tool in the development of these algorithms for use in the design of complex engineering systems.

This work was done by Sharon L. Padula and Jaroslaw Sobieszczanski-Sobieski of **Langley Research Center**. *For further information, Circle 70 on the TSP Request Card. LAR-13850*

Numerical Models for Control of Robots

Kinematic models are based on empirical data.

Marshall Space Flight Center, Alabama

An algorithm develops numerical models of the kinematics of robots for use in directing the movements of the robots. The numerical models can replace the analytical or iterative models used commonly.

While analytical models describe the movements of robots by algebraic equations and iterative models do so by successive approximations that home in on the true movements, numerical models simply predict movements from previous measurements of actual movements. Analytical models are difficult to develop and cannot be used for robots that are not wrist partitioned. Iterative models can be used for non-wrist-partitioned robots, but they cannot provide the data needed for control of the relative motion and velocity of end effectors. Iterative models, moreover, demand large computational capacities.

Both analytical and iterative models yield solutions for ideal robots. Real robots, however, depart from ideal behavior: inevitably, they embody manufacturing and design errors, and their linkages are not rigid but flex when loads are applied. Such deviations from the ideal are too complex to be included in these models.

The numerical models developed by the new algorithm, in contrast, transcend manufacturing and design errors because they are based on empirical data. No assumptions are made about the geometrical properties of a given robot. For the same reason, the numerical model of a robot is unaffected by flexure — a factor that can introduce large errors in conventional models if the robot is very large. The effects of loads are simply included in the numerical model of the robot, with loads as independent variables. In a similar manner, the algorithm can compensate for thermal contraction and expansion of links and joints by including the effect of temperature in the model and temperature as another independent variable. In addition, it readily produces the partial differential equations needed for relative-motion commands and control of velocity if the robot is not wrist partitioned.

Numerical models from the new algorithm were generated by B-spline fits to joint-coordinate data for two quite different robots — NASA's protoflight manipulator (PFMA) and Stanford University's robot manipulator. These models were analyzed in a computer simulation. The model of the PFMA was found to be accurate within thousandths of a degree, and that of the

Stanford machine within hundredths of a degree. For both models, the maximum error in the position of the end effector was less than 0.085 mm.

The data for the models must be measured by digital theodolites, laser-based instruments, or other highly-accurate measuring equipment. Rented equipment can be used for the measurements, inasmuch as new data are needed only when the characteristics of a robot change significantly — from wear or an accident, for example.

This work was done by Mary S. Waggener of Advanced Control Technologies, Inc., for **Marshall Space Flight Center**. *For further information, Circle 42 on the TSP Request Card.*

Inquiries concerning rights for the commercial use of this invention should be addressed to the Patent Counsel, Marshall Space Flight Center [see page 14]. Refer to MFS-28360

Books and Reports

These reports, studies, handbooks are available from NASA as Technical Support Packages (TSP's) when a Request Card number is cited; otherwise they are available from the National Technical Information Service.

Recursive Construction of Jacobian Matrix and its Time Derivative for Robot Arm

Quantities essential to linearization of control feedback are calculated.

A report discusses the recursive calculation of the Jacobian matrix (J) and the derivative of this matrix with respect to time ($\dot{J}$) for a robot arm that has multiple rotary joints. Such calculations can be used for the implementation of linearizing feedback in a digital control system for the arm. Once a recursive construction for $\dot{J}$ is available, the feedback can be linearized in a completely recursive manner by the use of previously known methods for the recursive computation of J and of the inverse dynamics of the arm.

The mathematical model of the robot is a standard N-link manipulator based in an inertial reference frame. The ith link vector is represented by $\mathbf{r}_i = \mathbf{O}_i - \mathbf{O}_{i-1}$, where $\mathbf{O}_i$ is the position vector of the origin of the moving reference frame that is based at the outer end of the ith link. The ith moving reference frame has inertial angular velocity $\mathbf{\Omega}_i$ and angular velocity $\boldsymbol{\omega}_i$ with respect to the $i-1$st reference frame.

First, the inertial linear velocity, $\mathbf{V}$, and angular velocity, $\mathbf{\Omega}$, of the end effector (Nth link) are expressed in terms of the $\mathbf{r}_i$ and $\boldsymbol{\omega}_i$. The angular displacement of the ith link with respect to the $i-1$st link is expressed as a rotation through angle q_i about the $\hat{\mathbf{z}}_{i-1}$ axis. Then

$$\boldsymbol{\omega}_i = \dot{q}_i \hat{\mathbf{z}}_{i-1}$$

(where the dot denotes the derivative with respect to time) is inserted into the equations for $\mathbf{V}$ and $\mathbf{\Omega}$. After some manipulation, the equations are transformed into an equation for J in terms of the $\hat{\mathbf{z}}_{i-1}$ and of vector products between the $\hat{\mathbf{z}}_{i-1}$ and the $\boldsymbol{\ell}_i = \mathbf{O}_N - \mathbf{O}_{i-1}$.

With proper attention to the rates of change of vector products in rotating reference frames, some further manipulation leads to an equation for $\dot{J}$ in terms of vector products and sums of vector products of the various position vectors and angular velocities. Because each succeeding element of J and $\dot{J}$ includes terms from the preceding element, these equations lend themselves directly to a recursive formulation. Two recursive algorithms are presented: one for the recursion from the end effector toward the base and one from the base toward the end effector.

This work was done by Kenneth K. Kreutz of Caltech for **NASA's Jet Propulsion Laboratory**. *To obtain a copy of the report, "Recursive Control of Jacobian Matrix and Its Time Derivative for Feedback Linearization of a Robot Arm," Circle 6 on the TSP Request Card. NPO-17364*

New on the Market

The IC-3 **fiber optic inspection adaptor** from Willow Bend, Chelmsford, MA, employs a 2mm flexible optical-grade fiber to illuminate areas which are difficult or impossible to access with conventional lights, such as deep borings, complex castings, and shrouded components. The monofilament fiber transmits light with over 90% efficiency at ten meters. The adaptor comes with 6", 12", and 18" fiber lengths.
Circle Reader Action Number 788.

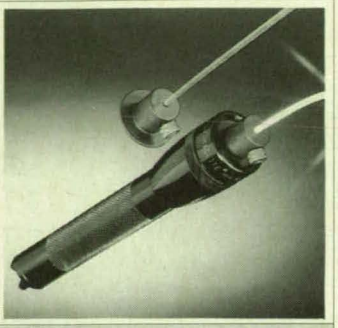

The RPLP-4 **rack and pinion low-profile wrench** from Raymond Engineering Inc., Middletown, CT, is suited for tight spots on flanges and areas with low clearances on heavy equipment, pipelines, turbines, in petrochemical and chemical industries, shipbuilding, mining, and drilling. The lightweight tool offers a 4000 ft.-lb. torque capacity, interchangeable heads, an adjustable drop-foot adaptor, and swivel hydraulic fittings for easy maneuverability without hose binding. The RPLP-4 is packaged with common wrench sizes in a compact carrying case.
Circle Reader Action Number 776.

A new interactive **voice recognition product** developed by Covox Inc., Eugene, OR, records and plays back speech and other sounds via the parallel printer port on any PC, PS/2, or compatible computer. Dubbed the Voice Master Key System II, the unit features a graphics-based sound editor for speech manipulation and a software program capable of recognizing 64 spoken words at a time. Speech can be introduced into application programs written in C, compiled Basic, GWBasic, and other languages. Priced at $219.95, the system is designed for use with multimedia presentations, in education, entertainment, foreign and remedial language training, and for voice mail over local area networks.
Circle Reader Action Number 780.

Thermalite, a three-layer **wire insulation** consisting of a Du Pont Teflon® fluoropolymer surrounded by Kapton® polyimide, with an outer sheath of Teflon, is available from Teledyne Thermatics, Elm City, NC. Designed for military, aerospace, and electronics applications, Thermalite is flexible, strippable, crack-resistant, and surpasses cross-linked ETFE in flammability resistance, smoke emissions, and fluid resistance. Conductors made with Thermalite have been shown to withstand temperatures from -65° to +260°C.
Circle Reader Action Number 782.

Acculex, Taunton, MA, has introduced the DPP-400 **panel printer** for laboratory, industrial, and field/mobile applications. The DPP-400 has a standard RS-232 serial interface for connection to a variety of computers, process controllers, modems, and terminals. It can be configured for baud rates ranging from 50 to 9600 baud, with choice of parity checking, character bit length, and number of stop bits. The printer provides full ASCII character support.
Circle Reader Action Number 774.

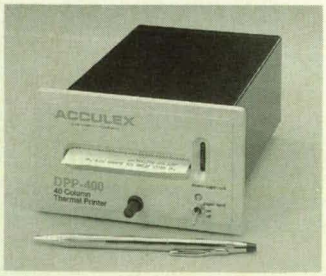

Offering up to 7.6 billion floating point instructions per second (GFlops) with 2 GBytes main memory and disk storage in excess of 100 GBytes, the iPSC®/860 **supercomputer** delivers Cray-level performance at one-tenth the cost, according to the manufacturer, Intel Scientific Computers, Beaverton, OR. The iPSC/860 is available in five field-upgradable models, delivering from 480 MFlops to 7.6 GFlops. System prices start at $265,000.
Circle Reader Action Number 766.

The HP 84130A **EMI commercial-compliance system** from the Hewlett Packard Company, Palo Alto, CA, allows full compliance testing, including open-area testing, for regulations of governing agencies. Its EMI receiver meets the recommendations of the International Special Committee on Radio Interference. The HP 84130A is configured with the HP 8568B spectrum analyzer and includes a quasi-peak adaptor, an RF preselector, a preamplifier, a transient limiter, and a receiver-functions downloadable program.
Circle Reader Action Number 770.

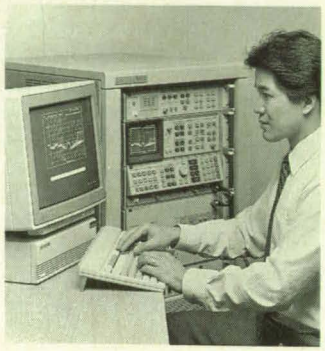

The XEU, an **electronic encryption device** from Xerox Corporation, McLean, VA, enables government computer users to send and receive classified and unclassified information on the same local area network. It is activated by inserting an electronic Crypto ignition key into a slot on the front of the unit and is deactivated when the key is removed. The key becomes unique to a specific XEU once it is used. The XEU, which is inserted between a workstation or a personal computer and a network connection, meets IEEE 802.3 and Ethernet specifications.
Circle Reader Action Number 796.

The MV-SPECTRUM single-channel, **VGA graphics overlay and frame grabber interface board** from Metrabyte Corp., Taunton, MA. is designed for real-time image processing and acquisition applications. The product combines video pictures, text, and graphics on the VGA-compatible monitor of an IBM PC/AT or compatible microcomputer and accepts any NTSC video input. A frame is digitized and displayed in 33 milliseconds.
Circle Reader Action Number 768.

A new four-channel **waveform recorder** from Scientific Recording Assoc., Watertown, CT, plugs into AT or PC style computers and offers an aggregate sampling rate of 800 kilo-samples per second. The model SRA1204 recorder features a flexible timebase which can be programmed to provide varying amounts of pre- and post-trigger information, enabling the user to accurately capture transient signals. The unit's highly accurate analog-to-digital converter provides 12-bit low-noise resolution.
Circle Reader Action Number 786.

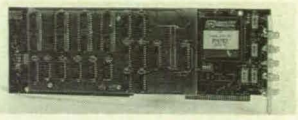

A new line of plastic **self-lubricating bearings** from Igus Bearings Inc., East Providence, RI, features high wear resistance and load capacity and can withstand temperatures to 221° C short term or 132° C in continuous use. According to the manufacturer, the Iglide L280 bearings offer up to five times the wear resistance of other plastic and metallic bushings when applied in rotary, linear and reciprocating motions. The oil-free bearings are available in 200 standard sizes and sleeve, flange, and thrust configurations.
Circle Reader Action Number 772.

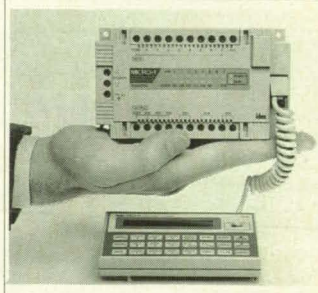

Only 5.5" x 3.2" x 2.75" in size, the microprocessor-based Micro 1 **controller** from Idec Corp., Sunnyvale, CA, matches the capacity of larger controllers and can replace 160 relays, 80 timers, and 45 counters. The product incorporates a CPU, eight DC inputs and six relay outputs. Its I/O capacity is easily expanded via a compact serial module that adds eight additional inputs and outputs. The Micro 1 uses EEPROM for heightened memory reliability.
Circle Reader Action Number 784.

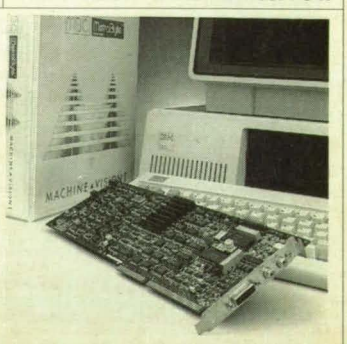

New on the Market

The model WL10 portable handheld **infrared (IR) heater** from Lux-Therm Products, Syracuse, NY, features a 1000w, 230v tubular quartz IR lamp assembly. When used with a 230v power supply, the WL10 emits 1000w to produce a surface temperature of 227°C within five minutes. Applications include plastic curing and forming, preheating, paint and adhesive curing, and surface treatment.
Circle Reader Action Number 794.

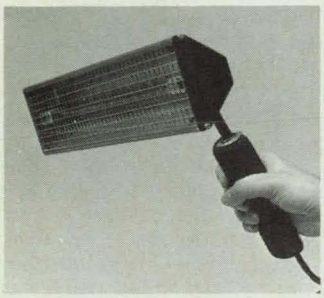

Replacing the prism viewfinder on a conventional Nikon F3 35mm camera with the PentaCam CCD color video head creates a hybrid **high-resolution TV and 35mm film camera.** For applications such as surveillance, monitoring, training, and documentation, the PentaCam system allows for simultaneous on-site and remote real-time viewing on a monitor, recording onto tape, direct transmission to electronic imaging systems, and conventional 35mm still photography. Developed by The Focal Point Inc., South Norwalk, CT, the PentaCam system includes the bracket for the F3, the video camera control unit (CCU) and a power supply .
Circle Reader Action Number 798.

A new **form entry device** allows users to keep both paper and electronic copies of important documents. Available from the Graphics Technology Co., Austin, TX, the device consists of an opaque clipboard attached to a computer. As the user writes with an ordinary pen on a form placed on the board, the device sends the information to the computer, which can store handwriting or, using recognition software, convert it to ASCII characters.
Circle Reader Action Number 792.

Sharp Electronics, Mahwah, NJ, has introduced the PC-E500, a programmable **pocket computer** with built-in engineering software. It features a full graphic display and 1101 functions, including 744 formulas, 124 constants, and 233 scientific calculation functions. Designed for portability, the 7" x 3" half-pound PC features a 40 character x 4 line screen, 32K byte RAM, a QWERTY keyboard, and a serial I/O interface. Options include a thermal printer, a pocket disk drive, and plug-in RAM cards. The PC-E500 retails for $299.
Circle Reader Action Number 800.

The CYD200 Series **digital thermometer** from OMEGA Engineering Inc., Stamford, CT, can measure temperatures from -271° to +200°C with an accuracy of 0.5°C and a resolution of 0.1°C. It features a four digit display and front panel selection of units in °C, °F, Kelvin, or the actual sensor voltage. Two models are available: a single channel indicator and an eight channel indicator.
Circle Reader Action Number 790.

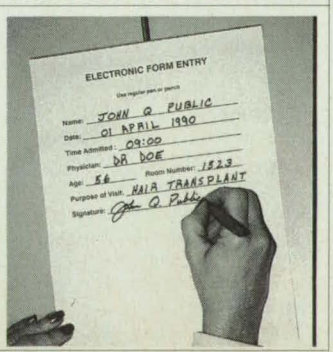

New Literature

Stock Drive Products' 768-page Handbook of Standardized Components features over 24,000 off-the-shelf **inch and metric drive parts**. Product categories include belt and chain drives, gears, speed reducers, motors, couplings, universal joints and flexible shafts, bearings, fasteners, vibration mounts, and unique components such as constant force springs and splined bushings. The catalog includes technical tables with conversion to small inch measurements, standards for inch size and metric threads, and American/metric equivalents.
Circle Reader Action Number 706.

A 20-page catalog from Power General, Canton, MA, provides basic electrical and mechanical specifications for over 400 **AC/DC switching power supplies and DC-DC converters.** Included are AC/DC power supplies from 25 to 200 watts in open-frame, enclosed, and encapsulated modules, as well as DC-DC converters from 1 to 100 watts. All products are machine-inserted, autotested, and monitored under statistical process control.
Circle Reader Action Number 710.

A 34-page catalog from AMP Inc., Harrisburg, PA, spotlights the Metrimate line of **pin and socket connectors** which includes square-grid connectors for free-hanging and/or panel mounting; free-hanging in-line connectors; square-grid and in-line pin and socket headers for printed circuit board mounting; and drawer connectors for rack and panel mounting with radial float. The catalog provides performance characteristics, dimensional specifications, and application tooling information.
Circle Reader Action Number 704.

A **digital timing analyzer** (DTA) offering both time-ordered and sample modes is described in a full-color brochure from International Test Instruments Inc., Irvine, CA. The DTA stores up to 524,000 continuous time-ordered measurements, for data rates up to 20 MHz at a resolution of 50 ps. For samples, it can record up to 10 billion measurements at data rates up to 200 MHz. Example screens of time-ordered and sample mode measurements are shown on the analyzer's 640 x 350 line EL flat-panel display.
Circle Reader Action Number 708.

Industrial Computer Source, San Diego, CA, has released the fourth edition of its Industrial Computer Source-Book/Supplement, featuring over 500 **industrial computer, data acquisition, industrial control, and communication products** for the IBM PC/XT/AT and compatibles. Available free of charge, the supplement includes an extended line of computer chassis products, as well as new 386SX and 386 CPU cards, 19" rack accessories, and A/D and communication cards.
Circle Reader Action Number 702.

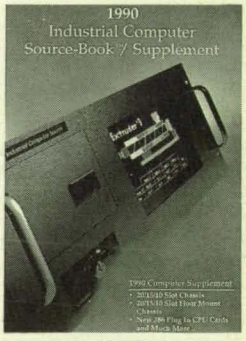

A 48-page **adhesive, ceramic, and high-temperature materials handbook** is available from Cotronics Corp., Brooklyn, NY. Product categories include insulation materials, machinable ceramics, ceramic and industrial cements, high-temperature epoxies, sealers and binders, high-temperature coatings, and welding and brazing supplies.
Circle Reader Action Number 726.

The Brushless DC Motor Handbook from Inland Motor, Radford, VA, provides basic design concepts, terms and definitions, and configurations of **brushless motor systems.** The handbook contains a brushless amplifier application note which relates the use of sinusoidal and trapezoidal back EMF waveform motors to the proper control electronics and discusses the advantages of both. A simplified approach to pulse-width modulation (PWM) is presented for both voltage and current control.
Circle Reader Action Number 712.

New Literature

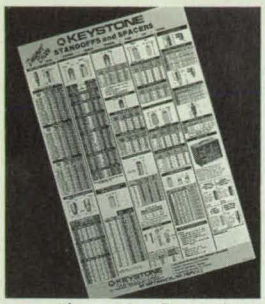

Keystone Electronics Corp., Astoria, NY, is offering a quick-reference wall chart detailing the company's various **spacer and standoff** types, sizes, styles and platings. The 14" x 22" multicolor chart contains complete specifications for Keystone's brass, aluminum, stainless steel, phenolic, nylon and ceramic spacers and standoffs. An additional feature highlights the company's wall-mount or stackable spacer kits which include inventories of the most frequently used spacers and standoffs in day-to-day operations.
Circle Reader Action Number 714.

Digital Equipment Corp., Maynard, MA, has published a handbook describing its new **VAX vector processing architecture** for the 6000 and 9000 series computers. The free 134-page publication provides an overview of vector processing and the VAX vector architecture, and discusses how the VAX FORTRAN compilier supports vector processing.
Circle Reader Action Number 724.

A six-page brochure from Datel Inc., Mansfield, MA, reviews the company's **data converter component** product lines, including sampling analog-to-digital converters, data acquisition systems, sample-hold amplifiers, general-purpose A/D converters, digital-to-analog converters, instrumentation amplifiers, isolation amplifiers, tunable active filters, multiplexers, and V/F converters. The brochure includes electrical specifications and pricing information.
Circle Reader Action Number 722.

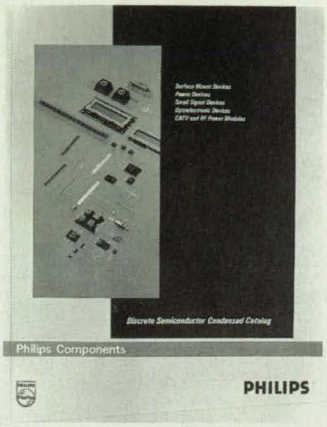

A 179-page **discrete semiconductor catalog** from Philips Components, Riviera Beach, FL, lists the company's full line of surface mount, power, small signal, and optoelectronic devices as well as CATV and RF power modules. The catalog contains a cross-referenced index with packaging specifications and outline drawings.
Circle Reader Action Number 716.

A 40-page **carbide tool catalog** from Niagara Cutter Inc., North Tonawanda, NY, features solid carbide end mill styles and sizes, as well as milling cutters, saws, special carbide tipped tools, and indexable insert tools. Carbide-tipped and indexable insert tools are available with titanium nitride coating.
Circle Reader Action Number 720.

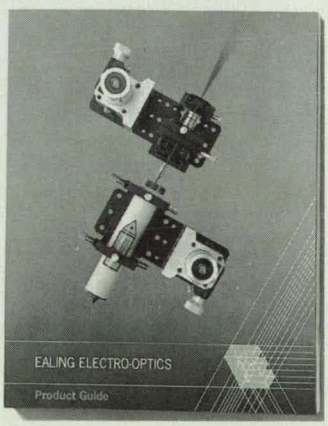

A new **electro-optics catalog** from Ealing Electro-Optics Inc., Hollis-ton, MA, describes the company's line of manual and motorized micropositioners, component mounts, light sources, lasers and accessories, monochromators and detectors, optical benches and tables, optical filters, and microscope components. Technical specifications and photos are provided for all products.
Circle Reader Action Number 718.

Subject Index

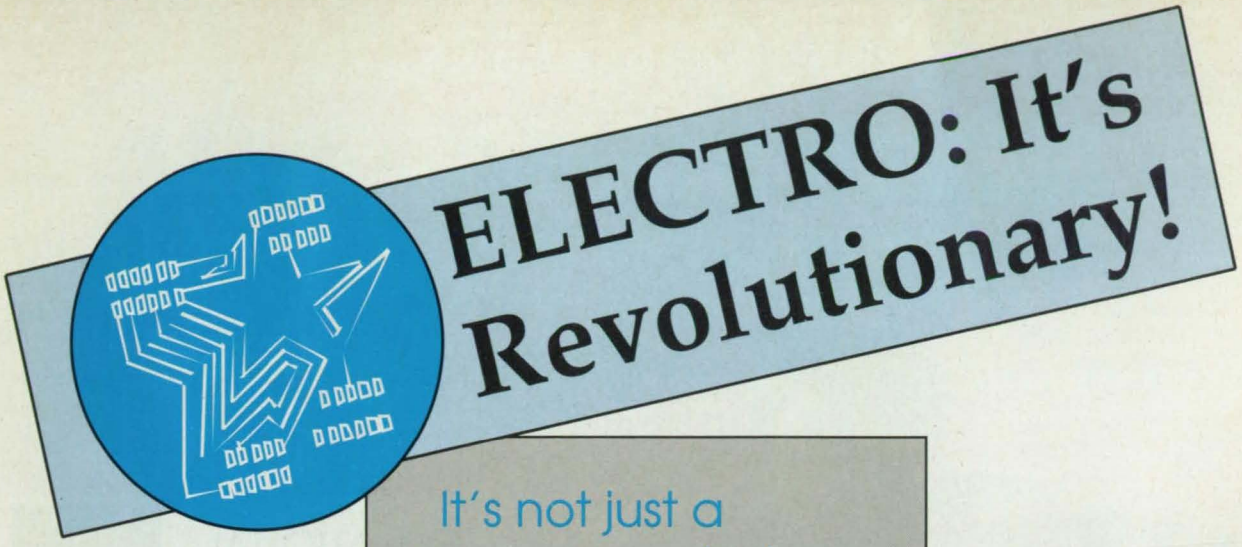

It's not just a components show, it's much more!

What distinguishes ELECTRO and sets it apart from all other conferences on the East Coast?

The breadth and depth of the many segments of the electronics industry gathered in one forum, at one time with the newest and most advanced electronics products and technologies. Only ELECTRO successfully integrates product presentations and updates on the current state of technology into a multidisciplinary concurrent engineering framework.

When you come to ELECTRO, it's like attending several vertical shows at once. Nowhere else can you see what's new in components, instruments, EDA tools, power supplies, production materials, engineering services and more at one industry event. No other conference offers you the wide variety of learning opportunities available at ELECTRO.

This revolutionary approach makes ELECTRO your best learning value and the one event YOU CANNOT MISS in 1990. Don't be left behind.

▲ More than 5,000 products being demonstrated by experts knowledgeable in their uses and applications

▲ More than 800 vendors

▲ 51 educational idea-generating tutorials and technical sessions organized in the following tracks: • Marketing • Devices • Electronic CAx • Mechanical CAx • CASE • Manufacturing CAx • Test • Quality • Education • General

▲ Keynote address by Thomas H. Bruggere, chairman of the board and chief executive officer of Mentor Graphics Corp.

▲ Purchasing conference on "Purchasing's Role in Corporate Success" with Frank Tahmoush, Polaroid Corp., and Robert Nahabit, Nahabit Associates

Electro®/90

The Boston T.E.A. Party

May 9-10-11, 1990

John B. Hynes Veterans Memorial Convention Center and Bayside Exposition Center in Boston, Mass.

For FREE registration and more information, call 213/215-EXPO

Sponsored by Region 1, CNEC and METSAC, IEEE and New England and New York Chapters, ERA

AUTOMATION NEVER STANDS STILL . . . NEITHER CAN YOU!

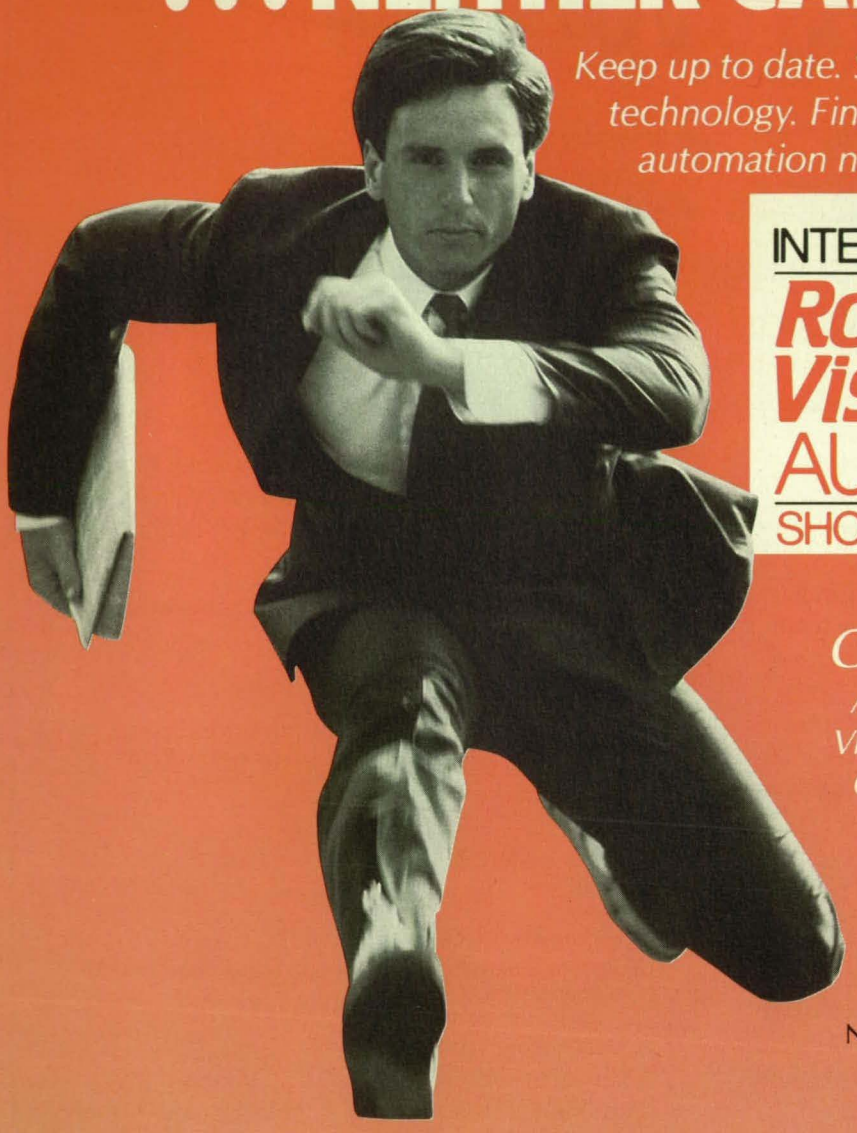

Keep up to date. See the newest technology. Find solutions for your automation needs. You must attend:

INTERNATIONAL
Robots & Vision
AUTOMATION
SHOW & CONFERENCE

June 5–7, 1990
Cobo Hall, Detroit

America's only Robots and Vision Automation Show and Conference, sponsored by

ria
Robotic Industries Association

NSRA
National Service Robot Association

AIA
Automated Imaging Association
(formerly Automated Vision Association)

Call or write now for your free show tickets. Be sure to ask for full details on America's most comprehensive Robots and Machine Vision Conference. Contact: Automation Show, 7901 Westpark Drive, McLean, VA 22102. (703) 827-5299.

Circle Reader Action No. 456

CLEO® / IQEC '90

ANAHEIM CONVENTION CENTER
ANAHEIM, CALIFORNIA

May 21–25, 1990 Conference • May 22–24, 1990 Exhibits

CLEO®
SPONSORED BY:
LASERS AND ELECTRO-OPTICS SOCIETY OF IEEE
OPTICAL SOCIETY OF AMERICA

IQEC
SPONSORED BY:
AMERICAN PHYSICAL SOCIETY
LASERS AND ELECTRO-OPTICS SOCIETY OF IEEE
OPTICAL SOCIETY OF AMERICA

The Exhibition and Product Presentations are free of charge to the qualified business professional.

The tenth annual Conference on Lasers and Electro-Optics (CLEO®) and the seventeenth International Quantum Electronics Conference (IQEC) combine to present the **world's largest** technical conference on lasers and electro-optics. The combined meeting—with approximately 1,000 technical papers anticipated—represents a broad forum for the distribution of information on all aspects of lasers and electro-optical technology from basic research to applied research to systems engineering to industrial applications. IQEC concentrates on basic research on and with lasers, while CLEO® spotlights the applications of laser and electro-optic technology. A unified technical exhibition will be open May 22–24.

DYNAMIC COMMERCIAL EXHIBIT

Attendees will find the latest in laser and electro-optical technology on display in the North and South Halls of the Anaheim Convention Center. The latest products and services from more than 400 leading manufacturers from around the world will be on display. Don't miss this opportunity to observe the finest commercial products in the laser industry!

FOCUSED PRODUCT DEMONSTRATIONS

Product demonstrations will be held on Tuesday, Wednesday, and Thursday. These product demonstrations allow a more-involved presentation of application-specific operation than is possible on the exhibit floor. A complete listing of demonstrations will be available at registration.

Check off the boxes below to identify the additional information you need, and mail this coupon to:
Meetings Department, Optical Society of America
1816 Jefferson Place, NW, Washington, DC 20036
or call CLEO® Exhibits Dept. (202) 223-9034. Or fax this coupon to: (202) 223-1096.

I need information on:

- ☐ technical conference registration
- ☐ exhibits-only attendance
- ☐ exhibiting my company's products
- ☐ focused product demonstrations

Send this information to:

Name _____ Job Title _____

Company _____

Address _____

City _____ State _____ Zip _____

Country _____ Telephone number ( ) _____

Circle Reader Action No. 411

Advertiser's Index

***RAC** stands for **Reader Action Card.** For further information on these advertisers, please circle the RAC number on the Reader Action Card elsewhere in this issue. This index has been compiled as a service to our readers and advertisers. Every precaution is taken to ensure its accuracy, but the publisher assumes no liability for errors or omissions.

NASA Tech Briefs, ISSN 0145-319X, USPS 750-070, copyright © 1990 in U.S., is published monthly by Associated Business Publications Co., Ltd. 41 E. 42nd St., New York, NY 10017-5391. The copyrighted information does not include the individual Tech Briefs which are supplied by NASA. Editorial, sales, production and circulation offices at 41 E. 42nd Street, New York, NY 10017-5391. Subscriptions for non-qualified subscribers in the U.S., Panama Canal Zone, and Puerto Rico, $75.00 for 1 year; $125.00 for 2 years; $200 for 3 years. Single copies $10.00. Remit by check, draft, postal or express orders. Other remittances at sender's risk. Address all communications for subscriptions or circulation to NASA Tech Briefs, 41 E. 42nd Street, New York, NY 10017-5391. Second-class postage paid at New York, NY and additional mailing offices.

POSTMASTER: please send address changes to NASA Tech Briefs, 41 E. 42nd Street, Suite 921, New York, NY 10017-5391.

The Tandem™ flashlight features an ergonomic design that borrows from NASA technology.

Mission Accomplished

To expedite the transfer of space-based technology to U.S. industry, NASA established a nationwide network of Industrial Applications Centers (IACs) that offers businesses access to over 100 million documents contained in the NASA data bank and some 400 other computerized databases. The IACs provide technical support and conduct literature searches to help clients investigate new or unfamiliar technology areas; stay abreast of advances in their own disciplines; examine competing activity; review patents; and resolve design or manufacturing problems.

One company that has benefited significantly from IAC assistance is the Rayovac Corporation, a leading battery and flashlight manufacturer located in Madison, Wisconsin. Rayovac engineers worked with NERAC Inc., a Connecticut-based IAC, in designing a new combination home, industrial, and work light called Tandem™ that offers both a wide-angle floodlight and a spotlight capable of illumination up to 50 feet. The square flood beam illuminates downward to afford safe walking while the spot beam projects forward at a scientifically-established angle for aiming ease. Tandem features krypton bulbs that are 100 percent brighter than regular flashlight bulbs; an ergonomic body constructed of extremely tough ABS plastic; and a heavy-duty magnetic nameplate that enables the flashlight to be affixed to any metal object. NERAC helped Rayovac researchers explore NASA ergonomic design concepts, as well as developments in krypton bulbs and new magnetic materials.

NERAC also assisted in the application of NASA technology to Rayovac's premier flashlight—the Luma 2™—which features a unique emergency backup system with an independent power cell, bulb, and switch. This technique of systems redundancy was first used by NASA to ensure the reliability of manned spacecraft components. The Luma 2 also sports such NASA innovations as the lithium power cell, which offers a ten-year shelf life, and a magnetic switch with corrosion-proof sealed contacts.

In addition to identifying technology advances incorporated into Rayovac's lighting products, NERAC aided the company in developing a zinc air battery for hearing aids. A key component in the product is a permselective film that permits oxygen ingress but prevents water ingress or outgo. NERAC helped researchers to locate permselective films that would improve battery performance and to ascertain that competing products offered no technological advantage over the Rayovac battery.

Commented David R. Schaller, head of Rayovac's Advanced Technologies Laboratory: "NERAC saves my group about $50,000 a year in research time and effort. It's like having an additional technical expert on our staff." ❑

For a complete listing of NASA's Industrial Applications Centers, turn to page 14.

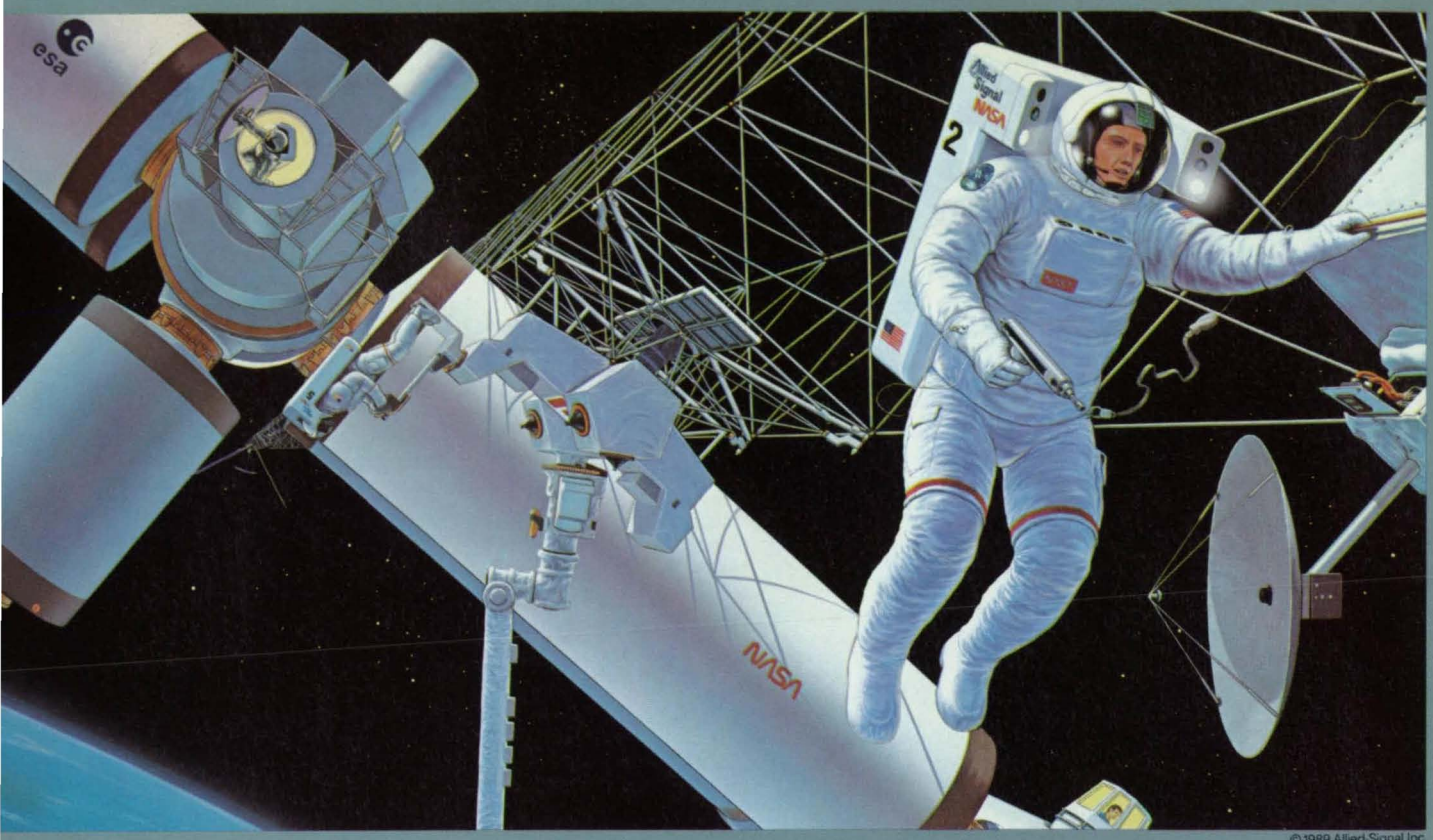

EXTRAVEHICULAR ACTIVE WEAR.

WE'RE THE FIRST AND LAST WORD IN EXTRAVEHICULAR ACTIVITY. WITH A PIONEERING PAST AS NASA'S ORIGINAL PORTABLE LIFE SUPPORT SYSTEM SUPPLIER. AND CONTINUING LEADERSHIP IN ENVIRONMENTAL CONTROL/LIFE SUPPORT SYSTEM TECHNOLOGY.

WE'VE WON THREE SPACE STATION FREEDOM PORTABLE LIFE SUPPORT SYSTEM TECHNOLOGY CONTRACTS. DEVELOPING EFFICIENT NEW SUBSYSTEMS FOR VENTILATION, THERMAL CONTROL AND CO_2 REMOVAL.

NOT ONLY HAVE WE LIVED WITH THIS UNPRECEDENTED NEW TECHNOLOGY FOR SEVERAL YEARS, WE ARE THE PERFECT PARTNER TO TURN IT INTO HARDWARE.

AIRESEARCH LOS ANGELES DIVISION 2525 WEST 190TH STREET TORRANCE CA 90509 (213) 512-5488. WHERE THE ULTIMATE EFFICIENCY IS RELIABILITY.

Allied-Signal Aerospace Company

Circle Reader Action No. 415

Allied Signal

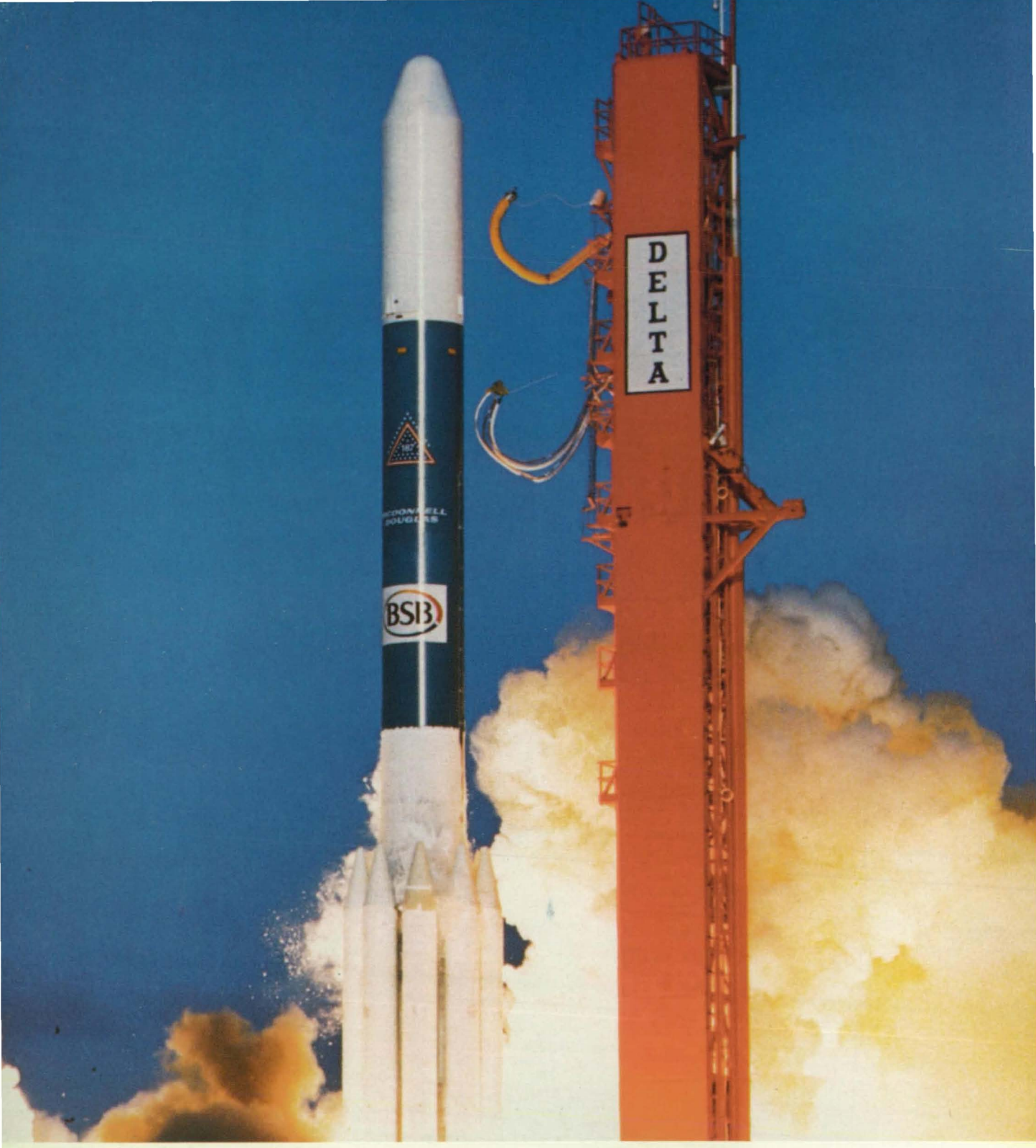

THE SHOT HEARD ROUND THE WORLD.

Recent launch of a British satellite by a McDonnell Douglas Delta booster marked the first commercial launch to orbit flown by a private U.S. company.

The satellite, owned by British Satellite Broadcasting, Ltd., will be teamed in geosynchronous orbit soon with an identical spacecraft launched by a Delta booster. The pair will provide direct-relay TV broadcasts on five channels to subscribers across The British Isles.

As it has for nearly 30 years, Delta leads the way into space.

MCDONNELL DOUGLAS

A company of leaders.

Circle Reader Action No. 501